

Multiscale Methods for Nuclear Reactor Analysis

by

Benjamin S. Collins

A dissertation submitted in partial fulfillment
of the requirements for the degree of
Doctor of Philosophy
(Nuclear Engineering and Radiological Sciences and Scientific Computing)
in The University of Michigan
2011

Doctoral Committee:

Professor Thomas Downar, Co-Chair
Assistant Research Scientist Volkan Seker, Co-Chair
Professor Edward Larsen
Professor William Martin
Assistant Professor Eric Johnsen
Professor Han Gyu Joo, Seoul National University
Engineer Yunlin Xu, Argonne National Laboratory

And whatever you do, in word or deed, do everything in the name of the Lord Jesus, giving thanks to God the Father through him.

— Colossians 3:17

... all of this through the precious blood of Christ Jesus

© Benjamin S. Collins

All Rights Reserved

2011

for Sarah, Ezekiel, and my parents
Thank you for all your love and support throughout this process

Acknowledgments

Several people have been instrumental in the development of this work. I would like to thank my co-advisors Dr. Thomas Downar and Dr. Volkan Seker for all of their encouragement, ideas, and patience. I would also like to show my extreme gratitude to Dr. Yunlin Xu. His advice, assistance, and willingness to teach me has been an invaluable part of my graduate career.

My committee has also been a great source of feedback throughout the development of this work, Dr. Edward Larsen, Dr. William Martin, Dr. Han Gyu Joo, and Dr. Eric Johnsen. The several discussions that we have had have been greatly appreciated. I would also like to thank the DOE NEUP program for sponsoring this work under grant NEUP-09-304.

My officemates and others in the department have provided a wonderful environment to work and learn. Specifically I would like to express my gratefulness to Andrew Ward, Daniel Jabaay, and Brendan Kochunas for always being around to bounce ideas off of, make me laugh, and provide a helping hand. I would also like to thank Artem Yankov for his assistance in running cases for this work.

Lastly I would like to express my great appreciation of my family. Sarah, you have been there for me every step of the way and your love and support has made all of this possible. Ezekiel, your smile makes everything seem better. My parents, your encouragement and support for the past 26 years has never wavered and I know you are the reason I have made it this far. Of course none of this would be possible without the gifts given to my by the Lord and Savior Jesus Christ whom all the glory should be given.

Table of Contents

Dedication	ii
Acknowledgments	iii
List of Tables	vi
List of Figures	vii
Abstract	ix
Chapter 1 Introduction	1
1.1 Multiscale Methods	3
1.2 Previous Work in Multiscale for Neutron Transport Calculations	5
1.3 Overview of Current Work	7
Chapter 2 Current Reactor Analysis Methodology	9
2.1 Neutron Transport Theory	9
2.2 Diffusion Theory	12
2.2.1 Nodal Diffusion	12
2.2.2 Fine Mesh Finite Difference Diffusion	17
2.3 Transport Methods	21
2.3.1 Method of Characteristics	22
2.3.2 Stochastic Methods	28
2.4 Coarse Mesh Finite Difference Acceleration	28
2.4.1 Few Group CMFD	29
2.4.2 Multigroup CMFD	29
2.4.3 CMFD Iteration Scheme	30
Chapter 3 Multiscale Neutronics Method	31
3.1 Boundary Response Function	31
3.1.1 Interface Approximations	32
3.2 Post-Refinement Multiscale Method	36
3.2.1 Post-Refinement Fixed Source Implementation	38
3.2.2 Post-Refinement Albedo Boundary Implementation	39

3.3	Embedded Iteration Method	39
3.3.1	Embedded Iteration Method Implementation	39
Chapter 4	Assessment of the Post-Refinement Multiscale Method	43
4.1	Figures of Merit for Analysis	43
4.2	One Dimensional Analysis	44
4.2.1	Assembly Layouts	45
4.2.2	LEU Core	46
4.2.3	MOX1 Core	47
4.2.4	MOX2 Core	54
4.3	Two Dimensional Analysis	57
4.3.1	Assembly Layouts	57
4.3.2	LEU Core	59
4.3.3	MOX Core	63
4.4	Discussion of Post-Refinement Methods	69
4.4.1	Same Energy and Mixed Energy Results	69
4.4.2	Impact of Buffer Region	69
4.4.3	Comparison of Post-Refinement Methods	70
4.4.4	Sensitivity Analysis	71
Chapter 5	Assessment of the Embedded Multiscale Method	78
5.1	One Dimensional Analysis	78
5.1.1	Embedded Region Around Peak Power Assembly	79
5.1.2	Embedded Region Around Fuel-Reflector Interface	85
5.1.3	Embedded Region Around Controlled Assembly	87
5.2	Discussion of Embedded Method	90
5.2.1	Impact of Multiple Embedded Levels	90
5.2.2	Prolongation Operators	91
Chapter 6	Summary and Conclusion	92
6.1	Summary of Work	92
6.2	Future Work	94
Bibliography	96

List of Tables

Table

4.1	One Dimensional Assembly Geometry	45
4.2	FOM Mixed Energy LEU Core	48
4.3	FOM Same Energy MOX 1 Core	49
4.4	FOM Mixed Energy MOX 1 Core	50
4.5	FOM Mixed Energy MOX 1 Core with 33 Groups	55
4.6	Figures of Merit for MOX 2 Core	56
4.7	Two Dimensional Assembly Geometry	57
4.8	FOM for 2D LEU Core	62
4.9	FOM for 2D MOX Core	66
5.1	Figures of Merit for LEU Core with Embedded Multiscale Method . .	81
5.2	Figures of Merit for MOX1 Core with Embedded Method	82
5.3	Figures of Merit for MOX 2 Core	84
5.4	Comparison of Level Structure for 33 Group Embedded Calculation .	85
5.5	Control Rod Worth for the LEU Core	88

List of Figures

Figure

1.1	Composite grid corresponding to each level	4
1.2	Traditional V-Cycle Iteration Strategy	5
1.3	W-Cycle Iteration Strategy with Multiple Levels	5
2.1	^{235}U and ^{239}Pu Total Cross-sections	10
2.2	Coordinate System for MOC Rays	23
2.3	Modular Rays	27
3.1	Reflective Boundary Condition	33
3.2	Flow Chart of the Post-Refinement Method	37
3.3	Flow Chart of the Embedded Iteration Method	40
4.1	LEU Assembly	45
4.2	MOX Assembly	45
4.3	LEU Core Layout	46
4.4	Multiscale Regions for 1-D LEU and MOX 1 Cores	46
4.5	Pin Error PPR for LEU Core	47
4.6	MOX 1 Core Layout	48
4.7	Pin Error PPR for Same Energy MOX 1 Core	49
4.8	Pin Error MS for Same Energy MOX 1 Core	50
4.9	Pin Error in MS for Mixed Energy MOX 1 Core	51
4.10	FOM Mixed Energy MOX 1 Core with Buffer Region	52
4.11	FOM Mixed Energy MOX 1 Core with Increased ROI and Buffer	53
4.12	Pin Error in MS for Mixed Energy MOX 1 Core with No Buffer	54
4.13	MOX 2 Core Layout	55
4.14	Multiscale Regions for 1-D MOX 2 Core	55
4.15	2-D LEU Assembly	58
4.16	2-D MOX Assembly	58
4.17	2-D LEU Core Layout	59
4.18	2-D LEU Core Multiscale Regions	60
4.19	Pin Error in PPR for 2D LEU Core	61
4.20	Assembly Error for 2D LEU Core	62

4.21	2-D MOX Core Layout	63
4.22	2-D MOX Core Multiscale Regions	64
4.23	Pin Error in PPR for 2D MOX Core	65
4.24	Pin Error in MS for 2D MOX Core with Increased ROI and Buffer . .	66
4.25	Assembly Error for 2D MOX Core	67
4.26	Pin Error in PPR for 2D MOX Core with Increased ROI and No Buffer	68
4.27	Domain Mapping Example	72
4.28	Sensitivity of Local Solver	77
5.1	Pin Power Error Distribution for Diffusion Solvers	80
5.2	Embedded Multiscale Regions for LEU and MOX 1 Core	80
5.3	PPR in MOX1 Core for Embedded Method	82
5.4	Additional Embedded Multiscale Region for MOX 1 Core	82
5.5	Impact of Extended MOC Region for MOX1 Core	83
5.6	Multiscale Regions for MOX2 Core	83
5.7	Multiscale Regions for 33 Group Embedded Calculation	84
5.8	Multiscale Regions in the Reflector for the Embedded Method	85
5.9	Impact of Embedded Regions in Reflector for the LEU Core	86
5.10	Impact of Embedded Regions in Reflector for the MOX 2 Core	87
5.11	Control Insertion Pattern	88
5.12	Multiscale Regions Used in Control Rod Analysis	88
5.13	Pin Power Errors with Control Rod Inserted	89

Abstract

The ability to accurately predict local pin powers in nuclear reactors is necessary to understand the mechanisms that cause fuel pin failure during steady state and transient operation. In the research presented here, methods are developed to improve the local solution using high order methods with boundary conditions from a low order global solution. Several different core configurations were tested to determine the improvement in the local pin powers compared to the standard techniques, that use diffusion theory and pin power reconstruction (PPR). Two different multiscale methods were developed and analyzed; the post-refinement multiscale method and the embedded multiscale method. The post-refinement multiscale methods use the global solution to determine boundary conditions for the local solution. The local solution is solved using either a fixed boundary source or an albedo boundary condition; this solution is “post-refinement” and thus has no impact on the global solution. The embedded multiscale method allows the local solver to change the global solution to provide an improved global and local solution.

The post-refinement multiscale method is assessed using three core designs. When the local solution has more energy groups, the fixed source method has some difficulties near the interface; however the albedo method works well for all cases. In order to remedy the issue with boundary condition errors for the fixed source method, a buffer region is used to act as a filter, which decreases the sensitivity of the solution to the boundary condition. Both the albedo and fixed source methods benefit from the use of a buffer region.

Unlike the post-refinement method, the embedded multiscale method alters the global solution. The ability to change the global solution allows for refinement in areas where the errors in the few group nodal diffusion are typically large. The embedded method is shown to improve the global solution when it is applied to a MOX/LEU assembly interface, the fuel/reflector interface, and assemblies where control rods are inserted. The embedded method also allows for multiple solution levels to be applied in a single calculation. The addition of intermediate levels to the solution improves the

accuracy of the method. Both multiscale methods considered here have benefits and drawbacks, but both can provide improvements over the current PPR methodology.

Chapter 1

Introduction

The determination of the neutron flux distribution in nuclear reactors is crucial for both safety and economic reasons. This is because the power produced in the fuel is directly proportional to the neutron flux. The ability to accurately predict the power distribution inside the core is important in determining the cooling requirements of the reactor during steady state operation and all hypothesized transients, including severe accidents. Economically, the ability to accurately predict the pin power distribution allows for better utilization of the fuel and decreases conservatism applied to the probability of fuel failures during overpower events. These requirements put a heavy burden on the codes responsible for calculating the neutron flux under various conditions.

Standard practice in the design and analysis of nuclear reactors is the use of nodal diffusion codes coupled to one dimensional thermal-fluid codes. Such coupled code systems have the ability to accurately predict the average assembly powers. Pin power reconstruction methods have been developed to modulate the heterogeneous pin power distribution for a single assembly lattice calculation onto the smooth full core solution. The efficiency of nodal diffusion codes makes them ideal to evaluate the neutron flux during both operational and accident analyses. Unfortunately, the underlying assumptions of diffusion theory prevent a detailed power distribution to be known with sufficient accuracy for complex geometries or in challenging transient conditions. For this reason, interest has increased in the development of advanced codes which are capable of solving the Boltzmann transport equation throughout the core [1, 2].

Although these full core transport solvers yield a detailed distribution of pin powers throughout the core, they are very computationally intensive. Full core transport solvers generally require the use of a computer cluster in order to solve the flux distribution in a reasonable time and hold the full problem domain in memory. Furthermore, the ability to solve full core transport transient problems are even more

computationally intensive, in some cases requiring weeks of computing time for a few seconds of transient simulation.

An important advantage that full core transport solvers have over the standard nodal diffusion codes is the ability to accurately describe the effects of neighboring assemblies. In nuclear reactors, there are several locations where the effect of neighboring assemblies can introduce errors into the calculation: the fuel-reflector interface, the insertion of control rods, and the interface of different fuel types. In the standard few group nodal diffusion methods, the homogenized cross sections are generated using an infinite medium neutron spectrum which can be very different from the conditions in a modern core that can have very different fuel types and compositions. A basic assumption of current methods is the validity of an asymptotic spectrum to generate homogeneous cross sections. Unfortunately, this has become less valid in highly heterogeneous fuel loadings currently used in industry.

One of the most common locations where diffusion theory does not work well is the fuel-reflector interface. For assemblies facing the reflector, the assumption of an infinite assembly does not accurately describe the correct energy spectrum inside the assembly. The reflector allows for a large leakage of high energy neutrons and a source of thermal energy neutrons which cause fission. The ability to resolve this interface requires special treatment during modeling. The most common practice is to use a two assembly calculation, which is comprised of the fuel assembly and a reflector region. In order to preserve the net current at the interface, a discontinuity factor is defined. Although this methodology is practical and improves the accuracy of the calculation of the fuel-reflector interface, the method is not robust. Generally, this type of calculation is only performed for a single fuel type with zero burnup, but in reality there are several fuel types that face a boundary and the burnup associated with the peripheral fuel is also not uniform.

Another common location where diffusion theory is inaccurate is in the vicinity of control rods. The introduction of control rods causes a sharp drop in the thermal neutron flux. Although the diffusion core solution does a good job of approximating the worth of a control rod, the pin power distribution in neighboring regions can have significant errors. The ability to calculate the pin power around control rods accurately can be very important when predicting the fuel performance during events such as a control rod ejection. In this kind of accident, the fuel pins facing the control rod can experience a higher deposition of energy than the assembly average.

Finally, another common region where diffusion theory introduces errors is at the interface of unlike fuel types. In recent years, interest has grown in the ability to load

mixed oxide (MOX) fuel into operating nuclear reactors in order to burn weapons grade Plutonium. The addition of these assemblies into the nuclear reactors creates a very heterogeneous system of standard low enriched Uranium (LEU) and MOX assemblies. The computational issues with these simulations are the fact that the energy spectrum of an LEU assembly and a MOX assembly can be very different. The existence of Plutonium in the MOX assemblies adds a large absorption resonance below 1 eV, which does not exist in standard LEU fuel. The LEU-MOX interface can be a significant source of error in nodal diffusion calculations, and a special treatment must be used in order to minimize the errors in the standard homogenized nodal methods.

The error in few group nodal diffusion in each of the cases noted above is directly attributable to localized transport effects. *The objective of this work is to increase the fidelity of the solver locally in regions where large errors are introduced by the few group diffusion approximation by employing a set of higher order methods locally, yet retaining the global nodal diffusion solution.* This is achieved through two different methods. The first is an a posteriori method in which the global solution is used to determine the boundary conditions for a local problem. This method does not provide any feedback to the global solver and will be referred to as the post-refinement method. The second method is an embedded calculation in which the global and local solutions are solved simultaneously to provide a consistent solution. The second method is much more consistent with traditional adaptive multiscale methods and will be referred to as the embedded method.

1.1 Multiscale Methods

Multiscale methods provide the framework to perform a detailed calculation locally while still relying on a coarser solution globally. The essential idea behind the multiscale method is to decompose the solution into suitable scales; macro, meso, micro, etc. The objective of these scales is to increase fidelity where important physics is occurring or the mathematical model of the macroscale is insufficient to capture the full physics. The goal is to optimize the computational cost of the multiscale scheme with the cost of a detailed global solution. That is, we desire:

$$\frac{\text{cost of multiscale method}}{\text{cost of smallest scale method on the full domain}} \ll 1 \quad (1.1)$$

One of the classical examples of the multiscale method is the multigrid method [3].

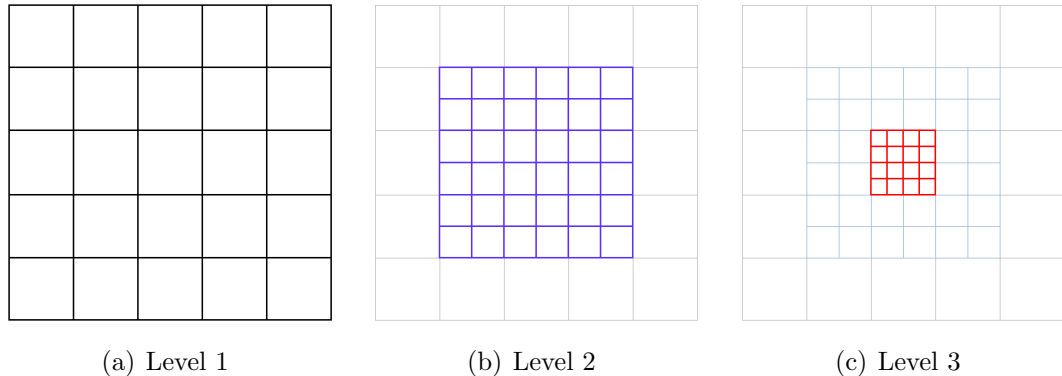


Figure 1.1: Composite grid corresponding to each level

In this method, the spatial grid is refined in order to decrease the discretization error. The grid refinement can be done on a global scale (full multigrid) and the multigrid scheme simply accelerates the solution of the smallest scale or it can be done on a local scale (adaptive multigrid) where the grid is reduced where the discretization error is large. The standard coarse mesh finite difference (CMFD) [4] procedure is an example of a full multigrid method.

The refinement of multiscale methods is performed adaptively and can be done either statically or dynamically. Static adaptive methods determine how to refine the grid using a predefined map, generally defined by the user. Dynamic adaptive methods, on the other hand, use criteria of the solution to determine if the grid should be refined. The criteria used can vary depending on the physics of interest. In principle, the two types of adaptive methods can be combined. In this case, the user would specify a location of interest and the rest of the domain would be refined dynamically. However, the focus of the work here is on static adaptive methods.

The adaptive multiscale method relies on a hierarchy of grids and methods. The first level represents the global domain with the macro-scale method. As the grid level increases, the grid is restricted to smaller and smaller subdomains and the method also increases in fidelity. Figure 1.1 shows the composite grid. Level 1 contains a coarse representation of the global domain. Levels 2 and 3 refine the grid and the method. The remainder of the coarse grid is depicted but the grayed out and is not used during the computation of the level.

In addition to determining and defining the levels, it is necessary to define an iteration strategy between the levels. There are several iteration strategies for maneuvering between levels [3]. The V cycle iteration is a basic iteration strategy which starts

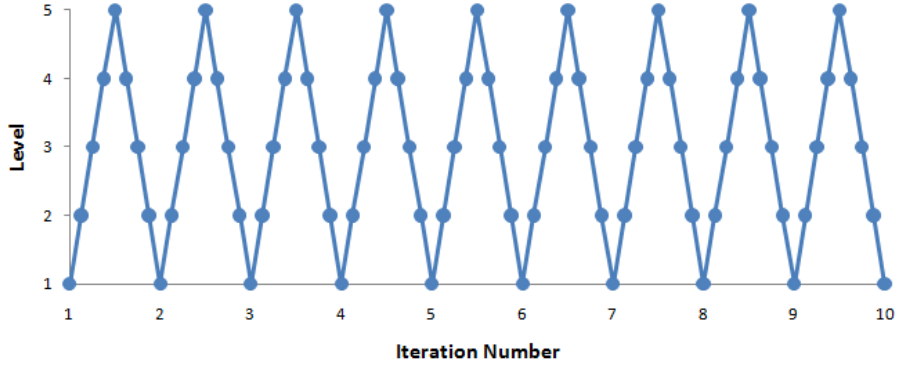


Figure 1.2: Traditional V-Cycle Iteration Strategy

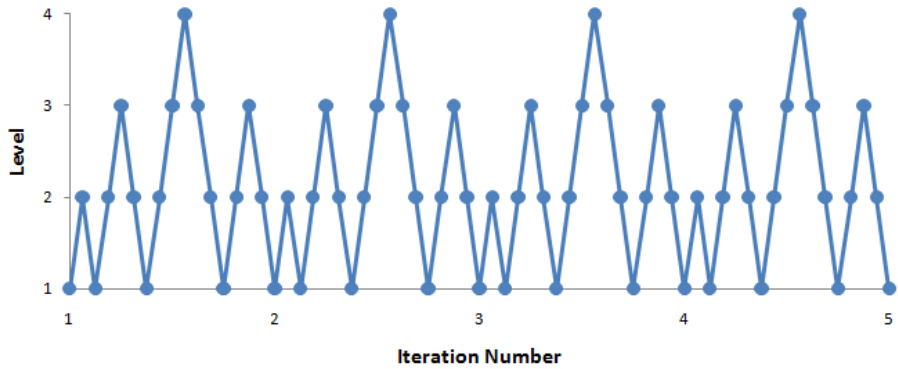


Figure 1.3: W-Cycle Iteration Strategy with Multiple Levels

at level 1 and gradually increases the levels until the maximum number of levels is reached and then gradually reduces the level back to 1. This type of iteration scheme is repeated until all levels reach their convergence as shown in Figure 1.2. Another iteration scheme, the W cycle, strives to limit the number of calls to the higher levels until the lower levels reach certain convergence criteria. This iteration strategy is depicted in Figure 1.3.

1.2 Previous Work in Multiscale for Neutron Transport Calculations

The ability to obtain detailed localized information in nuclear reactors has been the goal of several researchers over the past several decades. Some of the first research in this area was done in the 1970's by Wagner, Koebke, Grill, and Jonsson. The methods

they developed involved a posteriori imbedded calculations with more detail locally in order to reconstruct pin powers.

Koebke and Wagner [5] proposed a method called the “flux-lupe” method. Lupe appropriately is the German word for magnifying glass. In this technique, a full core nodal method is used to define partial incoming current boundary conditions for a local problem. The boundary conditions describe the coupling of the local problem to the global problem. The local problem is solved using a collision probability method. Overall, the results of the flux-lupe method show significant improvement over the pin power modulation method.

Grill and Jonsson [6, 7] also investigated imbedded calculations for the code ROCS/MC. The methods used are similar to Koebke, but instead of the local solver being collision probability, fine mesh finite difference diffusion was used. Partial incoming currents are still used as the boundary condition for the problem. In this method, the global and local solutions both used two energy groups. The results from this work also showed good agreement with the global fine mesh calculations.

Nissen [8] investigated several different methods for pin power reconstruction, including the flux-lupe methods and the modulation method that is the basis for current pin power reconstruction techniques. In addition to running cases with partial incoming current boundary conditions, albedo type boundary conditions were also considered. Several conclusions about the flux-lupe method were made in Nissen’s work. The flux-lupe method is sensitive to the accuracy of the actual boundary conditions. In cases where the boundary conditions are poorly approximated, the pin power shape did not represent the true solution. Another conclusion is that the albedo type boundary condition is a better method to determine accurate boundary conditions compared to the incoming partial current. The final conclusion is that the method is accurate if good boundary conditions can be applied but it is computationally inefficient if pin powers are desired in more than a few assemblies.

In a paper discussing the framework of modern nodal codes, Smith [9] contrasted the speed of the current pin power reconstruction methods to the computational burden that imbedded methods require. Smith recognized the superior accuracy possible with imbedded methods, but because of concerns with computational efficiency, he recommended the development of pin power reconstruction methods which have since become more popular than imbedded methods.

More recently, researchers have investigated refining one of the three independent variables in neutron transport; space, energy, and angle. The spatial variable has been considered by Jessee [10] and Wang [11]. Both of these methods looked at applying

dynamically adaptive multigrid mesh refinement schemes to discrete ordinates discretization of the transport equation. The spatial refinement shows good improvement in computational requirements in both studies.

The spatial and angular variable refinement has been considered by Yi [12, 13]. In this work, an embedded MOC solver is considered inside a discrete ordinates global solution. This allows for higher accuracy in the local region where the MOC solution is solved with accurate boundary conditions from the discrete ordinates calculation. At the interface between the two solvers, the angular flux is projected in space and angle for each energy group. This method is similar to the method discussed in the research here except the interface is between diffusion and transport, and the energy group structure is mixed. Both of these differences complicate the interface. In addition, different regions are allowed to have different quadrature sets. At the interface of two quadrature sets, the angular flux is projection is based on interpolation in angle space.

The energy variable has recently been considered by Forget [14, 15, 16, 17]. The discrete generalized multigroup method (DGMM) creates a framework to perform calculations with mixed energy. This is done by performing an intermediate fixed source calculation which solves for moments of a coarse energy structure to reconstruct a fine energy structure. The intermediate calculation provides a consistent method to reconstruct the projection operator while still maintaining the fidelity of the coarse energy group solution.

Another method that has been considered to obtain more detailed pin by pin information is to rerun the lattice code to generate few group cross-sections with a more accurate energy spectrum [18, 19, 20, 21, 22]. In this method, a lattice calculation is performed for every assembly several times. Each time the lattice calculation is performed, the boundary conditions are adjusted in order to match the global diffusion solution and the spatial, energy, and angular effects of the neighboring assemblies. At convergence, the solution becomes very similar to the global transport solution. In the case where the outgoing angular flux is transferred to the neighboring assembly, these methods are effectively a method to decompose the transport domain to increase parallelism and reduce computation time.

1.3 Overview of Current Work

The presentation of the research performed here is organized in four major sections:

1. An overview of the current computational reactor physics methods
2. A discussion of the theory and implementation of the multiscale neutron transport methods
3. A brief overview of the test cases and the methods for assessing the quality of the solution
4. The results of the test cases

In the overview section, several currently used methods are discussed to provide a background of standard definitions and methods used in computational reactor physics. A more detailed discussion is focused on the methods relevant to the multiscale code developed in this work.

The next section presents the theory of the multiscale method, including various approximations needed to transition between scales. After the theory is presented, the specifics of the multiscale methods for this work are presented. Two different multiscale methods are detailed with contrasting benefits. The first method is called the post-refinement method, and is similar to the flux-lupe method proposed by Koebke, except that two improvements are made to provide more consistent results. The first improvement is to allow for albedo type boundary conditions instead of incoming partial currents. The second improvement is to allow for a buffer region around the region of interest to minimize the impact of the boundary conditions. The second multiscale method embeds the local solver into the global solver. This method is more consistent with standard multiscale methods. In this section, a description of the iteration strategy and all special treatments between levels is also provided.

The third section outlines the test cases that are used to assess the accuracy of the method. Several cases are developed to test different attributes of the solvers. One- and two-dimensional cases are performed to examine the effects of the fuel-reflector interface, control rods, and the interface between different fuel types. Five different figures of merit are also described to determine any improvements of the solution over standard methods.

The fourth section contains the results of all the test cases. The results section is separated into two chapters. The first chapter deals with the results from the post-refinement method. After considering cases with and without a buffer region, a sensitivity study is performed to determine how sensitive the solution is to each of the boundary condition types (incoming partial current and albedo). The next chapter investigates the use of embedded or “two-way coupling” methods which is similar to the typical multiscale methods. In these cases, the global solution is changed by the embedded local solution.

Finally conclusions about both methods are discussed and future work is proposed.

Chapter 2

Current Reactor Analysis Methodology

2.1 Neutron Transport Theory

The steady-state neutron transport equation, which describes how neutrons stream, are lost through collision, and are born into six dimensional phase space, is shown in equation (2.1).

$$\begin{aligned}
 & \boldsymbol{\Omega} \cdot \nabla \psi(\mathbf{x}, \boldsymbol{\Omega}, E) + \Sigma_t(\mathbf{x}, E) \psi(\mathbf{x}, \boldsymbol{\Omega}, E) \\
 &= \int_{4\pi} \int_0^\infty \Sigma_s(\mathbf{x}, \boldsymbol{\Omega}' \cdot \boldsymbol{\Omega}, E' \rightarrow E) \psi(\mathbf{x}, \boldsymbol{\Omega}', E') dE' d\Omega' \\
 &+ \frac{\chi(E)}{4\pi k} \int_{4\pi} \int_0^\infty \nu \Sigma_f(\mathbf{x}, E') \psi(\mathbf{x}, \boldsymbol{\Omega}', E') dE' d\Omega' \\
 & \qquad \qquad \qquad \mathbf{x} \in V, \quad \boldsymbol{\Omega} \in 4\pi, \quad 0 < E < \infty \quad (2.1a)
 \end{aligned}$$

$$\psi(\mathbf{x}, \boldsymbol{\Omega}, E) = 0 \quad \mathbf{x} \in \partial V, \quad \boldsymbol{\Omega} \cdot \mathbf{n} < 0, \quad 0 < E < \infty \quad (2.1b)$$

In this equation, ψ is the angular neutron flux as a function of space (\mathbf{x}), angle ($\boldsymbol{\Omega}$), and energy (E). Σ_x is the macroscopic cross-section of type “ x ” which is total (t), fission, (f), or scattering (s). ν is the average number of neutrons generated per fission, $\chi(E)dE$ is the probability that a fission neutron is created in dE about energy E . k is the k-eigenvalue (multiplication factor) of the system. The k-eigenvalue modifies the number of neutrons produced by each fission to preserve the global balance of neutrons. The transport equation is complicated by the energy dependent coefficients and cross-sections, as shown in Figure 2.1.

The complexities of the neutron transport equation make it difficult to solve for full core problems. Several methods have been developed over the past decades to

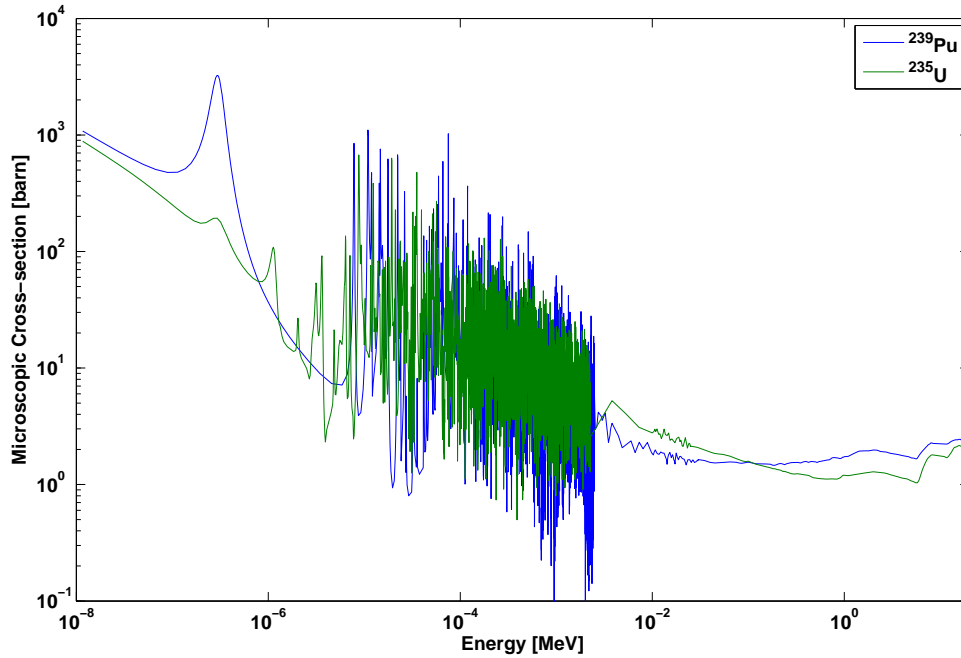


Figure 2.1: ^{235}U and ^{239}Pu Total Cross-sections

efficiently model standard reactor designs. Solutions of the transport equation can be broken up into two categories: deterministic and stochastic. Deterministic methods discretize each of the free variables, introducing discretization error into the solution. Stochastic methods model the random nature of the transport equation and thus do not have discretization errors, but instead have statistical errors.

Deterministic methods require the spatial, angular, and energy domain to be discretized. The spatial domain is generally divided into finite volumes, in which the transport equation is solved. The exact method of treating the spatial variables differ between different methods. The angular variable is generally treated in two ways. The first method is to discretize the angle across the unit sphere (discrete ordinates). The second method is to solve for integral moments of the angular variable (spherical harmonics). Almost all deterministic methods use the multigroup method to discretize the energy variable.

The multigroup method defines energy groups on which an average cross-section is defined for each group. The average cross-section is defined by preserving the reaction

rate inside the energy group.

$$\psi_g(\mathbf{x}, \boldsymbol{\Omega}) = \int_{E_g}^{E_{g-1}} \psi(\mathbf{x}, \boldsymbol{\Omega}, E) dE \quad (2.2a)$$

$$\Sigma_{x,g}(\mathbf{x}, \boldsymbol{\Omega}) = \frac{\int_{E_g}^{E_{g-1}} \Sigma_x(\mathbf{x}, E) \psi(\mathbf{x}, \boldsymbol{\Omega}, E) dE}{\psi_g(\mathbf{x}, \boldsymbol{\Omega})} \quad (2.2b)$$

$$\chi_g(\mathbf{x}) = \int_{E_g}^{E_{g-1}} \chi(\mathbf{x}, E) dE \quad (2.2c)$$

Generally an extra assumption is made that the angular flux is separable in energy and angle. This simplifies the definition of the multigroup cross-sections to only be a function of space.

$$\Sigma_{x,g}(\mathbf{x}) = \frac{\int_{E_g}^{E_{g-1}} \Sigma_x(\mathbf{x}, E) \phi(\mathbf{x}, E) dE}{\phi_g(\mathbf{x})} \quad (2.3)$$

These definitions yield the multigroup transport equation.

$$\begin{aligned} \boldsymbol{\Omega} \cdot \nabla \psi_g(\mathbf{x}, \boldsymbol{\Omega}) + \Sigma_{t,g}(\mathbf{x}) \psi_g(\mathbf{x}, \boldsymbol{\Omega}) \\ = \frac{\chi_g}{4\pi k} \sum_{g'=1}^G \int_{4\pi} \nu \Sigma_{f,g'}(\mathbf{x}) \psi_{g'}(\mathbf{x}, \boldsymbol{\Omega}') d\Omega' \\ + \sum_{g'=1}^G \int_{4\pi} \Sigma_{s,g' \rightarrow g}(\mathbf{x}, \boldsymbol{\Omega}' \cdot \boldsymbol{\Omega}) \psi_{g'}(\mathbf{x}, \boldsymbol{\Omega}') d\Omega' \end{aligned} \quad (2.4)$$

The principal problem with the multigroup equations is the need to know the continuous energy flux to correctly weight the continuous energy cross-sections. Several methods have been proposed to calculate multigroup cross-sections but, the two major methods are to assume an analytic shape for the flux or to calculate the point-wise continuous flux. Generally a combination of these two methods are used; analytic expressions where the flux solution is straightforward and well known, and point-wise continuous numerical solution in regions where the flux solution is non-trivial, such as the resonance region. The numerical solutions are generally computed on a significantly reduced spatial domain, which generally is zero- or one-dimensional in nature.

Another common assumption is to rewrite the differential scattering cross-section

as an infinite Legendre expansion:

$$\Sigma_s(\mathbf{x}, \boldsymbol{\Omega}' \cdot \boldsymbol{\Omega}) = \sum_{n=0}^{\infty} \frac{2n+1}{4\pi} \Sigma_{s,n}(\mathbf{x}) P_n(\boldsymbol{\Omega}' \cdot \boldsymbol{\Omega}) \quad (2.5)$$

The differential scattering can normally be well-approximated by truncating the infinite sum after the first or second moment. In this work, isotropic scattering, P_0 , will be assumed for simplicity. The resulting multigroup transport equation with isotropic scattering can be written as follows.

$$\begin{aligned} \boldsymbol{\Omega} \cdot \nabla \psi_g(\mathbf{x}, \boldsymbol{\Omega}) + \Sigma_{t,g}(\mathbf{x}) \psi_g(\mathbf{x}, \boldsymbol{\Omega}) \\ = \frac{\chi_g}{4\pi k} \sum_{g'=1}^G \nu \Sigma_{f,g'}(\mathbf{x}) \phi_{g'}(\mathbf{x}) + \frac{1}{4\pi} \sum_{g'=1}^G \Sigma_{s0,g' \rightarrow g}(\mathbf{x}) \phi_{g'}(\mathbf{x}) \end{aligned} \quad (2.6)$$

ϕ is the scalar flux which is simply the angle-integrated angular flux.

$$\phi_g(\mathbf{x}) = \int_{4\pi} \psi_g(\mathbf{x}, \boldsymbol{\Omega}) d\Omega \quad (2.7)$$

2.2 Diffusion Theory

2.2.1 Nodal Diffusion

Nodal diffusion codes have been the workhorse of reactor design and analysis for the past several decades. The nodal diffusion method is dependent on the diffusion form of the transport equation.

The Diffusion Equation

The diffusion equation is derived from the P_n class of methods, which expand moments of the angular flux using Legendre polynomials.

$$\psi_g(\mathbf{x}, \boldsymbol{\Omega}) = \sum_{n=0}^{\infty} \frac{2n+1}{4\pi} P_n(\boldsymbol{\Omega}) \phi_{g,n}(\mathbf{x}) \quad (2.8)$$

The P_1 equations are obtained by taking the zeroth and first angular moment of the transport equation and discarding the second angular moments:

$$\nabla \cdot \mathbf{J}_g(\mathbf{x}) + \Sigma_{t,g}(\mathbf{x}) \phi_g(\mathbf{x}) = \sum_{g'=1}^G \left(\frac{\chi_g}{k} \nu \Sigma_{f,g'}(\mathbf{x}) + \Sigma_{s0,g' \rightarrow g}(\mathbf{x}) \right) \phi_{g'}(\mathbf{x}) \quad (2.9a)$$

$$\frac{1}{3} \nabla \phi_g(\mathbf{x}) + \Sigma_{t,g}(\mathbf{x}) \mathbf{J}_g(\mathbf{x}) = \sum_{g'=1}^G \Sigma_{s1,g' \rightarrow g}(\mathbf{x}) \mathbf{J}_{g'}(\mathbf{x}) \quad (2.9b)$$

The P_1 equations are written solely in terms of the scalar flux ϕ and the net neutron current \mathbf{J} , which are defined as follows.

$$\phi_g(\mathbf{x}) = \int_{4\pi} \psi_g(\mathbf{x}, \boldsymbol{\Omega}) d\Omega \quad (2.10a)$$

$$\mathbf{J}_g(\mathbf{x}) = \int_{4\pi} \boldsymbol{\Omega} \psi_g(\mathbf{x}, \boldsymbol{\Omega}) d\Omega \quad (2.10b)$$

The diffusion equation and the P_1 equations differ in two ways. The first is that the time derivative of the current is assumed to be zero for the diffusion equation. Since only the steady state equations are shown here, this approximation is exact. The second assumption made is that the anisotropic scattering term, Σ_{s1} , can be simplified into a diagonal matrix. Since the scattering is assumed to be isotropic, this term is zero and this approximation becomes exact as well.

$$\Sigma_{tr,g}(\mathbf{x}) = (\Sigma_{t,g}(\mathbf{x}) - \Sigma_{s1,g,g'}(\mathbf{x})) \quad (2.11)$$

The diffusion equation is obtained by solving equation (2.9b) for the current and substituting that into equation (2.9a).

$$\begin{aligned} & -\frac{1}{3} \nabla \cdot \Sigma_{tr,g}^{-1} \nabla \phi_g(\mathbf{x}) + \Sigma_{t,g}(\mathbf{x}) \phi_g(\mathbf{x}) \\ & = \frac{\chi_g}{k} \sum_{g'=1}^G \nu \Sigma_{f,g'}(\mathbf{x}) \phi_{g'}(\mathbf{x}) + \sum_{g'=1}^G \Sigma_{s0,g' \rightarrow g}(\mathbf{x}) \phi_{g'}(\mathbf{x}) \end{aligned} \quad (2.12)$$

Equivalence Theory

Most nodal methods today are based on Equivalence Theory proposed by Koebke [23] and extended to Generalized Equivalence Theory by Smith [24]. In general, the

equivalence theories developed by Koebke and Smith aim to accurately represent a heterogeneous system using a homogeneous system through the introduction of additional parameters. Generalized Equivalence Theory uses a three-step approach for determining the power distribution in the reactor. The first step is to generate the transport multigroup cross-section library using zero or one dimensional methods. The transport library is generally between 50 to 200 energy groups but have special treatment to deal with resonance parameters.

The second step is to perform a two-dimensional assembly-level calculation for each assembly type using the transport library. Using the solution of this model, the cross-sections are homogenized in space and used to generate a few-group library, which typically has 2-8 energy groups. Other parameters are also computed to enforce equivalence between the assembly and core level solutions. In many cases where thermal hydraulic feedback is required, the few-group library is generated at different reference conditions (coolant density, fuel temperature, boron concentration, etc.).

In the third and final step, the nodal diffusion code uses the few-group library to solve the full core problem. The nodal diffusion code is normally coupled to one dimensional thermal hydraulic codes to provide the thermal hydraulic feedback in the core system.

Assembly-level (Lattice) Computation

The assembly-level computation relies on a code which is capable of solving the two dimensional transport equation. The single assembly model should accurately account for all of the geometric complexities in the lattice and have a sufficiently fine spatial mesh to accurately resolve the angular flux distribution in the assembly. Several methods have been used to solve the assembly-level problem, some of which are discussed in the Transport Methods section.

Homogenization and Discontinuity Factors

The spatial and energy flux distribution obtained from the assembly-level calculation is used to generate assembly homogenized few group cross-sections. The cross-sections are collapsed to preserve the average reaction rates.

$$\bar{\Sigma}_{x,g} = \frac{\int \sum_{h \in g} \Sigma_{x,h}(\mathbf{x}) \phi_h(\mathbf{x}) dV}{\int \sum_{h \in g} \phi_h(\mathbf{x}) dV} \quad (2.13)$$

where h is the fine group energy and g is the coarse group energy. The methodology to homogenize the transport cross-section is not as clear. Several methods have been proposed to do this, including flux weighting, inverse flux weighting, and current weighting. It has been found that flux weighting the transport cross-section in space, equation (2.14a), and flux weighting the inverse cross-section in energy, equation (2.14b), works best for reactor analysis [25].

$$\Sigma_{tr,h} = \frac{\int \Sigma_{tr,h}(\mathbf{x}) \phi_h(\mathbf{x}) dV}{\int \phi_h(\mathbf{x}) dV} \quad (2.14a)$$

$$\Sigma_{tr,g} = \frac{\sum_{h \in g} \phi_h}{\sum_{h \in g} \frac{\phi_h}{\Sigma_{tr,h}}} \quad (2.14b)$$

Generalized Equivalence Theory [24] provides an extra degree of freedom to match the assembly-level solution. This degree of freedom is captured in discontinuity factors, which account for the loss of spatial resolution at the interface during homogenization. Multiple discontinuity factors can be specified depending on the number of free variables the nodal method can accept. Side discontinuity factors specify the ratio of the surface flux calculated by the assembly-level calculation and the surface flux predicted by the nodal method.

$$SDF_{g,f} = \frac{\phi_{g,f}^{\text{Heterogeneous}}}{\phi_{g,f}^{\text{Homogeneous}}} \quad (2.15)$$

Here SDF is the side discontinuity factor, g is the few energy groups, and f is the surface. Other nodal methods can also utilize corner discontinuity factors; these are the ratio of the point flux calculated by the assembly-level calculation and the point flux predicted by the nodal method.

$$CDF_{g,c} = \frac{\phi_{g,c}^{\text{Heterogeneous}}}{\phi_{g,c}^{\text{Homogeneous}}} \quad (2.16)$$

Here CDF is the corner discontinuity factor and c represents the corner at which the flux is calculated.

The last piece of information extracted from the assembly-level calculation is the group-wise pin power form function (GFF). The GFF allows the pin powers to be

reconstructed in the entire core.

$$P_{i,j} = \sum_{g=1}^G GFF_{g,i,j} \tilde{\phi}_{g,i,j} \quad (2.17)$$

Here $GFF_{g,i,j}$ is the group form function for group g and pin position i, j and $\tilde{\phi}_{g,i,j}$ is the reconstructed scalar flux from the homogeneous diffusion solution of the lattice. The GFF is computed by taking the ratio of the power generated by group g as calculated using the assembly level calculation to the average pin flux as calculated by an equivalent diffusion model.

$$GFF_{g,i,j} = \frac{\kappa \sum_{f,g,i,j} \phi_{g,i,j}^{\text{Heterogeneous}}}{\phi_{g,i,j}^{\text{Homogeneous}}} \quad (2.18)$$

Core-level Computation

Once the lattice physics code generates all the parameters needed, a core wide computation can be performed. The core computation starts with the spatial discretization of the core. In the radial direction the assembly size is typically used. In the axial direction a grid is typically set to $10 - 20cm$. There are two common discretizations of the core wide diffusion problem. The first is to use the diffusion equation and apply a fine mesh finite difference method. This requires a further internal discretization of each assembly, which is typically made on a pin size level. The differential equation is then discretized using the finite difference approximation to solve the full core system.

A second method that is commonly used is a transverse leakage method. These methods convert the three dimensional differential equation into three one dimensional differential equations coupled through transverse leakage terms.

$$-D \frac{d^2}{dx_i^2} \phi(x_i) + \Sigma_t \phi(x_i) = Q(x_i) - L(x_i) \quad (2.19a)$$

$$L(x_i) = l_0 + l_1 P_1(x_i) + l_2 P_2(x_i) \quad (2.19b)$$

Here $L(x_i)$ is the transverse leakage sink and $P_n(x_i)$ is a function which defines the distribution of the leakage inside the node. Typically the transverse leakage is found by interpolating a shape function using the node average leakage of the current node and the neighboring nodes. Once the solution is cast into a one dimensional differential equation, the solution possibilities become much simpler.

Two standard options exist for solving the flux distribution inside a node. The first option is to expand the nodal flux and source using a polynomial basis set and solve for the node balance constraints (continuity of surface flux and current) as well as spatial moments of the differential equation. This method is known as the Nodal Expansion Method (NEM) [26].

The second option is to solve for the analytic solution of the nodal flux (ANM) [27]. With one energy group, this solution is trivial, but for reactor problems a minimum of two groups is needed. For two group problems, methods have been developed that use a spectral decomposition of the coupled differential equations to solve the groups simultaneously. For more energy groups, the spectral decomposition method is not as easy to derive. In this case, the system of equations can be written in such a way that solution becomes a matrix exponential. This can be evaluated using a variety of methods, but it can easily become ill-conditioned, and it can be difficult to implement boundary conditions.

The last option bridges the gap between the NEM and ANM. This method solves the analytic solution to the differential equation in which the source is expanded using a polynomial. This method is known as the Semi-Analytic Nodal Method (SANM) [28]. The group coupling is effectively removed from the analytic solution so groups do not need to be solved simultaneously. Once the analytic form of the flux is found, it is recast into a polynomial to update the source term. This method has advantages over the other two because the solution resembles the analytic result, reduces overshoots and undershoots from a pure polynomial method, and can be expanded to use an arbitrary number of groups. The main downside is the complication of implementation because the projection equations from analytic to polynomial can become quite complex.

All of the methods discussed above can be implemented with surface discontinuity factors. In some cases the corner discontinuity factors will be used in the calculation of the pin powers. The core calculation can produce very accurate results if the cross-sections and discontinuity factors are generated correctly.

2.2.2 Fine Mesh Finite Difference Diffusion

The fine mesh finite difference method is a common computational method that is used for many numerical solutions to partial differential equations. The methodology is well known for classical diffusion equations and is very similar for neutron transport. Like the classical solutions the node average flux is assumed to be the centroid flux and the derivative of the flux needed to determine the neutron current is calculated

using the first two terms of the Taylor expansion. There are two main features of neutron diffusion theory that differ from classical diffusion problems (such as heat conduction). The first is the presence of the collision operator in the neutron diffusion equation. The second difference is the use of discontinuity factors at the assembly interface.

Fine Mesh Finite Difference Formulation

The FMFD method starts by integrating the diffusion equation over a rectangular region. The neutron current at the surface of each face is balanced by the neutron source minus collision losses in each node.

$$\sum_{f=n,e,s,w} (\mathbf{J}_g \cdot \mathbf{A})_f + \Sigma_{t,P,g} \phi_{P,g} V = \sum_{g'=1}^G \Sigma_{s,P,g' \rightarrow g} \phi_{P,g'} V + \frac{\chi_{P,g}}{k} \sum_{g'=1}^G \nu \Sigma_{f,P,g'} \phi_{P,g'} V \quad (2.20)$$

Here n, e, s, w represent the north, east, south, and west faces respectively. The flow of neutrons at the surfaces is written in two different equations describing how neutrons flow from the node average values to the surface, then from the surface to the neighboring node. At the interface the discontinuity factor is applied.

$$J_e = D_P \frac{\phi_P - \phi_{P,e}}{0.5h_P} \quad (2.21a)$$

$$J_e = D_E \frac{\phi_{E,w} - \phi_E}{0.5h_E} \quad (2.21b)$$

$$f_{P,e} \phi_{P,e} = f_{E,w} \phi_{E,w} \quad (2.21c)$$

These three constraints are applied to construct the net current at the interface as a linear combination of the centroid value and the centroid of the neighboring cell.

$$J_e = \frac{2D_P D_E (f_{P,e} \phi_P - f_{E,w} \phi_E)}{D_E f_{P,e} h_P + D_P f_{E,w} h_E} \quad (2.22)$$

For the problems considered in this work the fine mesh is defined using the pin cell geometry, but the side discontinuity factors are only defined on the assembly level. In order to account for the difference in locations where the discontinuity factors are defined, the discontinuity factors are assumed to be unity for interior faces of the

assembly and adopt the assembly surface discontinuity factor for external faces of the assembly. The corner discontinuity factors are not utilized in this method. Lastly, the group form functions, which allow for the pin powers to be reconstructed from the homogenized solution, simply uses the node average flux which has been defined to be the average flux over the pin cell by nature of the FMFD method.

The last issue that must be addressed is the application of the boundary conditions of the global system. Generally, the boundary condition specified is an albedo boundary. For most diffusion codes the albedo is defined slightly different than the methodology described in the previous chapter. Instead, the α albedo is defined as the ratio of the net current and the surface flux for each energy group.

$$\alpha_g = \frac{\mathbf{J}_{g,s} \cdot \mathbf{n}}{\phi_{g,s}} \quad (2.23)$$

The definition of the albedo is substituted into the FMFD definition of the current to obtain a relationship between the boundary current and the node average flux.

$$J_e = D_P \frac{\phi_P - \phi_{P,e}}{0.5h_P} \quad (2.24a)$$

$$J_e = \alpha_e f_{P,e} \phi_{P,e} \quad (2.24b)$$

$$J_e = \frac{2\alpha_e D_P f_{P,e} \phi_P}{2D_p + \alpha_e f_{P,e} h_P} \quad (2.24c)$$

Source Iteration

Now that the diffusion equation is discretized and written in terms of the the average nodal flux and the average flux of the neighboring assemblies, the system of equations can be compiled in matrix form. The matrix is of dimension $N_{\text{node}G} \times N_{\text{node}G}$ and can be written in operator form as follows.

$$\mathbb{D}\phi + \mathbb{T}\phi = \mathbb{S}\phi + \frac{1}{k} \overrightarrow{\chi\nu\Sigma_f} \phi \quad (2.25a)$$

$$\mathbb{M} = \mathbb{D} + \mathbb{T} - \mathbb{S} \quad (2.25b)$$

$$\mathbb{F} = \chi\nu\Sigma_f^T \quad (2.25c)$$

$$\mathbb{M}\phi = \frac{1}{k}\mathbb{F}\phi = \lambda\mathbb{F}\phi \quad (2.25d)$$

In these equations, \mathbb{D} contains a matrix relating all of the streaming terms, \mathbb{T} is a diagonal matrix containing the total cross-section of each node and group, \mathbb{S} is a block diagonal matrix containing the scattering matrix of each node, \mathbb{F} is the fission operator defining the fission source in each node, and λ is the inverse of the multiplication factor.

The final form of the operator notation for the diffusion equation is an eigenvalue problem. Since the fundamental mode (largest multiplication factor) is the desired quantity for steady-state core analysis, the inverse power method is used to calculate the eigenvalue/eigenvector pair.

$$\mathbb{M}\phi^{(k+1)} = \lambda^{(k)}\mathbb{F}\phi^{(k)} \quad (2.26a)$$

$$\lambda^{(k+1)} = \frac{\|\mathbb{F}\phi^{(k)}\|}{\|\mathbb{F}\phi^{(k+1)}\|} \quad (2.26b)$$

Since $\phi^{(k)}$ is known at the beginning of the $k + 1$ iteration, equation (2.26a) is of the following form.

$$\mathbb{A}\mathbf{x} = \mathbf{b} \quad (2.27)$$

This equation can be solved using a direct linear equation solver such as Gaussian elimination, an iterative solver such as Gauss-Siedel or Jacobi methods, or using a Krylov subspace method such as GMRES or BiCGstab. Several solvers were implemented in the code developed and various methods were tested to determine the best results.

Wielandt Shift Acceleration

The source iteration method is slowly converging for cases with dominance ratios (the ratio of the second largest to the largest k) close to 1. One method that can accelerate the convergence of the source iteration is to shift part of the fission source to the left hand side of the equation.

$$(\mathbb{M} - \lambda_{\text{shift}}\mathbb{F})\phi = (\lambda - \lambda_{\text{shift}})\mathbb{F}\phi \quad (2.28)$$

Here λ_{shift} is the amount of the fission source that is moved to the left hand side of the equation and the inverse power method is applied to the shifted system.

Care must be taken when choosing the value of λ_{shift} . Since the inverse power method finds the eigenvalue closest to zero, it is possible to overshift the system and converge to an eigenvalue which does not represent the fundamental mode. One method to specify λ_{shift} is to fix the value to be $\frac{1}{k_{\text{max}}}$ where k_{max} is the maximum multiplication factor that is possible (3 is the default k_{max} used because it represents the average number of neutrons born per fission). Another method to specify λ_{shift} is to allow the user to input a fixed value for the shifted eigenvalue. The last method changes the shifted eigenvalue as the solution iterates to obtain an optimum shift. This is obtained by using the current estimate of the eigenvalue and the change in the eigenvalue between successive iterations.

$$\lambda_{\text{shift}}^{k+1} = \alpha_0 \lambda^k - \alpha_1 |\lambda^k - \lambda^{k-1}| \quad (2.29)$$

Here, α_0 is a constant less than 1 which does not allow the full eigenvalue to be shifted otherwise the matrix would become singular at convergence and α_1 is a constant which scales the error to prevent overshifting during the iteration. The values used in this work are $\alpha_0 = 0.95$ and $\alpha_1 = 5$.

2.3 Transport Methods

Limitations of nodal diffusion methods along with considerable advancements in computing technology are two of the main reasons that transport methods have found their way into reactor design and analysis. There are several classes of methods to solve the transport equation. This discussion will focus on a few of these methods. One of the most popular methods is the discrete ordinates method (S_N) [29], which assumes that the angular flux can be discretized into discrete angles each with a corresponding weight. These angles and weights are defined by a quadrature set. The quadrature sets used for 1-D problems are almost universally the Gauss-Legendre sets [30] but in 3-D problems there are many proposed quadrature sets. One of the most common quadrature sets for 3-D problems is the Level-Symmetric quadrature set [30].

The other common method for solving the full core transport problem is the Method of Characteristics, MOC [31]. In this method characteristic paths of flight are drawn across the domain with a user specified spatial and angular discretization.

The transport equation is then integrated along these characteristic directions. The computational burden for the application of 3-D MOC methods [32] to core problems is generally prohibitive for full core calculations. Approximate “2D-1D” methods have been developed [33] that are based on the assumption that the solution is separable in the radial and axial direction. The MOC equations are solved for each radial slice of the reactor and are coupled by a nodal diffusion solver in the axial direction. Other methods have been developed that model the axial direction using a one dimensional S_N solver [34].

2.3.1 Method of Characteristics

The Method of Characteristics is a solution to the transport equation in which rays are drawn across the global geometry in discrete angles and the transport equation is integrated along those rays.

Governing Equations

The MOC equations begin with the Boltzmann transport equation with isotropic scattering.

$$\begin{aligned} \boldsymbol{\Omega} \cdot \nabla \psi(\mathbf{x}, \boldsymbol{\Omega}, E) + \Sigma_t(\mathbf{x}, E) \psi(\mathbf{x}, \boldsymbol{\Omega}, E) \\ = \frac{\chi(E)}{4\pi k} \int_{4\pi} \int_0^\infty \nu \Sigma_f(\mathbf{x}, E') \psi(\mathbf{x}, \boldsymbol{\Omega}', E') dE' d\Omega' \\ + \frac{1}{4\pi} \int_{4\pi} \int_0^\infty \Sigma_{s_0}(\mathbf{x}, E' \rightarrow E) \psi(\mathbf{x}, \boldsymbol{\Omega}', E') dE' d\Omega' \end{aligned} \quad (2.30)$$

or

$$\boldsymbol{\Omega} \cdot \nabla \psi(\mathbf{x}, \boldsymbol{\Omega}, E) + \Sigma_t(\mathbf{x}, E) \psi(\mathbf{x}, \boldsymbol{\Omega}, E) = \frac{Q(\mathbf{x}, E)}{4\pi} \quad (2.31)$$

where Q is the isotropic fission and scattering source for position \mathbf{x} and energy E .

In order to obtain a solution along the ray, the angular coordinate system is recast in the direction of the ray, as shown in Figure 2.2.

$$\psi(\mathbf{x}, \boldsymbol{\Omega}, E) = \psi(\mathbf{x}_{m,0} + s\boldsymbol{\Omega}_m, E) \quad (2.32a)$$

$$\boldsymbol{\Omega} \cdot \nabla \psi(\mathbf{x}, \boldsymbol{\Omega}, E) = \frac{d}{ds} \psi(\mathbf{x}_{m,0} + s\boldsymbol{\Omega}_m, E) \quad (2.32b)$$

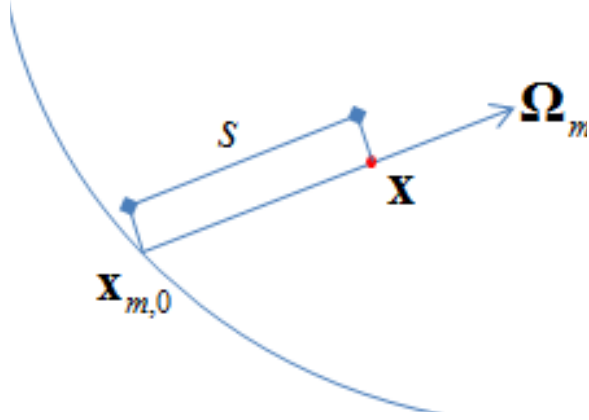


Figure 2.2: Coordinate System for MOC Rays

Using this definition the transport equation can be written in direction Ω_m as follows.

$$\frac{d}{ds}\psi(\mathbf{x}_{m,0} + s\Omega_m, E) + \Sigma_t(\mathbf{x}_{m,0} + s\Omega_m, E)\psi(\mathbf{x}_{m,0} + s\Omega_m, E) = \frac{Q(\mathbf{x}_{m,0} + s\Omega_m, E)}{4\pi} \quad (2.33)$$

The ordinary differential equation (2.33) has a solution which is shown below.

$$\begin{aligned} \psi(\mathbf{x}_{m,0} + s\Omega_m, E) &= \psi(\mathbf{x}_{m,0}, E) \exp\left(-\int_0^s \Sigma_t(\mathbf{x}_{m,0} + s'\Omega_m, E) ds'\right) \\ &+ \frac{1}{4\pi} \int_0^s Q(\mathbf{x}_{m,0} + s'\Omega_m, E) \exp\left(-\int_{s'}^s \Sigma_t(\mathbf{x}_{m,0} + s''\Omega_m, E) ds''\right) ds' \end{aligned} \quad (2.34)$$

Thus far the integral along a single ray with an arbitrary angle has been discussed. In reality, the solution is solved for a discrete number of angles. The angle is discretized using a product quadrature set, meaning that the polar and azimuthal angles are chosen separately and then combined. The azimuthal angles are chosen so that $4M$ angles are represented between 0 and 2π and the polar angles are chosen such that $2L$ angles between -1 and 1 . Weights are assigned to each angle such that the following relationship holds.

$$\int_{4\pi} \psi(\mathbf{x}, \Omega, E) d\Omega \approx \sum_{l=1}^{2L} \omega_l \sum_{m=1}^{4M} \omega_m \psi_{m,l}(\mathbf{x}, E) \quad (2.35)$$

Equation (2.34) is an exact representation of the transport equation along a line in direction $\mathbf{\Omega}_{m,l}$. Two major assumptions will now be applied to this equation in order to obtain the final form. The first assumption is that the domain is two dimensional and infinite in the axial direction. This simplification can allow the rays to be based in a plane with a correction for the azimuthal dependence of the flux.

$$\begin{aligned} \psi(\mathbf{x}_{m,0} + s\mathbf{\Omega}_{m,l}, \varphi_l, E) &= \psi(\mathbf{x}_{m,0}, \varphi_l, E) \exp\left(-\frac{\int_0^s \Sigma_t(\mathbf{x}_{m,0} + s'\mathbf{\Omega}_{m,l}, E) ds'}{\sin \varphi_l}\right) \\ &+ \frac{1}{4\pi} \int_0^s Q(\mathbf{x}_{m,0} + s'\mathbf{\Omega}_{m,l}, E) \exp\left(-\frac{\int_{s'}^s \Sigma_t(\mathbf{x}_{m,0} + s''\mathbf{\Omega}_{m,l}, E) ds''}{\sin \varphi_l}\right) ds' \end{aligned} \quad (2.36)$$

where φ_l is the polar angle.

The second assumption is that the ray is traced across a discrete geometry where inside a computational node, the cross-sections and the neutron source are constant. This assumption allows the integral over the entire ray to be broken up into segments where the outgoing angular flux is an algebraic expression instead of an integral expression.

$$\begin{aligned} \psi(\mathbf{x}_{m,r,0} + s\mathbf{\Omega}_{m,l}, \varphi_l, E) &= \psi(\mathbf{x}_{m,r,0}, \varphi_l, E) \exp\left(-\frac{\Sigma_{t,r}(E) s}{\sin \varphi_l}\right) \\ &+ \frac{Q_R(E)}{4\pi \Sigma_{t,r}(E)} \left(1 - \exp\left(-\frac{\Sigma_{t,r}(E) s}{\sin \varphi_l}\right)\right) \end{aligned} \quad (2.37)$$

Here r denotes a specific ray inside a flat source, flat cross-section node R . The incoming flux is determined by the boundary condition for nodes on the boundary or the outgoing angular flux from the previous region, which is determined by evaluating equation (2.37) at the length of cell r , $s_{m,r}$.

$$\begin{aligned} \psi_{m,l,r}^{\text{out}}(\varphi_l, E) &= \psi(\mathbf{x}_{m,r,0} + s_{m,r}\mathbf{\Omega}_{m,l}, \varphi_l, E) \\ &= \psi_{m,l,r}^{\text{in}}(\varphi_l, E) \exp\left(-\frac{\Sigma_{t,r}(E) s_{m,r}}{\sin \varphi_l}\right) + \frac{Q_R(E)}{4\pi \Sigma_{t,r}(E)} \left(1 - \exp\left(-\frac{\Sigma_{t,r}(E) s_{m,r}}{\sin \varphi_l}\right)\right) \end{aligned} \quad (2.38)$$

The average angular flux along a ray segment can be found by integrating equation (2.37) from 0 to $s_{m,r}$, the length of the cell, and dividing by the length of the cell.

$$\bar{\psi}_{m,l,r}(\varphi_l, E) = \frac{\int_0^{s_{m,r}} \psi(\mathbf{x}_{m,r,0} + s'\mathbf{\Omega}_{m,l}, \varphi_l, E) ds'}{s_{m,r}} \quad (2.39a)$$

$$\bar{\psi}_{m,l,r}(E) = \frac{\psi_{m,l,r}^{\text{in}}(E) - \psi_{m,l,r}^{\text{out}}(E)}{\frac{\Sigma_{t,r}(E) s_{m,r}}{\sin \varphi_l}} + \frac{Q_R(E)}{4\pi \Sigma_{t,r}(E)} \quad (2.39b)$$

So far one a single ray has been considered but in reality, several parallel rays are traced across the domain. The rays are laid out across the domain in each azimuthal direction with spacing Δ_m . In order to obtain the average angular flux in a region R , the average flux of each ray is weighted by the volume that ray occupies.

$$\bar{\psi}_{m,l,R}(E) = \frac{\sum_{r \in R} \bar{\psi}_{m,l,r}(E) \Delta_m s_{m,r}}{\sum_{r \in R} \Delta_m s_{m,r}} \quad (2.40)$$

The node average angular flux is used to calculate the node average scalar flux by using the angular weights described in equation (2.35).

$$\bar{\phi}_R(E) = 2 \sum_{l=1}^L \omega_l \sum_{m=1}^{4M} \omega_m \bar{\psi}_{m,l,R}(E) \quad (2.41)$$

Since the problem is two dimensional, only half of the polar angles need to be simulated and the weight is modified to account for the symmetry. The final step is to apply the multigroup method.

$$\bar{\psi}_{g,m,l,r} = \frac{\psi_{g,m,l,r}^{\text{in}} - \psi_{g,m,l,r}^{\text{out}}}{\frac{\Sigma_{t,g,r} s_{m,r}}{\sin \varphi_l}} + \frac{Q_{g,R}}{4\pi \Sigma_{t,g,r}} \quad (2.42a)$$

$$\bar{\psi}_{g,m,l,R} = \frac{\sum_{r \in R} \bar{\psi}_{g,m,l,r} \Delta_m s_{m,r}}{\sum_{r \in R} \Delta_m s_{m,r}} \quad (2.42b)$$

$$\bar{\phi}_{g,R} = 2 \sum_{l=1}^L \omega_l \sum_{m=1}^{4M} \omega_m \bar{\psi}_{g,m,l,R} \quad (2.42c)$$

The last remaining issue is to use the scalar flux in each group and region to determine the neutron source $Q_{g,R}$.

$$Q_{g,R} = \sum_{g'=1}^G \Sigma_{s_0,R,g' \rightarrow g} \phi_{g',R} + \frac{\chi_{g,R}}{k} \sum_{g'=1}^G \nu \Sigma_{f,g',R} \phi_{g',R} \quad (2.43)$$

Ray Tracing

So far we have assumed that the lengths of the rays, $s_{m,r}$, are known. Generation of all the ray segments for the whole core geometry requires enormous computational memory and programming effort. To avoid this problem, the ray segments are generated only for each cell type, and the rays defined for each cell are linked to the rays of the adjacent cells through path linking. For path linking, each ray must align itself exactly with its reflective counterpart at the cell boundary. To meet this condition, the ray spacing and azimuthal angle are adjusted from the evenly spaced initial angles and uniform ray spacing determined by the input parameters. In order to achieve an integer number of rays for a given angle the ceiling function is used which rounds up to the nearest integer.

$$N_x^m = \text{ceiling} \left(\frac{P}{\Delta_{m_0}} |\sin(\alpha_{m_0})| \right) \quad (2.44a)$$

$$N_y^m = \text{ceiling} \left(\frac{P}{\Delta_{m_0}} |\cos(\alpha_{m_0})| \right) \quad (2.44b)$$

$$\Delta_m = \frac{P}{\sqrt{(N_x^m)^2 + (N_y^m)^2}} \quad (2.44c)$$

$$\tan(\alpha_m) = \frac{N_x^m}{N_y^m} \quad (2.44d)$$

For PWR cores, the pin is normally the smallest repeated structure and is used as the cell. In a BWR, the assembly is the smallest repeated structure and is used as the cell. Since only PWR cores are considered in this work, the pin is always used as the cell. Figure 2.3 shows a typical pin cell with the modular rays.

The choice of modular rays has an impact on the quadrature set that imposed in the azimuthal direction. The weights chosen based on the solid angle represented by the adjusted angles. The polar angles and weights remain unchanged.

The pin cell is broken into 8 azimuthal segments and the user defines an arbitrary number of concentric circles located at the center of the pin cell. Each pin type is traced for each modular ray and direction to obtain the lengths inside the pin. The link between the incoming and outgoing ray is also stored in order to easily construct the path linking between neighboring pins. Once each pin type has been traced, the global rays are constructed using path linking. Instead of storing all of the structure inside a global ray, only the local pin index and the local ray index are stored for each

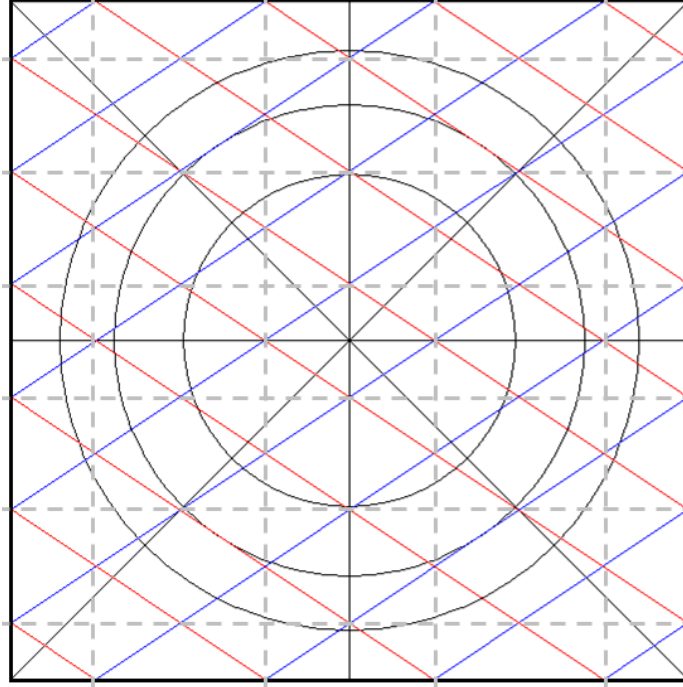


Figure 2.3: Modular Rays

part of the ray, greatly reducing the global storage requirements. As the global rays are traced in the MOC subroutine, the local ray information is recovered.

Another inherent problem with discrete rays is that the volume that the rays represent are not equivalent to the cell volume. Each ray represents a beam of neutrons that is rectangular. In curve-linear geometry, these rectangles do not accurately match the true geometry. Therefore the ray lengths are adjusted to conserve the total volume of each region. This is done by simply adjusting the lengths, $s_{m,r}$ to preserve the total volume in region R .

$$s_{m,r}^{\text{corr}} = \frac{s_{m,r} V_R}{\sum_{r \in R} s_{m,r} \Delta_m} \quad (2.45)$$

The corrected lengths are used for both the MOC ray sweeping routine and the calculation of the region average angular flux.

Source Iteration

The source iteration for the MOC calculation is slightly different than the diffusion equation because the scattering source is dependent on the angular flux from other angles. The number of free variables in MOC makes it difficult to set up into a matrix form. Two iteration loops are used in order to converge the scattering source and

the fission source. The outer most loop is the typical fission source iteration power method described for the FMFD case. Since the equations are not in matrix form, the application of Wielandt shift acceleration is not practical. An inner iteration loop is performed to converge the scattering source with a fixed fission source. It should be noted that the power method requires that the fission source does not change during a power iteration. Inside the inner loop, all rays inside each angle are swept from beginning to end. To minimize memory access, the ray is also swept in the reverse direction in the inner most loop.

2.3.2 Stochastic Methods

The Monte Carlo method is a stochastic method for solving the transport equation by simulating individual neutrons and computing a solution based on statistical averages. The Monte Carlo method is advantageous because there is no discretization error introduced in space, energy, or angle. Therefore the error encountered in the solution is purely statistical. The neutrons are simulated from their birth into the system and pseudo-random numbers are used to sample probability distribution functions to determine if; a reaction occurs, the type of reaction, and the secondary energy and angle of the particle. This process is repeated for millions of neutrons in the system. The statistical error in these calculations follows the Central Limit Theorem if $N \gg 1$.

$$\epsilon \approx \frac{C}{\sqrt{N}} \quad (2.46)$$

Therefore the statistical error decreases in inverse proportion, “inversely proportional”, to the square root of the number of particles simulated.

2.4 Coarse Mesh Finite Difference Acceleration

The Coarse Mesh Finite Difference method [4] is an acceleration technique that can take advantage of efficiency of the power method with Wielandt shift in the diffusion solver. CMFD uses the standard definition of node balance from the FMFD solution but a nonlinear correction factor is added to the current term at each nodes surface to account for the deficiencies of the diffusion method.

$$J_e = \frac{2D_P D_E (f_{P,e} \phi_P - f_{E,w} \phi_E)}{D_E f_{P,e} h_P + D_P f_{E,w} h_E} + \hat{D}_e (\phi_P + \phi_E) \quad (2.47)$$

The nonlinear correction factor \hat{D} is defined using the surface current from the MOC calculation.

$$\hat{D}_e = \frac{J_e^{MOC} - \frac{2D_P D_E (f_{P,e} \phi_P - f_{E,w} \phi_E)}{D_E f_{P,e} h_P + D_P f_{E,w} h_E}}{\phi_P + \phi_E} \quad (2.48)$$

The goal of the CMFD system is to quickly converge the fission source, thus limiting the number of times the MOC sweep algorithm is called. To do this efficiently, several layers of CMFD can be used in series that target different aspects of the global solution [1]. The layers of the iteration scheme are broken down into three main levels: few group CMFD, multigroup CMFD, and MOC sweeping.

2.4.1 Few Group CMFD

The few group CMFD is the lowest level of the acceleration method. The goal of this level is to contain the entire system into one matrix. In this work two group pin wise regions are selected as the computational grid. Two groups are sufficient to accurately couple the thermal and fast energy groups and allow for a quick and efficient solution of the global system.

When various layers are used, it is useful to limit the implementation of the power method to a single level of the method. The power method is implemented to the few group CMFD level because it allows for Wielandt shift to be implemented. The few group CMFD level determines the eigenvalue of the system and the spatial distribution of the fission source. The remaining levels use the fission source defined by the few group CMFD.

2.4.2 Multigroup CMFD

The multigroup CMFD solver uses the same number of energy groups as the MOC solution and pin-wise spatial regions. Because the number of energy groups can be very large, it is not efficient to solve the entire multigroup CMFD system at once with group coupling. Therefore, the multigroup CMFD method is solved group-wise, starting from the highest energy group and sweeping downward, and a second iteration is performed over all groups that have upscattering sources.

2.4.3 CMFD Iteration Scheme

The global CMFD iteration scheme is based on a V-cycle iteration. The few group CMFD first solves for the eigenvalue with cross-sections homogenized based on a uniform global flux and the nonlinear correction factors are assumed to be zero. This gives a very good initial condition for the fission source. Then the multigroup CMFD system is solved to resolve the global spectral effects. This is followed by the first MOC sweep. Once the MOC sweep is complete, the pin average cross-sections, fluxes, and surface currents are determined and nonlinear correction factors are determined for the multigroup CMFD. The multigroup CMFD is solved again and the solution is reduced to the few group CMFD. This method is repeated until the fission source stops changing, the eigenvalue is converged, and the residual in the multigroup residual is less than a given tolerance.

Chapter 3

Multiscale Neutronics Method

3.1 Boundary Response Function

In order to determine how different levels of the multiscale solution interact, the interface between the high order local solver, level l , and the low order global solution, level $l - 1$, must be defined. The interface between level l and level $l - 1$ requires a method to determine the boundary conditions for the local solution. The boundary response function relates the incoming angular flux to the outgoing angular flux. In this analysis the local domain is considered convex, so that neutrons leaving the local system must interact with the surrounding medium to return into the local domain. The assumption of domain convexity is consistent with practical problems that will be solved in this work. The angular flux at boundary of the local domain can be described in equation (3.1).

$$\psi(\mathbf{x}, \boldsymbol{\Omega}, E) = \int_0^\infty \int_{\boldsymbol{\Omega} \cdot \mathbf{n} < 0} \int_{\delta R} A(k_{eff}, \mathbf{x}' \rightarrow \mathbf{x}, \boldsymbol{\Omega}' \rightarrow \boldsymbol{\Omega}, E' \rightarrow E) \psi(\mathbf{x}', \boldsymbol{\Omega}', E') d\mathbf{x}' d\boldsymbol{\Omega}' dE'$$

$$\mathbf{x} \in \delta R, \quad \boldsymbol{\Omega} \cdot \mathbf{n} > 0, \quad 0 < E < \infty \quad (3.1)$$

Here A is the boundary response function, which describes the relationship between the outgoing angular flux and the incoming angular flux at all points on the surface δR , all energies E , and all outgoing angles $\boldsymbol{\Omega}$. If the boundary response function is known, the reduced domain transport problem can be run without approximation. Unfortunately, the computational demand required to calculate the response function is significantly greater than calculating the full domain with the transport solver. Approximate response functions are constructed to preserve the level $l - 1$ solution but also model as much physics as possible. Various levels of approximation are introduced in this work with increasing levels of complexity.

3.1.1 Interface Approximations

The restriction of outgoing for level l at the boundary is can easily be done by calculating the low order moments of the solution. The prolongation from the level $l - 1$ solution to level l requires approximations to be made. The simplest method for approximating the boundary function across multiscale levels is to preserve the level $l - 1$ solution but assume the distribution is flat. In space the response function is simply a delta function on the surface. A neutron leaving the local boundary is assumed to reenter at the identical point in space. In angle the incoming angular flux is assume to be isotropic but the net current across the interface is preserved, which is equivalent to the double P_0 or DP_0 assumption. In energy the multigroup global solution is assumed to be a histogram in energy. Since the multigroup angular flux is an integral parameter in energy, the magnitude of the angular flux must be divided by the width of the multigroup bin. Using these three approximations, the local solution boundary equation can be written as follows.

$$\psi(\mathbf{x}, \boldsymbol{\Omega}, E) \approx \frac{\phi_g(\mathbf{x}) + 2\mathbf{n} \cdot \mathbf{J}_g(\mathbf{x})}{4\pi(E_{g-1} - E_g)} \quad \mathbf{x} \in \delta R, \quad \boldsymbol{\Omega} \cdot \mathbf{n} > 0, \quad E_g < E < E_{g-1} \quad (3.2)$$

If the local solver is also a multigroup method with H energy groups, the response function can be written as follows.

$$\psi_h(\mathbf{x}, \boldsymbol{\Omega}) = \frac{\phi_g(\mathbf{x}) + 2\mathbf{n} \cdot \mathbf{J}_g(\mathbf{x})}{4\pi} \frac{E_{h-1} - E_h}{E_{g-1} - E_g} \quad \mathbf{x} \in \delta R, \quad \boldsymbol{\Omega} \cdot \mathbf{n} > 0, \quad E_h \in E_g \quad (3.3)$$

This equation assumes that the coarse energy group structure is aligned with the fine energy group structure. The remaining approximations discussed here focus on improving the three variables; space, angle, and energy. The approximations in each variable can generally be paired together to generate a response function that has the desired level of detail.

Angle

An improvement to the DP_0 approximation in angle is to use the P_1 approximation, where the angular flux is a linear function of angle. This is the natural form of the diffusion equation which is likely to be the global solver. The form of the response equation is very similar to the DP_0 but is also a function of incoming angle.

$$\psi(\mathbf{x}, \boldsymbol{\Omega}, E) \approx \frac{\phi_g(\mathbf{x}) + 3\boldsymbol{\Omega} \cdot \mathbf{J}_g(\mathbf{x})}{4\pi(E_{g-1} - E_g)} \quad \mathbf{x} \in \delta R, \quad \boldsymbol{\Omega} \cdot \mathbf{n} > 0, \quad E_g < E < E_{g-1} \quad (3.4)$$

Another improvement that can be made is to use the lattice calculation to determine predefined angular shape factors which describe the ratio of the incoming angular flux and the partial incoming current. Although this method gives a more accurate description of the angular flux shape, it also requires a significant amount of data to be saved in the lattice calculation.

$$\psi(\mathbf{x}, \boldsymbol{\Omega}, E) \approx \frac{\phi_g(\mathbf{x}) + 2\mathbf{n} \cdot \mathbf{J}_g(\mathbf{x})}{4\pi(E_{g-1} - E_g)} \frac{f(\boldsymbol{\Omega} \cdot \mathbf{n})}{2} \quad \mathbf{x} \in \delta R, \quad \boldsymbol{\Omega} \cdot \mathbf{n} > 0, \quad E_g < E < E_{g-1} \quad (3.5)$$

So far the response function has not been a function of the outgoing angular flux. In the next method, the shape of the incoming flux is influenced by the outgoing flux. The simplest method is to reflect the outgoing flux back into the domain and scale the magnitude to preserve the partial currents obtained from the global solution, as shown in Figure 3.1.

$$\psi(\mathbf{x}, \boldsymbol{\Omega}, E) = \frac{\phi_g(\mathbf{x}) + 2\mathbf{n} \cdot \mathbf{J}_g(\mathbf{x})}{\phi_g(\mathbf{x}) - 2\mathbf{n} \cdot \mathbf{J}_g(\mathbf{x})} \frac{\psi_g(\mathbf{x}, \boldsymbol{\Omega}')}{E_{g-1} - E_g} \quad \mathbf{x} \in \delta R, \quad \boldsymbol{\Omega} \cdot \mathbf{n} > 0, \quad E_g < E < E_{g-1} \quad (3.6a)$$

$$\boldsymbol{\Omega}' = \boldsymbol{\Omega} - 2\mathbf{n}(\boldsymbol{\Omega} \cdot \mathbf{n}) \quad (3.6b)$$

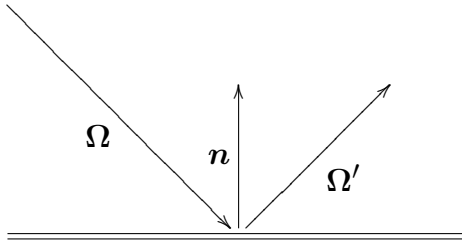


Figure 3.1: Reflective Boundary Condition

Energy

The energy variable is much more difficult to handle for two reasons. The first is because the general multigroup formulation is only a zeroth order method, so no high order moments exist to allow for reconstruction of the energy grid. The second reason

is because of the tight coupling between energy groups. A good boundary response function must be able to account for fast neutrons leaking out of the local domain to return with lower energies as well as thermal neutrons leaving, causing fission, and returning at higher energies. These two methods will be dealt with in separate sections. First, methods to prolongate the energy variable from the few group structure to the fine group structure will be discussed. After a fine group structure is obtained, the methodology is developed to allow for the transfer of neutrons between energy groups when interacting with the local system boundary.

The simplest method for expanding the few group global solution to a fine group local boundary condition is to use a shaping function, $f_g(E)$, to reconstruct the energy variable. This shaping function can be defined using an analytic shape or calculated from the lattice calculation.

$$\psi(\mathbf{x}, \boldsymbol{\Omega}, E) = \frac{\phi_g(\mathbf{x}) + 2\mathbf{n} \cdot \mathbf{J}_g(\mathbf{x})}{4\pi} f_g(E) \quad \mathbf{x} \in \delta R, \quad \boldsymbol{\Omega} \cdot \mathbf{n} > 0, \quad E_g < E < E_{g-1} \quad (3.7)$$

The shape function can be used to describe the original method of assuming neutrons were evenly distributed in energy.

$$f_g(E) = \frac{1}{E_{g-1} - E_g} \quad E_g < E < E_{g-1} \quad (3.8)$$

The form of the multigroup shape function can be written as a discrete function coupling few group energy g to the fine group energy h .

$$\psi_h(\mathbf{x}, \boldsymbol{\Omega}) = \frac{\phi_g(\mathbf{x}) + 2\mathbf{n} \cdot \mathbf{J}_g(\mathbf{x})}{4\pi} f_{g \rightarrow h} \quad \mathbf{x} \in \delta R, \quad \boldsymbol{\Omega} \cdot \mathbf{n} > 0, \quad E_h \in E_g \quad (3.9)$$

Another method for the shape parameter is to use the outgoing angular flux to define the shaping function. There is no physical reason for the outgoing and incoming angular flux to have the same energy shape, but this approximation should provide sufficiently accurate results if the flux is fairly asymptotic.

$$f_g(E) = \frac{\int_{\boldsymbol{\Omega} \cdot \mathbf{n} > 0} (\boldsymbol{\Omega} \cdot \mathbf{n}) \psi(\mathbf{x}, \boldsymbol{\Omega}, E) d\boldsymbol{\Omega}}{\int_{E_g}^{E_{g-1}} \int_{\boldsymbol{\Omega} \cdot \mathbf{n} > 0} (\boldsymbol{\Omega} \cdot \mathbf{n}) \psi(\mathbf{x}, \boldsymbol{\Omega}, E) d\boldsymbol{\Omega} dE} \quad (3.10)$$

The final method considered is to solve an extra set of fixed source equations to calculate flux moments in energy. One method for calculating these moments is the Discrete Generalized Multigroup Method [15, 16, 17]. Forget has proposed a mixed

energy calculation in which energy moments are tracked in a region surrounding the multigroup region. These energy moments allow for the fine energy flux to be reconstructed on the boundary of the fine/coarse energy interface without needing to assume a shape for prolongation. In this case, the approximation is made at the interface where the moments are chosen to be tracked. The region where the moments are tracked provides an identical low level solution, but also provides a buffer region to reconstruct the fine energy group fluxes.

Now that methods have been developed to determine the fine group energy structure at the interface, methods to describe the transfer of neutrons between energy groups at the local interface are discussed. The simplest method is to not assume any transfer between energy groups. Since the currents at the surface have already been determined, this method simply enforces that condition.

Developing a method that allows the outgoing neutrons to change energy when returning to the system is a much more difficult problem. Since the net incoming and outgoing flow of neutrons across the local domain boundary are known, the remaining unknown is a function that relates them. The construction of a G^2 response function from $2G$ inputs, where G is the number of energy groups, requires additional information. The additional information in this case comes from the source term in the neighboring assembly. The source term describes how neutrons appear in the region close to the assembly. Since neutrons do not move very far from the boundary before interacting, the source term of the adjacent assembly is a reasonable approach.

Space

The spatial variable is also difficult to accurately quantify. When neutrons leave the local system, they move through the surrounding medium and can reenter the local system. The distance a neutron travels is directly proportional to the mean free path of a neutron in the system. In the reactor systems considered in this work, the mean free path of a neutron is on the order of $2 - 3$ cm. This suggests that the average neutron will only move a few pins away from the point where the neutron leaves the local system. High energy neutrons do have mean free paths that are significantly longer than the average mean free path but it is difficult to determine where on the surface these neutrons will interact, if they ever do.

The approach taken so far in this chapter is that the spatial response is treated as a delta function. This means that a neutron reenters the local system at the exact point it leaves. Although there are limitations to this assumption, it provides sufficient

accuracy and is the only method used in this work.

A few methods have been considered to treat the spatial coupling and will briefly be discussed here. The first method is to pre-tabulate a spatial response function on a limited domain. Since the neutrons are not expected to travel very far after leaving the limited domain, a response function could be introduced to distribute the neutrons across the pins close to the exiting location. The extent of this local response would be determined by the ability of the surrounding medium to transport a neutron away from the point at which it leaves the local domain. A second method to determine the spatial coupling is to use the global solution to calculate a series of fixed source problems to determine the spatial response function. Since the global solution can be solved efficiently, this method is not expected to greatly increase the computational burden. The last method is to use the global solution but obtain a polynomial expansion at the interface to better resolve high order details [35]. Since fine mesh details are already known in the FMFD global solution, the polynomial expansion is not considered.

3.2 Post-Refinement Multiscale Method

Post-Refinement methods are one-way coupling methods from the nodal diffusion solver back to the higher order transport solver, as shown in Figure 3.2. These methods impose the core level solution by assigning either an albedo type boundary condition or a fixed boundary source problem. These boundary assignments have a fundamentally different solution technique which must be applied. The albedo boundary condition provides the ratio of the incoming angular flux to the outgoing angular flux. With these boundary conditions, the problem becomes an eigenvalue problem and a new eigenvalue is determined which represents the scaling of the fission source for the local domain. The fixed boundary source problem is not an eigenvalue problem. In this method the angular flux at the boundary is specified and the fission source is scaled with the eigenvalue from the global calculation. Both methods have advantages and disadvantages in the solution technique and implementation.

The solution procedure for the post-refinement method begins with a full core nodal diffusion calculation. Once the diffusion calculation has converged to the given tolerance, the surface fluxes and net currents are extracted at the boundary of the multiscale region. In the albedo method, the ratio of the incoming and outgoing partial currents are used for all angles, and are assigned to all fine groups which the coarse group solution represents. For the incoming angular flux, the surface flux and

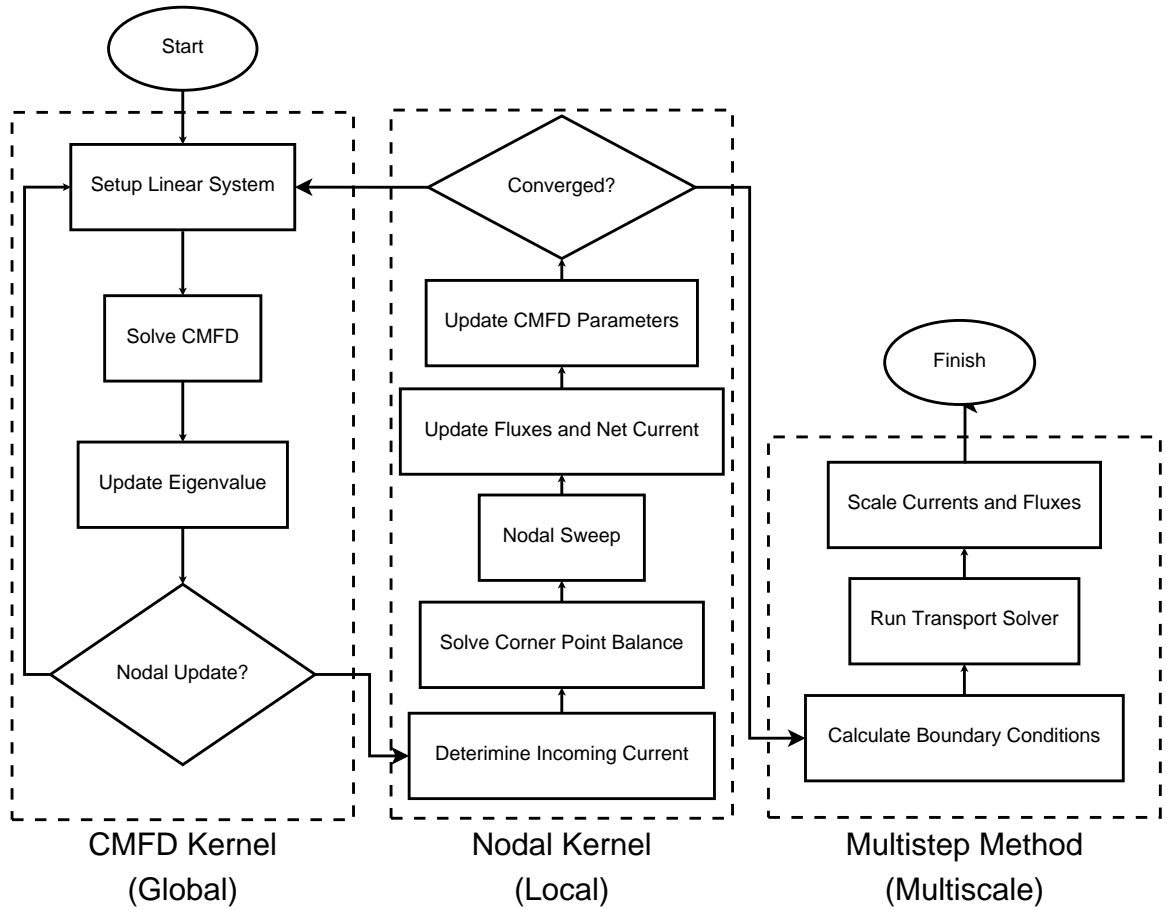


Figure 3.2: Flow Chart of the Post-Refinement Method

net current are used to project angular and energy shapes using one of the expansion methods mentioned above. Finally, the local problem is solved, and the pin power shape is normalized and projected onto the global solution. There are no changes made to the global solution except the shape of the pin power distribution.

The projection of the pin powers onto the global solution is one of the main shortfalls of the post-refinement method because it is completely dependent on the global solution. For example, if the assembly power is off by two percent, then the pin powers in that assembly will also be off by two percent. The post-refinement method does have some benefits as well. First of all, the post-refinement method could be implemented into any code system with only minor modifications. The second is that the post-refinement method can allow the user to specify a buffer region where the local solution may not be accurate. The buffer region only serves to decrease the impact of the boundary condition on the solution. When the pin power projection is determined, only the solution outside the buffer region is used.

3.2.1 Post-Refinement Fixed Source Implementation

The post-refinement methods use the global CMFD solver to fully converge the global FMFD linear system. The net current and surface flux from the global solution are calculated on the boundary of the multiscale region. The incoming angular flux at the boundary of the multiscale region is defined using the P_1 angular distribution. The energy projection is performed using a predefined flux distribution obtained from the energy shape of the surface fluxes of the lattice calculation.

During the fixed boundary source calculation the fission source is scaled by the eigenvalue calculated from the global solution. Since the fixed source problem is not an eigenvalue problem, the acceleration scheme is slightly different. The CMFD solution is rewritten to have boundary sources instead of albedo boundary conditions. Since an eigenvalue iteration does not need to be performed, the fission and scattering sources can be moved to the left hand side of the equation, leaving only the boundary source on the right hand side of the system of equations.

$$(\mathbb{M} - \lambda_{\text{global}}\mathbb{F})\boldsymbol{\phi} = \mathbf{C}_0\mathbf{J}_{in} \quad (3.11)$$

Here λ_{global} is the eigenvalue from the global calculations and must be used to scale the fission source. There are physical cases where the a steady state solution does not exist for the fixed source transport equation. This occurs when the production of neutrons through fission is greater than or equal to the loss of neutrons through absorption and leakage. This occurs when the eigenvalue of the scaled transport equation is greater than or equal to one. Equation (3.12) shows the eigenvalue problem for k . Since only the largest eigenvalue is required, the spectral radius of the matrix is taken to determine k .

$$\left(\mathbb{M} - \frac{1}{k}(\lambda_{\text{global}}\mathbb{F})\right)\boldsymbol{\phi} = 0 \quad (3.12a)$$

$$k = \rho\left(\frac{\mathbb{M}^{-1}\mathbb{F}}{k_{\text{global}}}\right) \quad (3.12b)$$

Since the maximum eigenvalue of $\mathbb{M}^{-1}\mathbb{F}$ is, by definition, the eigenvalue of the subdomain, k can be written as the ratio of the local high order and global low order eigenvalue.

$$k = \frac{k_{\text{subdomain}}}{k_{\text{global}}} \quad (3.13)$$

Although it is possible for this ratio to be greater than one, the leakage from the subdomain for most multiscale cases will make this ratio substantially smaller than 1.

The matrix \mathbb{M} is slightly modified to handle the fact that the boundary currents are on the source side of the equations. The nonlinear correction factors from the CMFD are still added into the migration matrix to preserve the higher order net current.

3.2.2 Post-Refinement Albedo Boundary Implementation

The net current and surface flux from the global FMFD solution are combined to calculate the ratio of the incoming and outgoing partial currents.

$$\beta = \frac{\phi + 2\mathbf{J}^{\text{net}} \cdot \mathbf{n}}{\phi - 2\mathbf{J}^{\text{net}} \cdot \mathbf{n}} \quad (3.14)$$

The albedos are applied to the local boundary and then a local eigenvalue calculation is performed. The local eigenvalue calculation is identical to the global, except the extent of the domain is expanded. The albedo is applied uniformly for all fine energy groups contained in the coarse energy groups.

3.3 Embedded Iteration Method

The embedded iteration method couples all simulation levels together to ensure that the interface between the levels provide a consistent balance of neutrons. The local solvers are directly embedded into the global solution and neutrons are strictly preserved at the interfaces. The iteration strategy for the embedded method is shown in Figure 3.3.

The embedded iteration methodology can also be used to implement a more detailed transport calculation such as 3-D MOC into a global transport solution such as S_N or 2D-1D MOC. The major difference would be preserving the angular flux at the interface.

3.3.1 Embedded Iteration Method Implementation

The embedded iteration method implemented in the research here relies on three major solvers to be interfaced together. The first is assembly-wise diffusion, in which the assembly is collapsed into one homogeneous material with discontinuity factors defined on the surfaces. The second solver is a pin-wise diffusion solver, in which

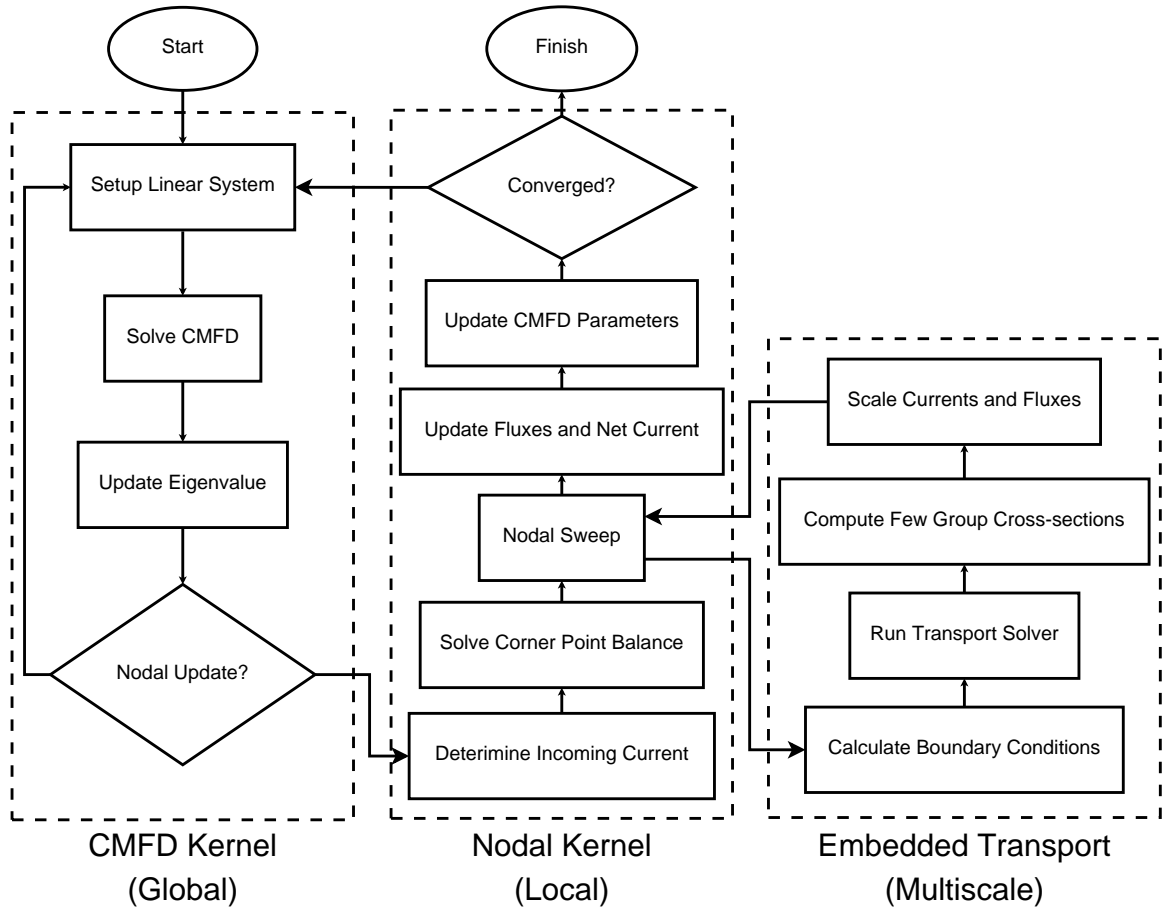


Figure 3.3: Flow Chart of the Embedded Iteration Method

each pin cell is collapsed into a homogeneous material with discontinuity factors defined on the surfaces of each pin cell. The third solver is the MOC, which solves the transport equation with explicit geometry specifications. The diffusion based methods are capable of being solved with any energy group structure during the simulation, and the MOC only uses the finest energy group structure.

The levels are defined so that level 1 always solves 2 group assembly-wise diffusion, which is consistent with the standard nodal methods. Levels 2 and 3 generally involve pin-wise diffusion with more energy groups. The highest level MOC solver is used to obtain the transport solution on a very localized region. Level 1 is the only level that performs the eigenvalue search, because it is the only level that contains the global information. All subsequent levels are solved as a standard fixed source problem with fission sources defined by the level 1 solution.

The levels are coupled together using the CMFD framework. Similar to standard multiscale methods, the higher levels provide information to the lower levels to ensure

consistency between the levels. Standard multiscale methods do this through the use of a source term, but since the original problem is an eigenvalue problem, another method must be chosen. Instead of adding a source term, nonlinear correction factors, \hat{D} , are used here to preserve the neutron balance.

The integration of both the assembly-wise and pin-wise diffusion solvers into the CMFD framework is straightforward. The projection of the partial currents between level l and level $l + 1$ is simply an energy prolongation. For these energy prolongation operators, the outgoing partial current spectrum is used.

The interface between a diffusion solver and the MOC solver is more difficult because the differences between diffusion theory and transport must be defined consistently. In order to do this correctly, a discontinuity factor must be defined on the MOC side of the interface to ensure an accurate partial current is used for the boundary condition of the interface. This discontinuity factor arises because of the differences in the definition of the surface flux between the two different methods. In diffusion theory, the surface flux is directly related to the two partial currents on the interface as shown in equation (3.15), but in transport theory, these two quantities are not algebraically related.

$$\phi_{s,diff} = 2 (J^+ + J^-) \quad (3.15)$$

The difference in the definitions of the surface fluxes must be taken into account to ensure the net current is calculated consistently at the interface.

$$f_{MOC} = \frac{\phi_{s,MOC}}{2 (J_{MOC}^+ + J_{MOC}^-)} \quad (3.16)$$

Since the MOC discontinuity factor is not known before the calculation begins, it is iteratively obtained during the solution.

Then the incoming partial current can be calculated with the MOC discontinuity factor.

$$J_{MOC}^{in} = \frac{\phi_s}{4f_{MOC}} \pm \frac{J^{net}}{2} \quad (3.17)$$

Once the incoming partial current is obtained, it can be projected in energy and angle. The energy projection uses the outgoing partial current spectrum and the angle projection uses a predefined shape from the lattice calculation.

The last step required to complete the embedded iteration is to restrict the solution from level l to level $l - 1$. The cross-sections are collapsed using the standard method depending on the reaction type. Nonlinear correction factors are defined on the surface

of each of each pin to preserve the net current from level l in most cases. However, the interface again needs special treatment to ensure a smoothly converging solution. In order to obtain the net current at the interface, the response of the level $l - 1$ solver to the level l outgoing partial current must be determined. This response is obtained by doing a single node solve. A single node is constructed with two boundary conditions: the incoming partial current on the interface and the average node flux from the previous iteration. The FMFD method provides an algebraic relationship between these two boundary conditions.

$$J_{\text{diff}}^{\text{in}} = \frac{\phi_s}{4f_{\text{dif}}} \pm \frac{J^{\text{net}}}{2} \quad (3.18\text{a})$$

$$J_{\text{diff}}^{\text{out}} = \frac{2D\phi - (4D - h) J_{\text{diff}}^{\text{in}}}{(4D + h)} \quad (3.18\text{b})$$

$$J^{\text{net}} = \pm (J_{\text{diff}}^{\text{in}} - J_{\text{diff}}^{\text{out}}) \quad (3.18\text{c})$$

$$\phi_s = 2 (J_{\text{diff}}^{\text{in}} + J_{\text{diff}}^{\text{out}}) f_{\text{diff}} \quad (3.18\text{d})$$

Once the partial currents are determined, the net current and surface flux can be calculated and the nonlinear correction factors can be determined for the interface.

The iteration strategy used is the standard “V-cycle”. Level 1 is solved first to obtain the global fission source and eigenvalue. The levels are increased step by step until the maximum level is reached. The levels are then decreased back to 1. This process is repeated until the global fission source norm and the eigenvalue both reach their convergence tolerance. More sophisticated iteration strategies could be implemented to minimize the computation in higher levels, such as the “W-cycle”, but have not been considered in this work.

Chapter 4

Assessment of the Post-Refinement Multiscale Method

In order to test the accuracy and speed-up of the post-refinement multiscale method, a series of one dimensional test problems have been developed to determine the performance of these methods in various geometric regions. First, an all (Low Enriched Uranium) LEU core will be analyzed; then two (Mixed Oxide / Low Enriched Uranium) MOX/LEU cores will be examined to see how the method works with a more heterogeneous flux shape.

4.1 Figures of Merit for Analysis

Six figures of merit are chosen to determine the effectiveness of the multiscale method. The first figure of merit is the speedup factor. This is the ratio of the time to perform the full core transport solution divided by the time to run the multiscale solution.

$$\tau = \frac{t^{\text{MOC}}}{t^{\text{MS}}} \quad (4.1)$$

The next figure of merit compares the eigenvalue calculated in the solution. For the fixed boundary source method, the eigenvalue is identical to the global diffusion eigenvalue but when the albedo boundary conditions are specified, a new eigenvalue is calculated for the local region. When albedo boundary conditions are used, the local eigenvalue will be compared but in all other cases, the global eigenvalue is compared. The traditional way to display eigenvalue differences for nuclear reactor problems is to show the difference in percent milli-k (pcm).

$$\Delta k = (k^{\text{MOC}} - k^{\text{MS}}) \times 10^5 \quad (4.2)$$

The next four figures of merit deal with the accuracy of the local and global

solution by looking at the pin powers. The first FOM is the error in the peak pin power. This is defined as the absolute difference between the maximum pin power from the MOC solution and the multiscale solution.

$$E^{\text{peak}} = |\max(P^{\text{MOC}}) - \max(P^{\text{MS}})| \quad (4.3)$$

The second FOM is the maximum error in the pin powers. This is the maximum absolute difference in any pin in the core between the MOC solution and the multiscale solution.

$$E^{\text{max}} = \max(|P^{\text{MOC}} - P^{\text{MS}}|) \quad (4.4)$$

The third FOM is the root mean square of the pin power error in the whole core.

$$E^{\text{RMS}} = \sqrt{\frac{\sum_{i=1}^{N_{\text{global}}} |P_i^{\text{MOC}} - P_i^{\text{MS}}|^2}{N_{\text{global}}}} \quad (4.5)$$

The last FOM is the root mean square of the pin power shape in the peak assembly. This figure of merit was developed to ensure that multiscale method improves the shape, and the results are not due to cancellation of projection errors.

$$E^{\text{RMS shape}} = \sqrt{\frac{\sum_{i=1}^{N_{\text{local}}} \left| \frac{P_i^{\text{MOC}}}{\bar{P}^{\text{MOC}}} - \frac{P_i^{\text{MS}}}{\bar{P}^{\text{MS}}} \right|^2}{N_{\text{local}}}} \quad (4.6)$$

4.2 One Dimensional Analysis

Three different reactor core models are developed for the purpose of testing the various methods. The assembly designs are based on the well established C5G7 benchmark [36]. The assemblies are approximated into one dimensional assemblies by preserving the pin pitch and the fuel to moderator ratio. Cross-sections provided for each material from the C5G7 benchmark are used for 7 group calculations. Another set of 33 group cross-sections for the C5G7 benchmark were provided by Forget [37]. The 33 group cross-sections provide a more realistic representation of the group structure traditionally used for transport calculations.

Table 4.1: One Dimensional Assembly Geometry

Assembly Pitch	21.42 cm
Pin Pitch	1.26 cm
Fuel Radius	0.36 cm

4.2.1 Assembly Layouts

The assemblies shown in this work are based on 17x17 PWR fuel assemblies defined in the C5G7 benchmark. The one dimensional assembly is comprised of 16 fuel pins and a water hole which approximately preserves the ratio of water holes to fuel pins in the actual assembly. In the case where a control rod is inserted into the assembly, the water hole is filled with a control slab the same dimension as the fuel surrounded by water. Table 4.1 describes the dimensions of the pins and assembly.

Two different assemblies are defined. The first is a LEU assembly. All of the pins are uniformly enriched to 3.7%. The geometry can be seen in Figure 4.1. The second



Figure 4.1: LEU Assembly

assembly is a MOX assembly, three different pin enrichments are used to flatten the power profile of the assembly and is shown in Figure 4.2. Lastly, a reflector assembly

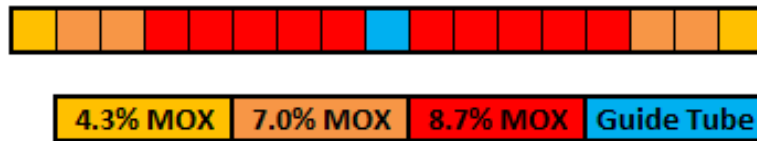


Figure 4.2: MOX Assembly

is defined as an assembly pitch in width filled with the moderator material.

4.2.2 LEU Core

The first core design is comprised of seven LEU assemblies with a reflector assembly on the right side. A reflective boundary condition is imposed on the left boundary and a vacuum boundary condition on the right. Figure 4.3 shows the assembly layout.



Figure 4.3: LEU Core Layout

Multiscale Regions

Three multiscale regions are run for the post-refinement cases. Figure 4.4 shows the region of interest and buffer regions.

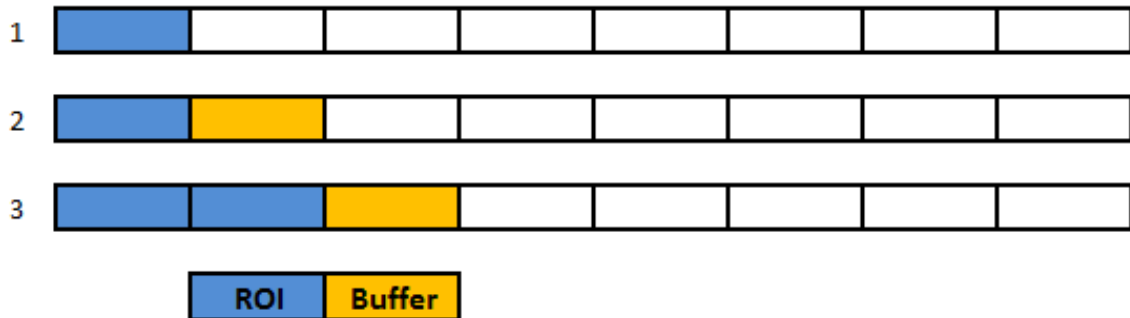


Figure 4.4: Multiscale Regions for 1-D LEU and MOX 1 Cores

The first multiscale region is a single assembly and does not have a buffer region. The second multiscale region is two assemblies, one of which is a buffer. The last multiscale region is three assemblies, one of which is a buffer. The inclusion of two assemblies into the region of interest will help minimize the impact of assembly errors by making the region larger.

Results for LEU Core

The one dimensional LEU core is the simplest case because of the fairly homogeneous fuel loading. For this case, the current pin power reconstruction (PPR) methodology

produces good pin powers in throughout reactor. The error in the diffusion solution with pin power reconstruction is shown in Figure 4.5.

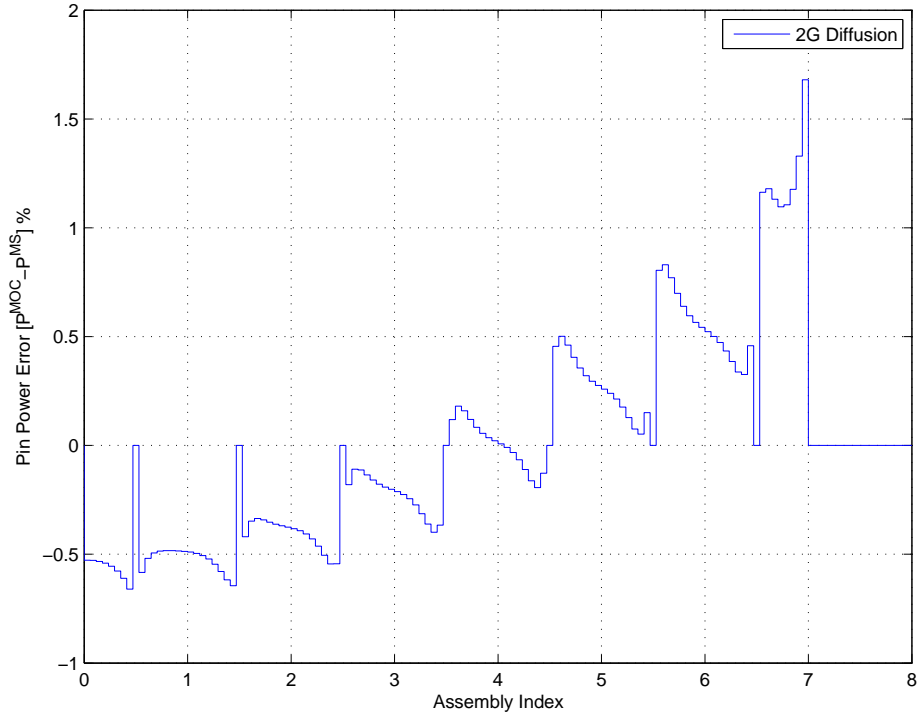


Figure 4.5: Pin Power Error in PPR for Mixed Energy LEU Core

The largest error in the LEU core occurs at the core-reflector interface. Generally, errors at this interface are acceptable because the peak power does not occur near the reflector. Since the diffusion solution has very little error, the multiscale method does not provide much advantage as seen in Table 4.2. The same energy multiscale cases all slightly increase the accuracy of the LEU core, but with the mixed energy cases it is possible to make the solution worse. Even though the solutions can get worse, it is informative to examine the performance of all multiscale methods for cases where the standard methodology is not sufficient.

4.2.3 MOX1 Core

Two MOX cores are designed to test different behaviors. The first is designed to test the heterogeneity caused by the addition of MOX into the reactor. Four LEU and three MOX assemblies are laid out in the core and a single reflector assembly is located on the right side. Figure 4.6 shows the layout of the assemblies.

Table 4.2: FOM for Mixed Energy LEU Core

	τ	E^{peak}	E^{max}	E^{RMS}	$E^{\text{RMS shape}}$
Diffusion	262.2	-1.00%	5.13%	0.79%	0.03%
Fixed Source - without Buffer	2.7	-0.40%	5.13%	0.84%	0.57%
Fixed Source - with Buffer	1.3	-0.94%	5.13%	0.79%	0.00%
Albedo - without Buffer	7.7	-1.03%	5.13%	0.79%	0.10%
Albedo - with Buffer	3.9	-0.94%	5.13%	0.79%	0.01%



Figure 4.6: MOX 1 Core Layout

The multiscale regions used for the MOX1 core are identical to the LEU core, Figure 4.4, because the assembly with the peak power is also at the center of the core.

Results for MOX 1 Core

The addition of MOX assemblies into the core adds heterogeneity that is difficult to model with the current methodology. The assumption that the few group cross-sections and form functions can be generated from an infinite assembly creates issues at the LEU MOX interface because the assemblies are very different. Figure 4.7 shows the pin errors in the diffusion solution for the same energy case.

Unlike the LEU core, the average pin power errors are much larger and spikes in the pin error can be seen at all of the interfaces of LEU and MOX assemblies.

Same Energy Results for MOX1 Core

When the multiscale method is applied to the center assembly of the MOX 1 core, all methods reduce the pin power errors. The same energy multiscale cases does not use a buffer region because energy projection is not required. Table 4.2.3 shows the figures of merit for the two multiscale methods.

The fixed source boundary method gives the best improvement on local quantities such as the peak pin error and the local pin power shape RMS. It also runs the fastest of the two methods. Figure 4.8 shows the spatial pin errors for diffusion, the fixed

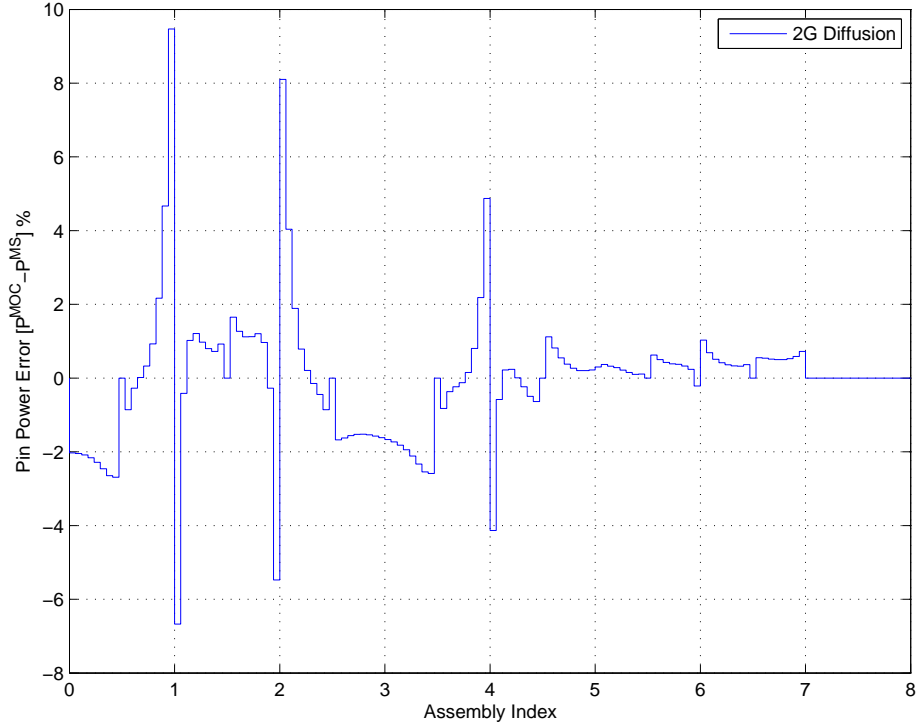


Figure 4.7: Pin Power Error in PPR for Same Energy MOX 1 Core

Table 4.3: Figure of Merits for Same Energy MOX 1 Core

	τ	Δk^1	E^{peak}	E^{max}	E^{RMS}	$E^{\text{RMS shape}}$
2G Diffusion	29.3	59.8	2.69%	9.47%	2.01%	1.50%
2G Fixed Source	9.8	59.8	0.54%	8.10%	1.63%	0.33%
2G Albedo	6.0	-114.4	1.09%	8.10%	1.75%	0.86%

boundary source, and the albedo method.

Both multiscale methods perform well for cases in which the global and local solvers are both solved with the same energy group structure. The next step is to move toward a more realistic case in which the local solver uses more energy groups than the global solution.

Mixed Energy Results for MOX1 Core

The mixed energy results without a buffer region are quite different from the results with the same energy structure. Table 4.2.3 shows the error in the PPR solution for the mixed energy multiscale methods without a buffer region.

¹For albedo method, local eigenvalue is compared.

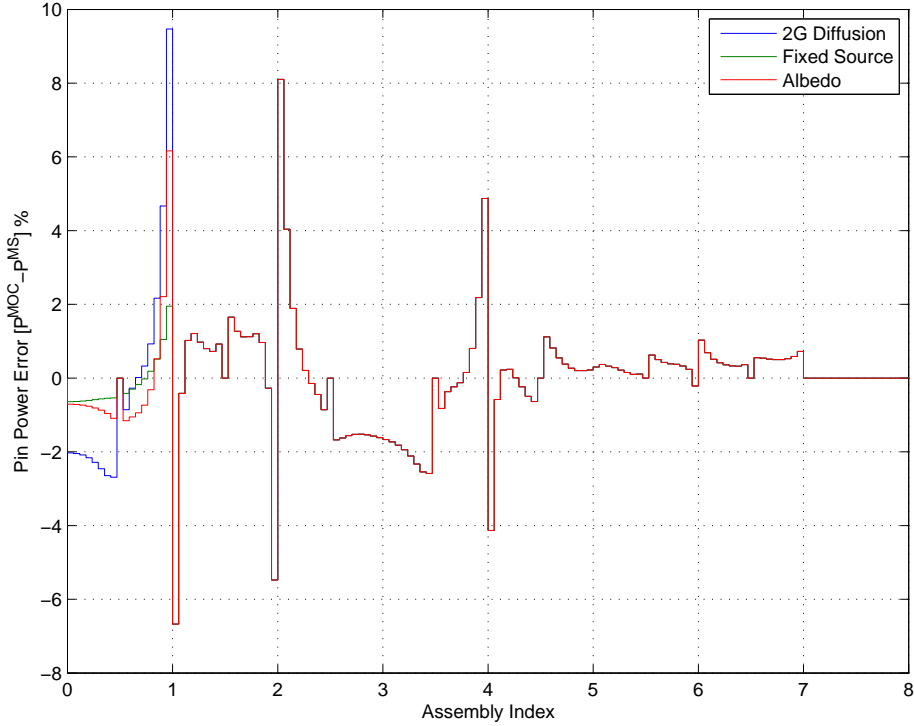


Figure 4.8: Pin Power Error in Multiscale for Same Energy MOX 1 Core

Table 4.4: FOM for Mixed Energy MOX 1 Core without Buffer Region

	τ	E^{peak}	E^{max}	E^{RMS}	$E^{\text{RMS shape}}$
Diffusion	256.6	-1.07%	15.03%	2.66%	1.47%
Fixed Source	10.9	-6.24%	40.96%	4.88%	5.84%
Albedo	7.6	-1.40%	15.03%	2.48%	0.48%

The results with mixed energy groups are in considerable contrast to the results with the same energy groups. The fixed boundary source method is worse than PPR in most of the figures of merit. The albedo method maintains a better solution than diffusion. In order to understand why the fixed boundary source method is worse, Figure 4.9 shows the spatial distribution of the pin power error for PPR, the fixed boundary source method, and the albedo method. From this figure, the main source of error can be seen to occur at the interface. For the fixed source boundary condition, the source of the error is the assumption that the precalculated energy shape is sufficient to project the flux. As indicated, this assumption results in large errors in the pin powers near the boundary.

Another interesting observation of the fixed boundary source solution is that the pin power error is large at the interface, but a few pins away from the interface the

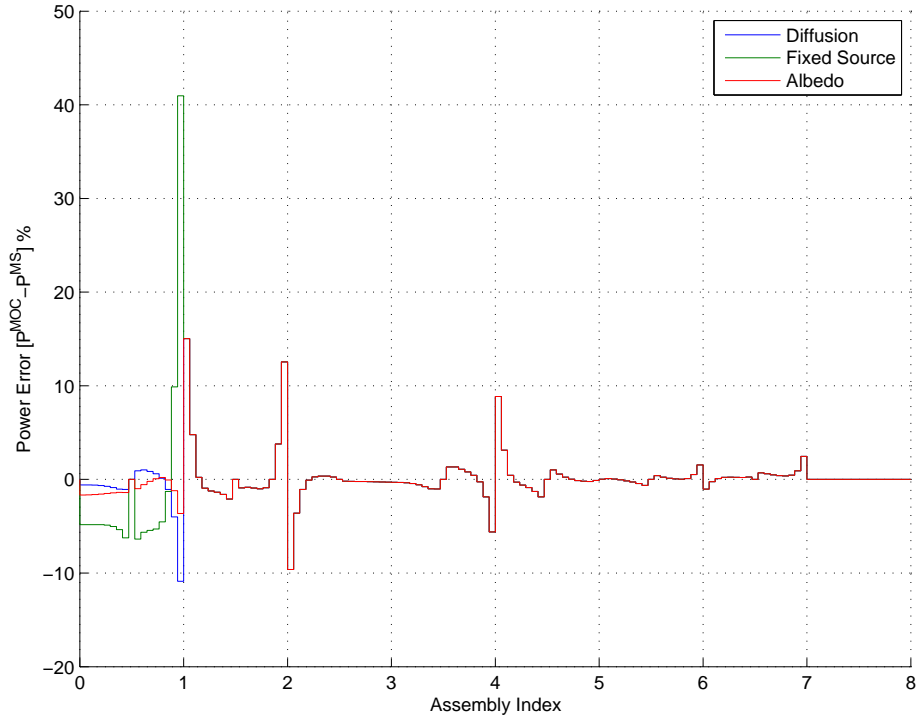


Figure 4.9: Pin Power Error in Multiscale for Mixed Energy MOX 1 Core without Buffer

errors are comparable to the diffusion solution. This seems to suggest that a region in which the solution is allowed to develop but is not applied to the final solution would considerably increase the accuracy of these methods. In this work, this region is called the buffer region. The next set of results show a buffer region applied to both the albedo and fixed boundary source regions to provide a better angular and energy distribution of the flux.

The inclusion of a buffer region in the post-refinement methods increases the computational burden but provides a region where the boundary errors can adjust to the local region geometry and energy group structure without negatively impacting the solution. The method that seems to gain the most from the buffer region is the post-refinement fixed boundary source problem. It was shown that the boundary condition causes significant errors in the pins closest to the boundary. The buffer region suppresses these errors by ignoring the solution in that region. Figure 4.10 shows the error when a buffer region is included in the local computation. In all cases shown here, the buffer region is the size of a single assembly.

For both post-refinement methods the buffer region increases the accuracy of the multiscale calculation. Even though the albedo solution was much better without the

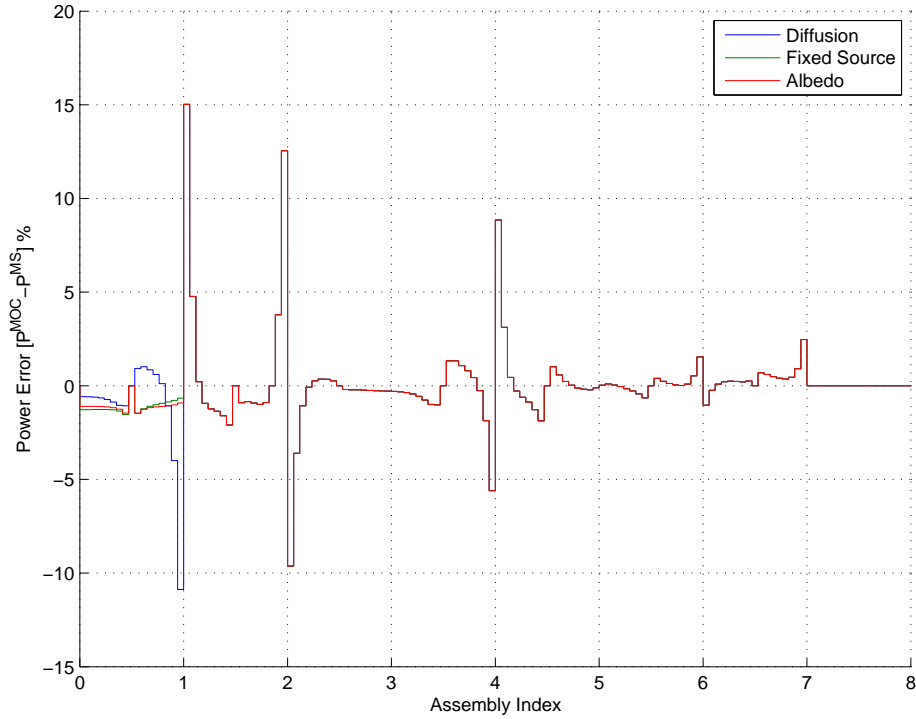


Figure 4.10: FOM for Mixed Energy MOX 1 Core with Buffer Region

buffer region, the two methods produce an almost identical result when the buffer region is added.

The next extension is to increase the region of interest to two assemblies. This will eliminate the dependency of the assembly error. Instead, the power generated in the entire region of interest is used to determine the local pin powers. In general the error associated with a larger region is less than the error of a smaller region. This is because the power is normalized so as the region grows larger, the average error approaches zero. There are cases in which the local diffusion error of a single assembly is small but the surrounding assemblies have larger errors. In this case, making the region of interest larger can increase the region average error and negatively impact the pin power errors. This effect is not seen in either of the MOX cores but was observed in the LEU core. Figure 4.11 shows the error in both methods over diffusion when another assembly is added to the region of interest. In both cases, the error is greatly reduced by expanding the region of interest.

A natural question is whether the buffer region is needed for the albedo method. For the single assembly without a buffer region, the albedo method results show a good improvement in the solution. It is advantageous if a buffer region is not needed because the computational requirements are reduced. The post-refinement methods for

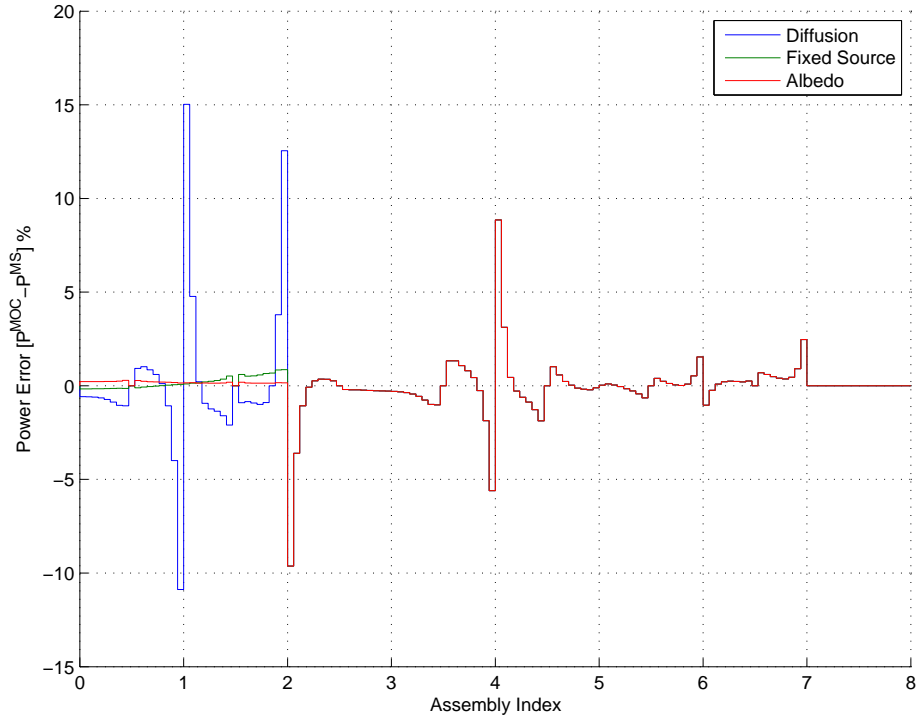


Figure 4.11: FOM for Mixed Energy MOX 1 Core with Increased Region of Interest and Buffer Region

the albedo case are repeated only if the buffer region is added to the region of interest. The two assembly region of interest problem can be performed with computational requirements similar to the single assembly problem with a buffer region, and the three assembly region of interest problem can be performed with computational requirements similar to the two assembly problem with a buffer region. The results of these cases are shown in Figure 4.12.

It can be quickly seen that the boundary condition for the two-assembly region of interest causes slightly larger pin power errors than the diffusion solution at the boundary. These errors are considerably less than pin errors introduced by the fixed source problem. The remainder of the solution shows considerable improvement over the single assembly. The three assembly region of interest has a less accurate solution than the equivalent computational demand case with a two assembly region of interest and a buffer region. This is caused by a cancellation of assembly power errors in the first two assemblies. The addition of a third assembly increases the region of interest average power error and makes the powers worse. It should also be noted that the error in the pin power shape of both cases are identical for the assembly containing the peak pin, so increasing the region of interest is only an effort to try to reduce the

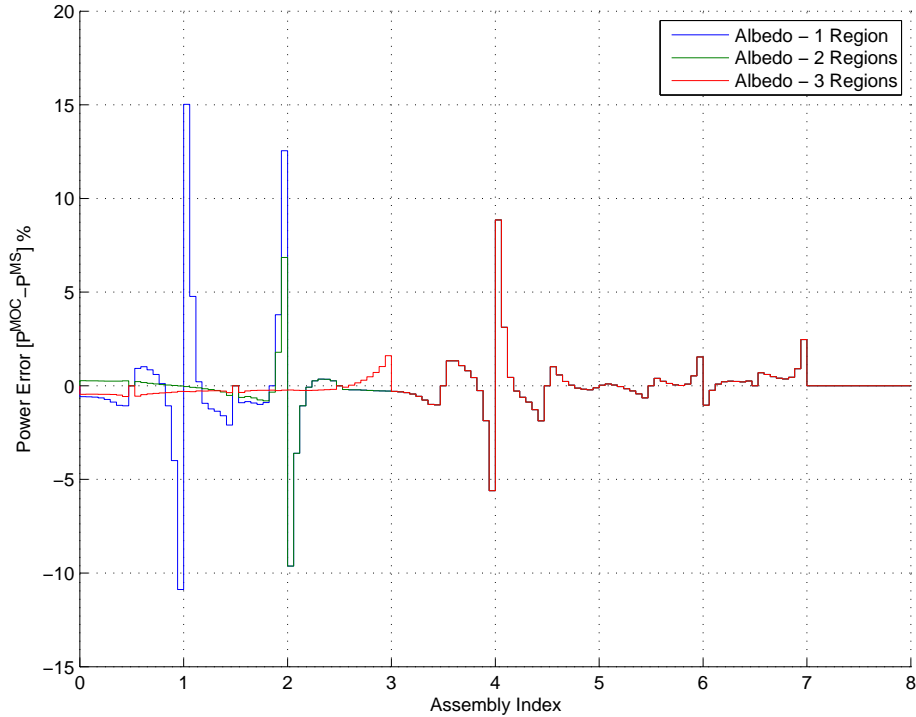


Figure 4.12: Pin Power Error in Multiscale Mixed Energy MOX 1 Core with No Buffer Region

effect of individual assembly errors and does not improve the shape. Ultimately, it seems to be better to include a buffer region instead of increasing the region of interest to eliminate the potential impact of the boundary condition onto the global pin power solution.

The method is also analyzed with the 33 group cross-section library as shown in Table 4.5. The size of this library is more consistent with the size of standard cross-section libraries used for transport calculations. It is important to determine if the post-refinement method can handle projections from 2 to 33 energy groups. Cases are run with and without a buffer region using both the fixed boundary source and albedo methods. In both cases, the buffer region is necessary to accurately capture the difference in the spectral effects. In fact, the fixed source method did not converge without a buffer region.

4.2.4 MOX2 Core

The second MOX core is designed to test the effect of the multiscale methods for the case in which the peak assembly is not on the left boundary. This requires a two sided

Table 4.5: FOM for Mixed Energy MOX 1 Core with 33 Groups

	τ	E^{peak}	E^{max}	E^{RMS}	$E^{\text{RMS shape}}$
Diffusion	1220.6	-1.16%	18.55%	3.23%	1.70%
Fixed Source - with Buffer	4.5	-2.25%	18.55%	3.00%	0.10%
Albedo - without Buffer	6.4	-2.20%	18.55%	3.03%	0.65%
Albedo - with Buffer	2.5	-2.59%	18.55%	3.01%	0.17%

multiscale interface around the assembly with the peak power instead of a single sided interface. Again, four LEU and three MOX assemblies are laid out in the core with a single reflector assembly is located on the right side. Figure 4.13 shows the layout of the assemblies.



Figure 4.13: MOX 2 Core Layout

Multiscale Regions

The MOX 2 core has a slightly different layout for the multiscale regions because the peak power is not located near the boundary. Figure 4.14 shows the region of interest and buffer regions that the post-refinement cases will use.



Figure 4.14: Multiscale Regions for 1-D MOX 2 Core

The first multiscale region is a region of interest in the assembly with the peak pin power. The second multiscale region adds a buffer region on both sides of the peak

Table 4.6: Figures of Merit for MOX 2 Core

	τ	E^{peak}	E^{max}	E^{RMS}	$E^{\text{RMS shape}}$
Diffusion	256.6	-1.07%	15.03%	2.66%	1.47%
Fixed Source - MS 1	10.9	-6.24%	40.96%	4.88%	5.84%
Fixed Source - MS 2	2.8	-1.54%	15.03%	2.46%	0.04%
Fixed Source - MS 3	0.8	-0.14%	9.63%	1.49%	0.04%
Albedo - MS 1	7.6	-1.40%	15.03%	2.48%	0.48%
Albedo - MS 2	3.1	-1.46%	15.03%	2.46%	0.04%
Albedo - MS 3	2.6	0.28%	9.63%	1.49%	0.00%

assembly. The last multiscale region spans five assemblies with a buffer region in the outer assemblies.

Results for MOX2 Core

The second MOX core is introduced to ensure that the multiscale methods work if the region of interest does not coincide with a boundary. In this case, the boundary condition must be estimated for both the left and right face of the local domain. When a buffer region is added, it is added to both sides, and when the region of interest is expanded, it is expanded in both directions. The MOX 2 core has a similar behavior as the MOX 1 core. For the same energy cases, all methods show improvement over the diffusion solution. In the more practical mixed energy case, the fixed boundary source method without a buffer region does not perform well. The albedo method performs well for all cases. The fixed boundary source method with a buffer region also performs well. Since two boundary conditions must be approximated instead of one, it makes sense that the improvements are less than the MOX 1 core. The figures of merit are summarized in Table 4.6.

Overall, the one dimensional results provide several interesting insights about the behavior of the multiscale methods. Using these insights, the number of two dimensional tests is reduced to only consider the post-refinement albedo method with mixed energy.

4.3 Two Dimensional Analysis

The two reactors analyzed here are both based on a 156 assembly core modeled with quarter core symmetry. The first core uses a uniformly enriched LEU assembly surrounded by a water reflector. The second core contains both LEU and MOX assemblies loaded in an arrangement to flatten the power shape and push the peak pin power away from the center of the core. There are 64 MOX assemblies and 92 LEU assemblies loaded into the reactor.

4.3.1 Assembly Layouts

The layout of the two dimensional reactors is based on the assembly design from the C5G7 benchmark. The assembly is designed with an array of 17x17 pins; 264 are fuel pins, 24 are guide tubes for control rods, and the center pin contains a fission chamber. The geometry is specified by the benchmark, but key dimensions are repeated in Table 4.7.

Table 4.7: Two Dimensional Assembly Geometry

Assembly Pitch	21.42 cm
Pin Pitch	1.26 cm
Fuel Radius	0.54 cm

The LEU assembly is a uniform arrangement of fuel pins with the same enrichment. The assembly layout is shown in Figure 4.15. The MOX assembly has three enrichment zones and the layout is shown in Figure 4.16. Lastly, a reflector assembly is defined to have an assembly pitch and filled with the moderator material. In the case where control rods are inserted into the assembly, the guide tube is replaced by the control rod material with the same radius as the fuel pin.

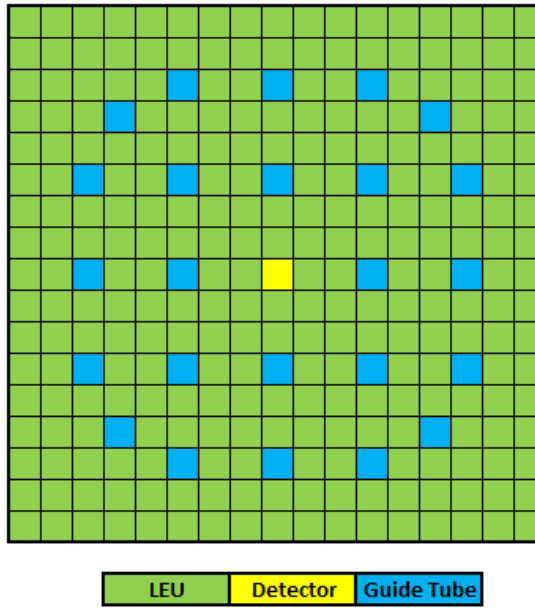


Figure 4.15: 2-D LEU Assembly

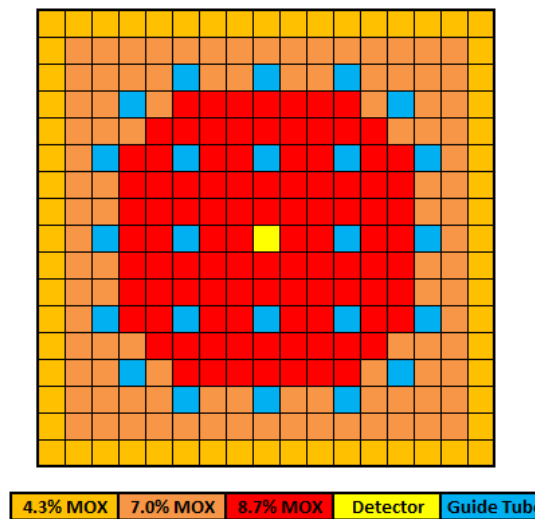


Figure 4.16: 2-D MOX Assembly

4.3.2 LEU Core

The LEU core is loaded completely with the same fuel type in all locations. The computational model only considers one quarter symmetry which places reflective boundary conditions on the left and bottom boundary of the computational domain. The right and top boundaries have a zero incoming current boundary condition. The LEU core is shown in Figure 4.17.

Refl	Refl	Refl	Refl	Refl	Refl	Refl	Refl
LEU	LEU	LEU	Refl	Refl	Refl	Refl	Refl
LEU	LEU	LEU	LEU	Refl	Refl	Refl	Refl
LEU	LEU	LEU	LEU	LEU	Refl	Refl	Refl
LEU	LEU	LEU	LEU	LEU	LEU	Refl	Refl
LEU	LEU	LEU	LEU	LEU	LEU	LEU	Refl
LEU	LEU	LEU	LEU	LEU	LEU	LEU	Refl
LEU	LEU	LEU	LEU	LEU	LEU	LEU	Refl

Figure 4.17: 2-D LEU Core Layout

Multiscale Regions

Three multiscale regions are defined for each core. Since the peak power is in the center assembly for the LEU core, the multiscale regions are based around the symmetry boundary. Figure 4.18 shows the three trust regions.

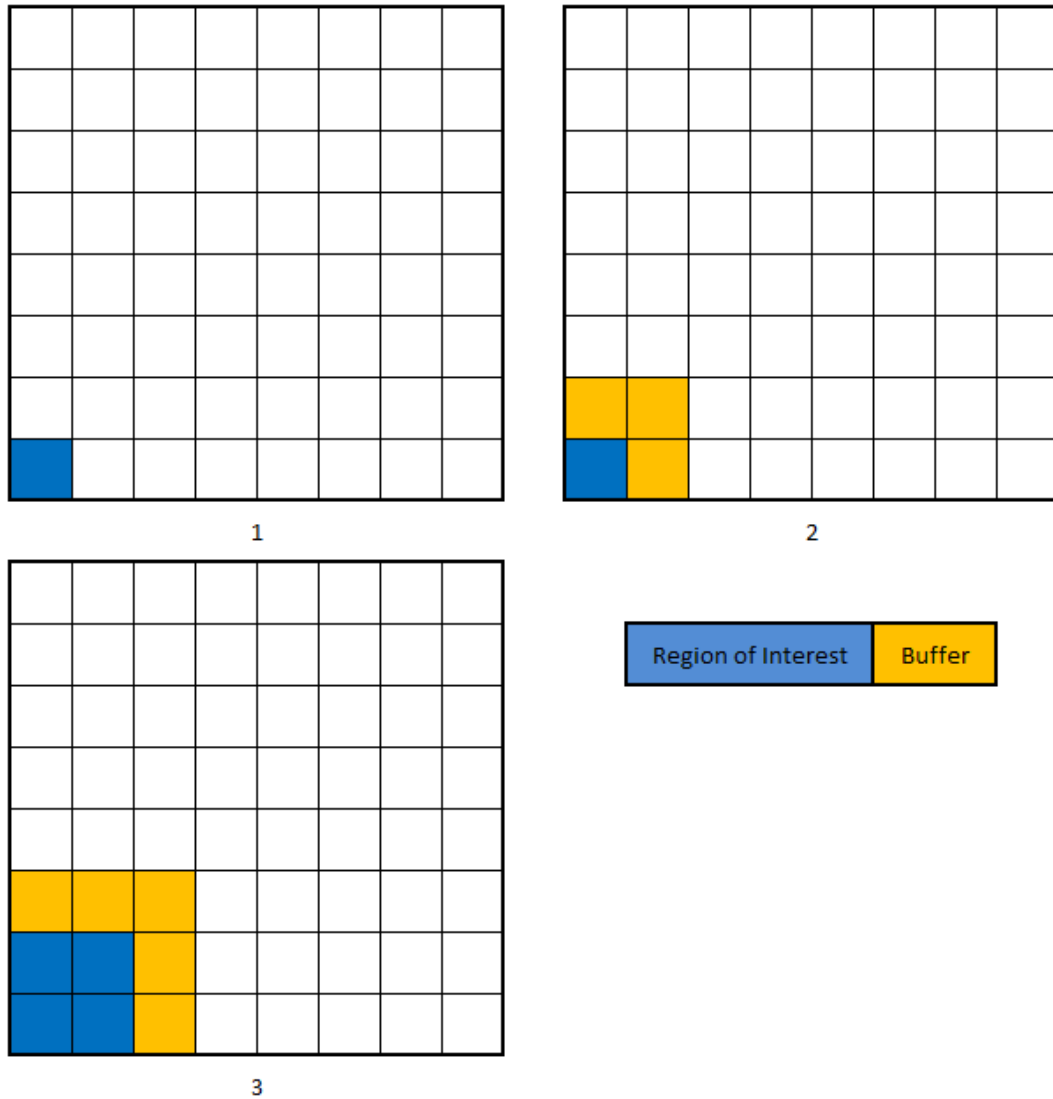


Figure 4.18: 2-D LEU Core Multiscale Regions

The first multiscale region is a single assembly with no buffer region surrounding it. The second multiscale region is a single region of interest with buffer region surrounding it. The last is a two by two assembly region of interest with a buffer region surrounding it.

Results for LEU Core

The two dimensional LEU core is a designed to test the initial performance of the post-refinement albedo method in two dimensions. As with the pure LEU case in one dimension, the diffusion solution with PPR already produces very good results. The major source of error occurs at the core reflector interface, where pin errors of approximately 10 percent are found. Figure 4.19 shows the spatial distribution of pin power error in the diffusion solution.

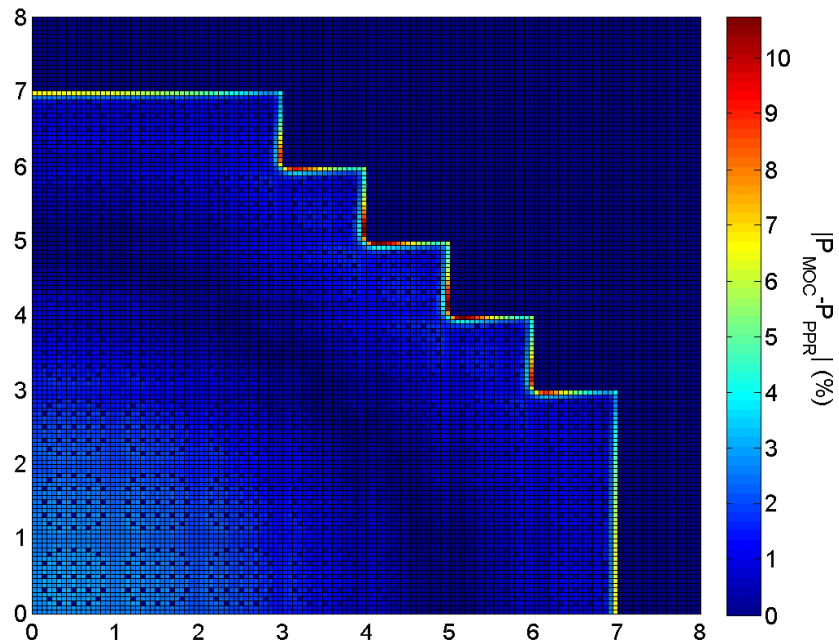


Figure 4.19: Pin Power Error in PPR for 2D LEU Core

The post-refinement albedo method shows marginal improvements in the solution for all of the trust regions, as shown in Table 4.8. However, the error in the pin power shape increases slightly over the diffusion solution. This means that the error in the peak pin power is completely driven by the error in the assembly powers which the post-refinement methods cannot change. The error in the assembly powers are shown in Figure 4.20. The region of interest would have to be expanded several assemblies in order for the region average error to become small.

Table 4.8: FOM for 2D LEU Core

	τ	E^{peak}	E^{max}	E^{RMS}	$E^{\text{RMS shape}}$
2G Diffusion	200.1	3.06%	10.72%	1.62%	0.03%
MS - 1	52.1	3.08%	10.72%	1.62%	0.01%
MS - 2	15.8	3.06%	10.72%	1.62%	0.01%
MS - 3	8.9	2.97%	10.72%	1.62%	0.01%

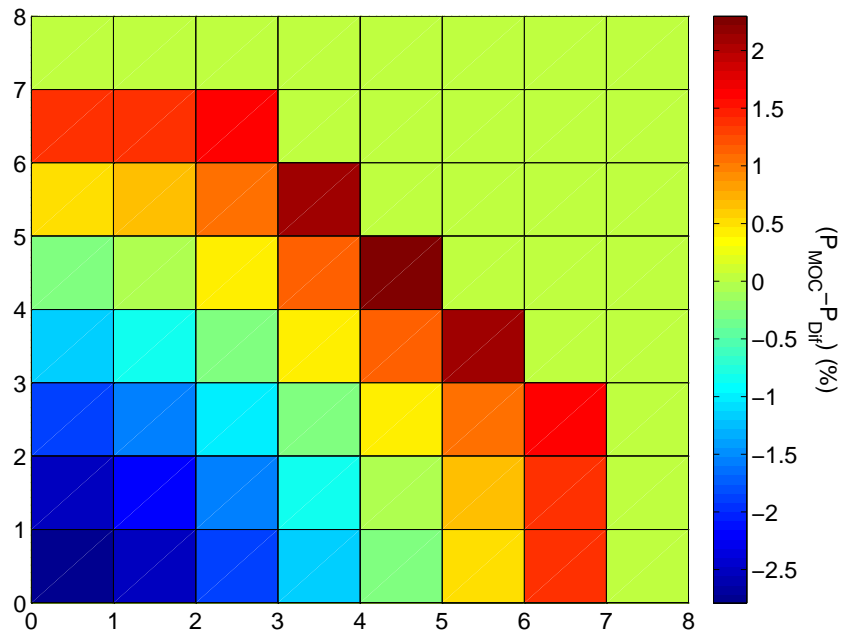


Figure 4.20: Assembly Average Power Error in Diffusion Solution for 2D LEU Core

4.3.3 MOX Core

The MOX core, Figure 4.21, is very similar to the LEU core except 16 of the LEU assemblies are replaced by MOX assemblies. MOX assemblies are loaded in the center of the core to push the peak power away from the center. This is done in order to test the multiscale method for a peak power away from the symmetry boundary.

Refl	Refl	Refl	Refl	Refl	Refl	Refl	Refl
LEU	LEU	LEU	Refl	Refl	Refl	Refl	Refl
LEU	MOX	LEU	LEU	Refl	Refl	Refl	Refl
MOX	LEU	MOX	LEU	LEU	Refl	Refl	Refl
LEU	MOX	MOX	LEU	LEU	LEU	Refl	Refl
MOX	LEU	LEU	MOX	MOX	LEU	LEU	Refl
MOX	MOX	LEU	MOX	LEU	MOX	LEU	Refl
MOX	MOX	MOX	LEU	MOX	LEU	LEU	Refl

Figure 4.21: 2-D MOX Core Layout

Multiscale Regions

The MOX core has the peak power in the (3,3) assembly and the region of interest surrounds this point as shown in Figure 4.22. The first multiscale region is only the single assembly without a buffer region. The second multiscale region surrounds the assembly with a buffer region. The last multiscale region expands the region of interest to include 9 assemblies and surrounds that region with a buffer region.

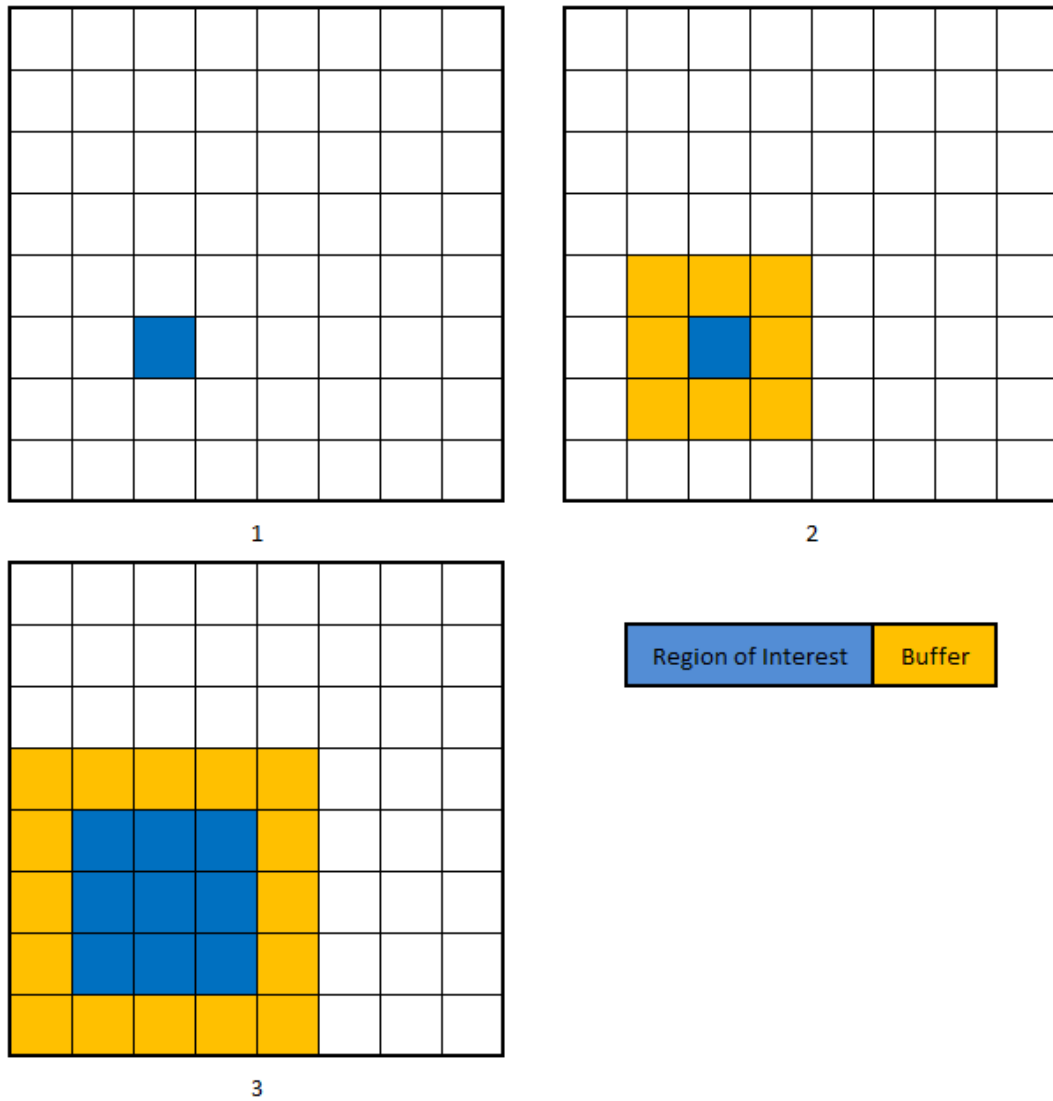


Figure 4.22: 2-D MOX Core Multiscale Regions

Results for MOX Core

The two dimensional MOX core adds a considerable amount of heterogeneity that diffusion with PPR does not handle well. The error in the pin powers are shown in Figure 4.23. Errors occur at all of the LEU MOX interfaces, with pin errors ranging from about 10 to 15 percent. At the core reflector interface, pin errors can be found ranging up to 25 percent. Even with large errors at the assembly interface, the pin power errors in the center of the assembly are small.

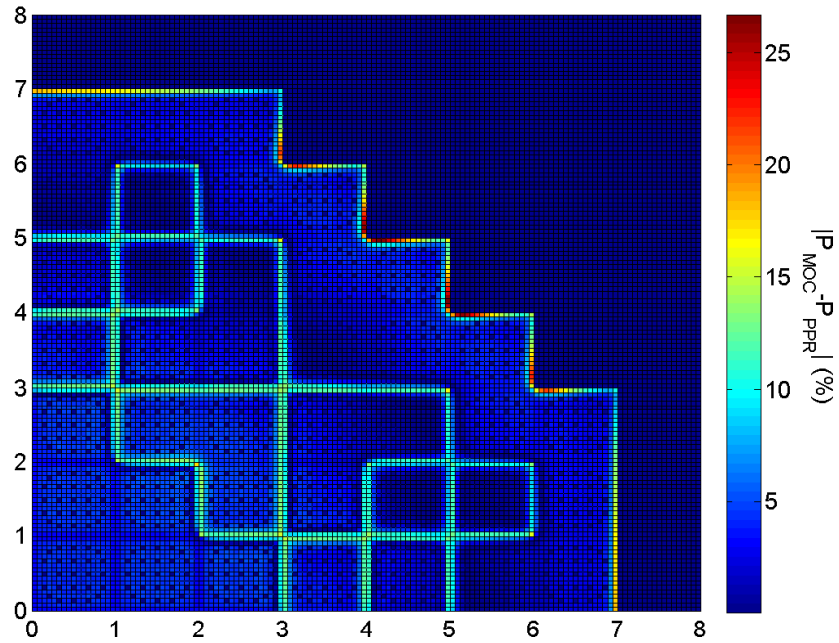


Figure 4.23: Pin Power Error in PPR for for 2D MOX Core

The multiscale method applied to the single assembly without a buffer region slightly improves the pin power errors. Adding a buffer region around the single assembly improves the shape of the solution but the error in the assembly power error makes the peak pin power error worse than PPR. When the multiscale is applied when the region of interest is increased to a three by three set of assemblies surrounded by a buffer region, the pin power errors are greatly reduced in the entire region of interest as shown in Figure 4.24.

Just as in the one dimensional cases, increasing the region of interest decreases the error in the region-wise power, as shown in Table 4.9. Figure 4.25 shows the assembly power errors in the diffusion solution for the MOX core. The assembly with the peak power is about 5 percent below the MOC assembly average power, but the

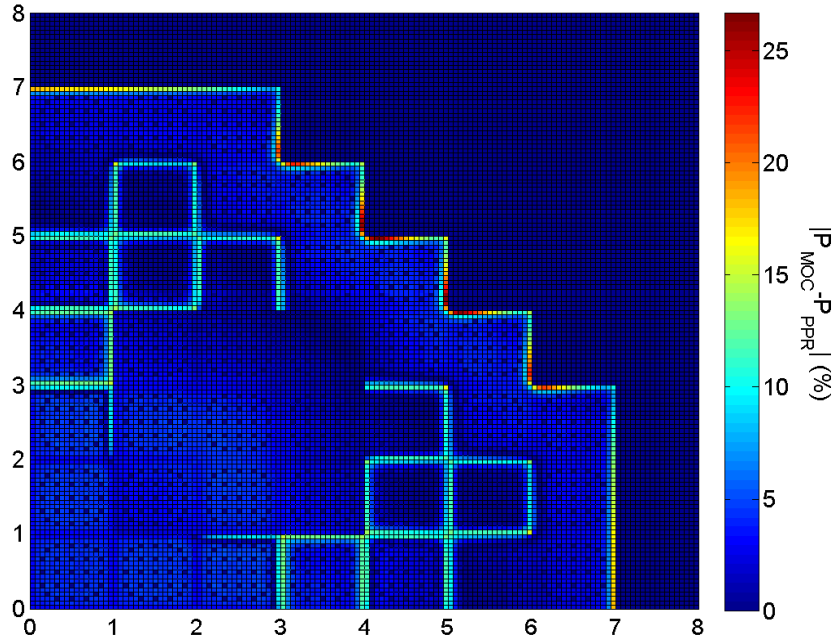


Figure 4.24: Pin Power Error of Multiscale Solution for 2D MOX Core with Increased Region of Interest and Buffer Region

surrounding assemblies are a mix of errors above and below the MOC solution. The average error for the three-by-three region of interest is 2.5 percent.

Table 4.9: FOM for 2D MOX Core

	τ	E^{peak}	E^{max}	E^{RMS}	$E^{\text{RMS shape}}$
2G Diffusion	235.5	4.93%	26.65%	5.25%	2.13%
MS - 1	48.5	6.77%	26.65%	5.23%	0.26%
MS - 2	6.9	6.76%	26.65%	5.23%	0.24%
MS - 3	2.6	4.79%	26.65%	4.73%	0.24%

Another case that was considered is the three-by-three region of interest without a buffer region. As seen in the one dimensional results, it is possible to obtain very good results using the albedo method without a buffer region, but there are some cases where not having a buffer region can cause local pin errors. Since the pin errors on the periphery are already relatively large, it may be worthwhile to remove the buffer region to reduce some of the computational burden. Figure 4.26 shows the resulting pin power error for the case where the buffer is removed from the expanded region of interest. The results from this case are improved over the case with a single assembly

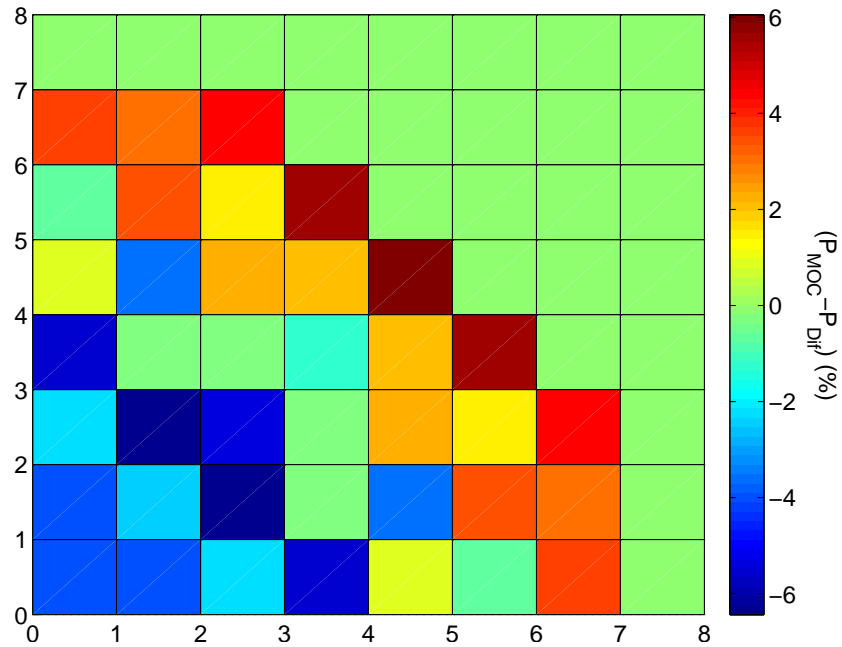


Figure 4.25: Assembly Average Power Error in Diffusion Solution for 2D MOX Core

with a buffer region which has similar computational cost, but the expanded region of interest with a buffer layer still has better results in all categories.

Although these results show that the case without a buffer region can provide good results, it is important to note that when a buffer region is not used, the results appear to vary case by case. If the assembly power error distribution is known, it may be practical to decide if a buffer region is needed. In the end, the user should be cautious when not using a buffer region, because the influence of the boundary condition to pins near the boundary could give solutions less accurate than the original diffusion solution with pin power reconstruction (PPR).

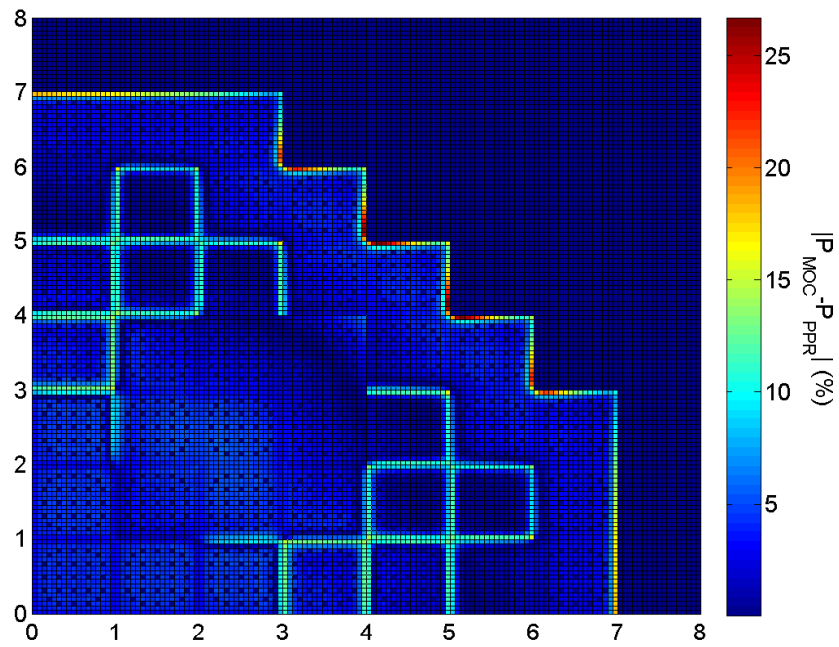


Figure 4.26: Pin Power Error in Multiscale Solution for 2D MOX Core with Increased Region of Interest and No Buffer Region

4.4 Discussion of Post-Refinement Methods

The results given in the previous section provide important insights into the behavior of the post-refinement multiscale method. Several conclusions are drawn from the information obtained, and the results are analyzed to offer a set of best practice guidelines when developing post-refinement multiscale methods for reactor analysis.

4.4.1 Same Energy and Mixed Energy Results

The issue of energy projection is a crucial question of this work. In general, diffusion codes are designed to solve 2, 4, or 8 energy group calculations, but the lattice codes that are used to generate cross-sections in the multiscale approach use many more energy groups ($\sim 50-200$). The projection in energy is a necessary step for the multiscale method to work correctly.

In the one dimensional results, the same energy cases were performed to test the impact of angular coupling. For the same energy cases, all of the cores and multiscale configurations analyzed produced results that were improved over the diffusion solution with pin power reconstruction. This means that the angular dependence on the solution is secondary to the spatial and energy dependence. Since the same energy grid was used, no projection was necessary in the energy variable.

The mixed energy results were then considered, and the results were very different. The post-refinement fixed boundary source method provided results that were considerably worse than the diffusion solution with PPR, especially near the local domain boundary. The albedo results showed modest improvements over diffusion by assuming that the albedo is a constant function of energy for the projection. Without the use of buffer regions, the energy projection methods discussed here cannot sufficiently describe the energy distribution of neutrons at the interface.

4.4.2 Impact of Buffer Region

The use of a buffer provides a region in which the flux can adjust to all of the differences in the local solution; different energy grid, different angular grid, and discrete pins instead of homogenized cross-sections. Most importantly, the buffer region appears to be able to filter out the impact of boundary conditions that have errors. From the results, it appears as though a few pin pitches is a sufficient buffer to obtain a correct energy distribution, but because of practical implementation issues in the test

code used for these problems, only assembly size buffer regions could be used. The thickness of a buffer for these methods is not limited by the method, but by the code in which the method is implemented.

The one-way coupling methods showed consistent improvement when the buffer was added. For this reason it is always suggested that a buffer region be used for one-way coupling methods.

4.4.3 Comparison of Post-Refinement Methods

The post-refinement methods both suffer from the same flaws mentioned in the previous section. In order to choose the best method, the fixed boundary source and albedo methods need to be examined in greater detail. The first category to consider is the ease of implementation into existing high order methods. Many of the target high order codes (DeCART, DENOVO, and MCNP) considered for implementation already have the functionality to solve an eigenvalue problem given an albedo boundary condition. In many cases, the albedo boundary condition is not as generalized as this method requires. Development issues would involve making the albedo dependent on space and energy at the pin cell level. The work required to do this is modest. Some of the target lattice codes also have the ability to define an incoming angular flux. Again, modification would need to be made to define the angular flux as a function of space, angle, and energy on the entire domain. Another minor modification would be for the fixed source solver to accept an arbitrary eigenvalue that would be determined by the global solver. Ultimately, the implementation of the albedo method appears to be a better fit for the lattice codes considered for implementation.

A second consideration is execution time. The computational cost for both methods is approximately equal for the same size domain. The main difference is that for the albedo method, it is not essential to have a buffer region. The removal of the buffer region makes the method much more computationally advantageous.

A third consideration is the sensitivity of the method to errors in the input data. The global solution has inherent errors in the solution, and thus the boundary conditions of the local solver derived from the global solution also have errors. It is useful to understand how these errors affect the solution. To better understand the difference in the way the fixed boundary source and albedo methods propagate errors, a sensitivity analysis was performed to determine which method is more stable.

4.4.4 Sensitivity Analysis

To better understand the two methods, the solution methodology in both approaches are analyzed using Matrix-Operator notation. After it is understood how the errors are introduced in each method, several cases will be performed with small perturbations in the solution to test the sensitivity of the figures of merit to the derived input data. The impact of small perturbations on the solution has been studied by Rahnema et al. [38, 39, 40, 41, 42]. However, the majority of this work focuses on sensitivities to the eigenvalue using perturbation theory. Since the eigenvector is of more interest for this analysis, spectral analysis of the matrices will be used.

The propagation of error in these method can best be understood by considering a domain mapping problem shown in Figures 4.27(a) and 4.27(b). The mapping begins by considering the physical location where the source term (left) is mapped using matrix A to the solution (right). Then two cases are considered; the well conditioned case, 4.27(a), where a small perturbation in the source term produces a small perturbation in the solution (red line), or a small perturbation in the mapping matrix A produces a small perturbation in the solution (green line). In both of these cases the introduction of error does not have a significant impact on the solution. The second case is considered to be ill conditioned, 4.27(b). This is where the same small perturbation in the source term (red) or mapping matrix (green) creates large changes in the solution. The same idea can be applied to the eigenvalue system, except that the error occurs in A, and the solution error is in the eigenvalue/eigenvector combination.

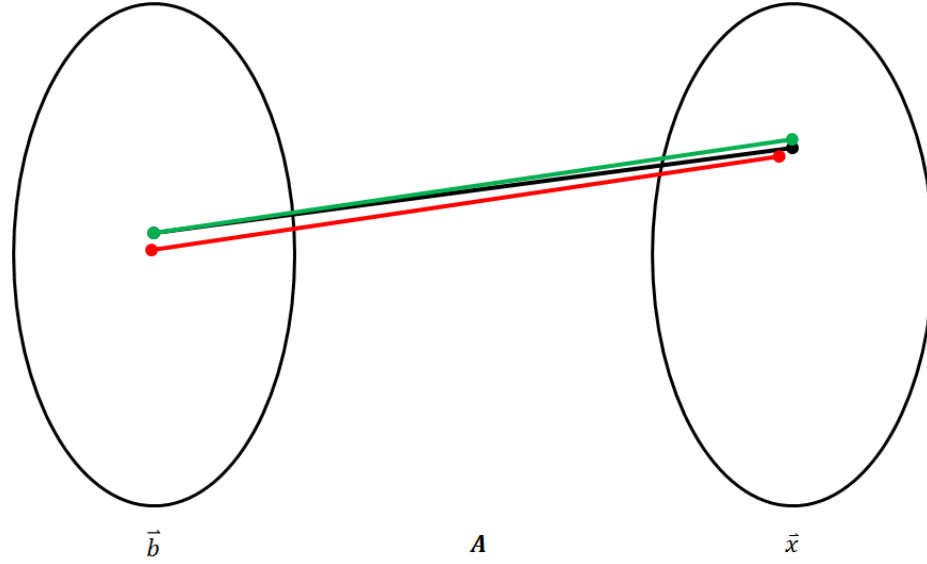
In order to analyze how the error propagates through the fixed source and albedo problems, both multiscale methods are compared to the high order solution. The high order solution for the full domain can be written in matrix-operator notation as shown in equation (4.7).

$$\left(\tilde{\mathbb{M}}^H + \lambda^H \tilde{\mathbb{F}}^H\right) \tilde{\psi}^H = 0 \quad (4.7)$$

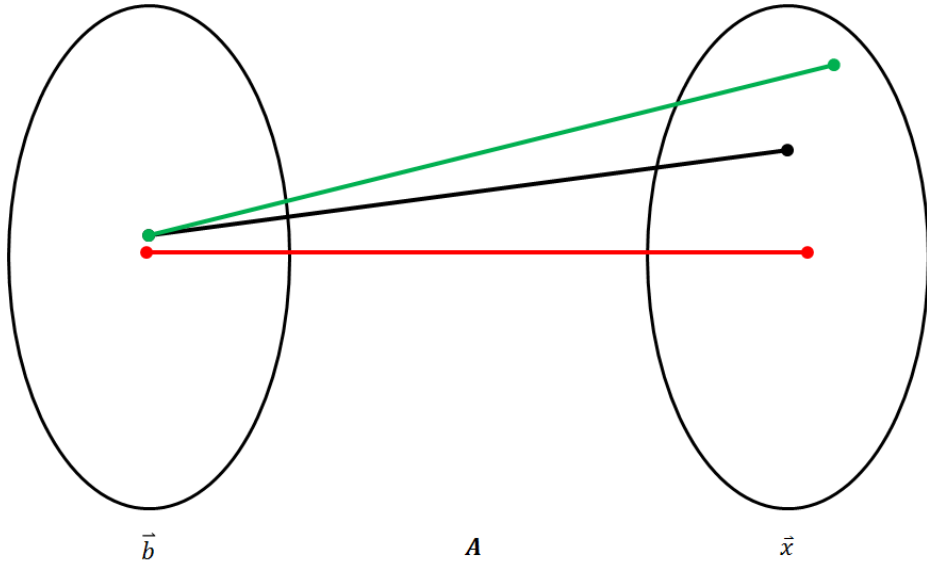
In this equation $\tilde{\mathbb{M}}^H$ is the streaming, collision, and scattering operator for the transport solution for the global domain, $\tilde{\mathbb{F}}^H$ is the fission operator for the global solution, λ^H is the eigenvalue of the high order solution, and $\tilde{\psi}^H$ is the flux distribution for the entire domain. Similarly, equation (4.8) is written for the global low order solution.

$$\left(\tilde{\mathbb{M}}^L + \lambda^L \tilde{\mathbb{F}}^L\right) \tilde{\psi}^L = 0 \quad (4.8)$$

The local high order solution of the fixed source problem can be written in



(a) Well Conditioned System



(b) Ill Conditioned System

Figure 4.27: Domain Mapping Example

equation (4.9).

$$(\mathbb{M}^H + \lambda^H \mathbb{F}^H) \psi^H = \psi_b^H \quad (4.9)$$

The matrices \mathbb{M} and \mathbb{F} are subsets of the global matrices $\tilde{\mathbb{M}}$ and $\tilde{\mathbb{F}}$ for the local solution. If ψ_b is defined using the global high order solution, the local flux distribution ψ is a subset of the global solution $\tilde{\psi}$. Unfortunately, the high order global solution is not known. Instead, the low order global solution is used to determine the eigenvalue and

boundary source as shown in equation (4.10).

$$(\mathbb{M}^H - \lambda^L \mathbb{F}^H) \psi^{\text{FS}} = \psi_b^L \quad (4.10)$$

The difference between the high order local solution (4.9) and the multiscale approximation (4.10) can be rearranged to obtain the error in the flux distribution.

$$(\mathbb{M}^H - \lambda^H \mathbb{F}^H) \psi^H - (\mathbb{M}^H - \lambda^L \mathbb{F}^H) \psi^{\text{FS}} = \psi_b^H - \psi_b^L \quad (4.11a)$$

$$(\mathbb{M}^H - \lambda^L \mathbb{F}^H) (\psi^H - \psi^{\text{FS}}) = \psi_b^H - \psi_b^L - (\lambda^H - \lambda^L) \mathbb{F}^H \psi^H \quad (4.11b)$$

$$(\psi^H - \psi^{\text{FS}}) = (\mathbb{M}^H - \lambda^L \mathbb{F}^H)^{-1} (\psi_b^H - \psi_b^L - (\lambda^H - \lambda^L) \mathbb{F}^H \psi^H) \quad (4.11c)$$

Although it is useful to consider the complete error vector, it is more instructive to consider some vector norm of the error. To obtain a bound on the error, a series of operations are applied to equation (4.11c). First an arbitrary norm is taken of both sides of equation (4.11c). Then the Cauchy-Schwartz inequality is applied, (4.12b), which states that the norm of a product is less than or equal to the product of the norms. The same inequality is applied to a rearranged version of the high order solution, (4.12c). The error equation is then divided by the norm of the high order solution to obtain an error bound for the multiscale fixed source system, (4.12d).

$$\|\psi^H - \psi^{\text{FS}}\| = \|(\mathbb{M}^H - \lambda^L \mathbb{F}^H)^{-1} (\psi_b^H - \psi_b^L - (\lambda^H - \lambda^L) \mathbb{F}^H \psi^H)\| \quad (4.12a)$$

$$\|\psi^H - \psi^{\text{FS}}\| \leq \|(\mathbb{M}^H - \lambda^L \mathbb{F}^H)^{-1}\| \|\psi_b^H - \psi_b^L - (\lambda^H - \lambda^L) \mathbb{F}^H \psi^H\| \quad (4.12b)$$

$$\|\mathbb{M}^H - \lambda^L \mathbb{F}^H\| \|\psi^H\| \geq \|\psi_b^H + (\lambda^H - \lambda^L) \mathbb{F}^H \psi^H\| \quad (4.12c)$$

$$\frac{\|\psi^H - \psi^{\text{FS}}\|}{\|\mathbb{M}^H - \lambda^L \mathbb{F}^H\| \|\psi^H\|} \leq \|(\mathbb{M}^H - \lambda^L \mathbb{F}^H)^{-1}\| \frac{\|\psi_b^H - \psi_b^L - (\lambda^H - \lambda^L) \mathbb{F}^H \psi^H\|}{\|\psi_b^H + (\lambda^H - \lambda^L) \mathbb{F}^H \psi^H\|} \quad (4.12d)$$

$$\kappa (\mathbb{M}^H - \lambda^L \mathbb{F}^H) = \|\mathbb{M}^H - \lambda^L \mathbb{F}^H\| \|(\mathbb{M}^H - \lambda^L \mathbb{F}^H)^{-1}\| \quad (4.12e)$$

$$\frac{\|\psi^{\text{H}} - \psi^{\text{FS}}\|}{\|\psi^{\text{H}}\|} \leq \kappa (\mathbb{M}^{\text{H}} - \lambda^{\text{L}} \mathbb{F}^{\text{H}}) \frac{\|\psi_b^{\text{H}} - \psi_b^{\text{L}} - (\lambda^{\text{H}} - \lambda^{\text{L}}) \mathbb{F}^{\text{H}} \psi^{\text{H}}\|}{\|\psi_b^{\text{H}} + (\lambda^{\text{H}} - \lambda^{\text{L}}) \mathbb{F}^{\text{H}} \psi^{\text{H}}\|} \quad (4.12\text{f})$$

The relative error norm in the angular flux is proportional to the condition number of the coefficient matrix multiplied by the relative error from the low order solution. The error bound provided by this relationship is similar to the standard error bound for a linear system [43].

Now that the fixed boundary source has been examined, the albedo method will be considered. This method requires a different approach because it is an eigenvalue problem. The boundary conditions for the local multiscale problem are determined by modifying the migration/collision matrix with the albedo boundary condition.

$$(\mathbb{M}^{\text{H}} + \Delta\mathbb{M}^{\text{H}} - \lambda^{\text{H}} \mathbb{F}^{\text{H}}) \psi^{\text{H}} = 0 \quad (4.13\text{a})$$

$$\Delta\mathbb{M}^{\text{H}} \psi^{\text{H}} = -\psi_b^{\text{H}} \quad (4.13\text{b})$$

Unfortunately, in order to formulate the matrix $\Delta\mathbb{M}^{\text{H}}$ it is necessary to calculate the global high order transport solution. Instead, the low order global solution can be used to estimate the matrix, $\mathbb{M}^{\text{H}} \approx \mathbb{M}^{\text{L}}$.

$$(\mathbb{M}^{\text{H}} + \Delta\mathbb{M}^{\text{L}} - \lambda^{\beta} \mathbb{F}^{\text{H}}) \psi^{\beta} = 0 \quad (4.14\text{a})$$

$$\Delta\mathbb{M}^{\text{L}} \psi^{\text{L}} = -\psi_b^{\text{L}} \quad (4.14\text{b})$$

The last operation that must be done is to recast the albedo equations into a standard eigenvalue problem.

$$\left((\mathbb{M}^{\text{H}} + \Delta\mathbb{M}^{\text{H}})^{-1} \mathbb{F}^{\text{H}} - \frac{1}{\lambda^{\text{H}}} \mathbb{I} \right) \psi^{\text{H}} = 0 \quad (4.15)$$

$$\left((\mathbb{M}^{\text{H}} + \Delta\mathbb{M}^{\text{L}})^{-1} \mathbb{F}^{\text{H}} - \frac{1}{\lambda^{\beta}} \mathbb{I} \right) \psi^{\beta} = 0 \quad (4.16)$$

A simplification to the notation is made to replace $(\mathbb{M}^{\text{H}} + \Delta\mathbb{M}^{\text{H}})^{-1} \mathbb{F}^{\text{H}}$ with \mathbb{A}^{H} , $(\mathbb{M}^{\text{H}} + \Delta\mathbb{M}^{\text{L}})^{-1} \mathbb{F}^{\text{H}}$ with \mathbb{A}^{L} , and the inverse of λ with the k-eigenvalue.

Perturbation theory for eigenvalue systems is much more complex [44]. The per-

turbation analysis gives two condition numbers, one for the eigenvalue and another for the eigenvector.

$$\frac{k^{\text{H}} - k^{\beta}}{k^{\text{H}}} \leq \kappa_k(\mathbb{A}^{\text{H}}) \frac{\|\mathbb{A}^{\text{H}} - \mathbb{A}^{\text{L}}\|}{\|\mathbb{A}^{\text{H}}\|} \quad (4.17\text{a})$$

$$\frac{\|\psi^{\text{H}} - \psi^{\beta}\|}{\|\psi^{\text{H}}\|} \leq \kappa_{\psi}(\mathbb{A}^{\text{H}}) \frac{\|\mathbb{A}^{\text{H}} - \mathbb{A}^{\text{L}}\|}{\|\mathbb{A}^{\text{H}}\|} \quad (4.17\text{b})$$

The condition number for the eigenvalue, κ_k , is inversely proportional to the angle between the left and right eigenvectors associated with the eigenvalue of interest. The condition number of the eigenvector, κ_{ψ} , requires a full spectral analysis of the matrix \mathbb{A}^{H} . The determination of the eigenvector condition number can only be estimated using numerical perturbations of the system since the full transport matrix is never constructed for practical applications.

Numerical Results

In order to compare the sensitivity of the boundary conditions for the two different methods, a series of perturbations are applied to the boundary condition. The one dimensional MOX 1 core is used with a single multiscale region. Since the full core MOC solution has been determined the exact boundary conditions are known for this case. A weighting parameter is defined which provides a linear interpolation between the true high order solution and the low order estimation of the boundary. For the fixed source problem, the eigenvalue and boundary flux are determined using the following relationships.

$$\lambda(\gamma) = \lambda^{\text{H}} + \gamma(\lambda^{\text{L}} - \lambda^{\text{H}}) \quad (4.18\text{a})$$

$$\psi_b(\gamma) = \psi_b^{\text{H}} + \gamma(\psi_b^{\text{L}} - \psi_b^{\text{H}}) \quad (4.18\text{b})$$

The boundary condition perturbation for the albedo method uses the following relationship.

$$\Delta\mathbb{M}(\gamma) = \Delta\mathbb{M}^{\text{H}} + \gamma(\Delta\mathbb{M}^{\text{L}} - \Delta\mathbb{M}^{\text{H}}) \quad (4.19)$$

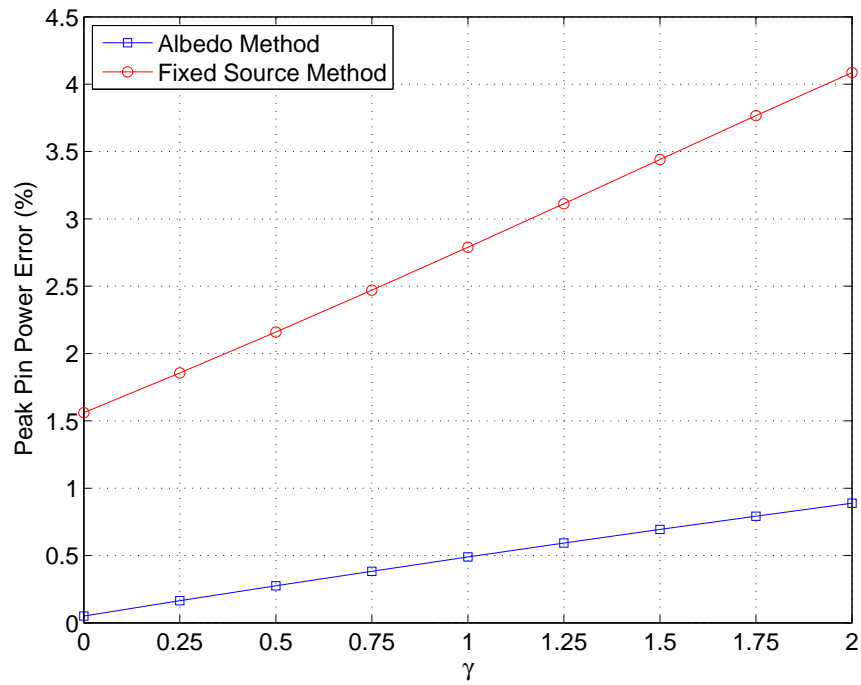
Although the high order solution is known in both angle and energy, only the energy shape will be used for the high order solution. This is because both methods always rely on the accuracy of the diffusion solution for the angular shape. The high order solution used preserves both partial currents for the each energy group. Also, the assembly error that is associated with the post-refinement method is set to zero so

there is not an offset in the error.

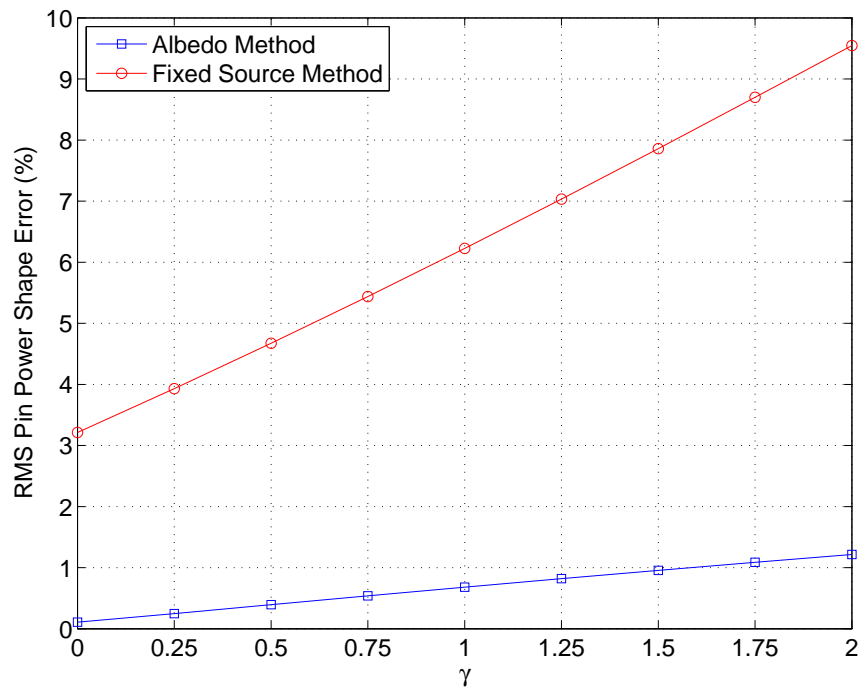
Calculations are performed with both methods for values of γ ranging from zero to two. The peak pin power and pin power shape errors are plotted in Figure 4.28 for both methods. It can be seen that the albedo method is much less sensitive to the perturbations in the boundary condition. The errors in the albedo method increase gradually from zero as the boundary condition error is increased. The errors in the fixed source method are nonzero when the incoming current is identical to the high order method. The sensitivity to the angular distribution cannot be remedied for the multiscale methods discussed here. More importantly than the initial error, the increase in the error is considerably greater with the fixed source method than with the albedo method.

The sensitivity analysis shows that the albedo method is less sensitive to errors in the initial boundary conditions. In addition, the albedo was perturbed uniformly. Generally, errors to ratios tend to be much smaller than errors of the absolute value of a measurement. This is because the incoming and outgoing currents tend to have similar errors, causing the ratio to be much more reliable than the absolute incoming current.

Because the albedo method could be easier to implement, is more computationally efficient, and less sensitive to boundary condition errors, it was chosen to be implemented into the two dimensional cases and is recommended for further use where the multiscale method is applied. The post-refinement albedo method provides a flexible framework in which the local solution can be obtained with very good accuracy for all cases.



(a) Peak Pin Power Error



(b) Pin Power Shape Error

Figure 4.28: Sensitivity of Local Solver

Chapter 5

Assessment of the Embedded Multiscale Method

Unlike the post-refinement method, the embedded method allows the global solution to adjust to the refined local solution. Since the global solution is altered, it can be beneficial to define refined local regions in which the standard nodal diffusion methods have problems; not just around the peak assembly.

In this chapter the embedded multiscale method will be applied to several regions in the reactor. The first cases that are considered are identical to the cases looked at with the post-refinement method. Another location that can have a significant impact on the global solution is the fuel-reflector interface, since calculating the correct leakage in the core can have a significant impact on the global tilt of the error. By embedding the solver into the reflector region, the leakage out of the system can be calculated more accurately. The last location that is considered is around a control rod, which can be important since a strong absorber causes a significant dip in the local flux. Although the standard method can do reasonably well in predicting the worth of the control rod, the pin powers around the control rod can have significant errors.

5.1 One Dimensional Analysis

The same one dimensional cores used in the previous chapter are used to assess the performance of the embedded method. As noted in the descriptions of the assemblies, when a control rod is inserted into an assembly the center water hole is replaced with control rod material.

Another difference between the post-refinement method and the embedded method is that multiple levels can be embedded into the calculation. This analysis will investigate the use of up to four levels of embedded solvers. The first level's solver is

always the assembly homogenized two group diffusion solver. Three additional solvers are added to increase the accuracy of the embedded calculation: a fine group MOC solver, a fine group pin homogenized diffusion solution, and an intermediate group pin homogenized diffusion solver. The MOC solver will be placed where the most accuracy is desired, with the other two solvers surrounding to decrease the effects of prolongation at the boundary. As in the previous chapter, a series of three multiscale calculations are performed. The first is with the MOC solver in the region of interest. The second adds the fine group pin homogenized diffusion solution on both sides of the region, and the last adds the intermediate group pin homogenized diffusion solver.

In order to determine the choice of intermediate group structures to use between the two group diffusion solver and the fine group MOC solver, the impact of intermediate level energy group levels on the accuracy of the solution were evaluated using the MOX1 core. Figure 5.1 shows the spatial distribution of the pin power errors in the MOX 1 core for diffusion solvers with 2, 4, and 7 energy groups. The error in the two group assembly homogenized diffusion solver with pin power reconstruction (2G Diffusion in the Figure) is compared to the error in the pin homogenized diffusion solver with 2, 4, and 7 energy groups.

At the interface between dissimilar fuel assemblies, the error is significantly reduced as the number of groups is increased. The difference in the assembly and pin homogenized two group cross-sections is small, and the impact of pin homogeneous cross-sections appears to be negligible in the one dimensional problem. The four group cross-section set captures the majority of the spectral effects, but increasing to seven groups does show some additional improvement in the solution. Even with seven group cross-sections, the diffusion solution still has significant errors at the MOX/LEU interfaces. These differences can be attributed to the effect of spatially homogenizing cross-sections using a single infinite assembly spectrum, as well as transport effects at the boundary. Because the seven group pin homogenized diffusion solver provides a considerably improved solution, it is used in the region surrounding the MOC region. In cases where the multiscale region needs to be expanded, the four group pin homogenized diffusion solver will be added.

5.1.1 Embedded Region Around Peak Power Assembly

Like the post-refinement method, the embedded method can be used to resolve local pin power peaking to obtain a more accurate prediction of the peak pin power. The multiscale regions used for the LEU and MOX1 cores is shown in Figure 5.2.

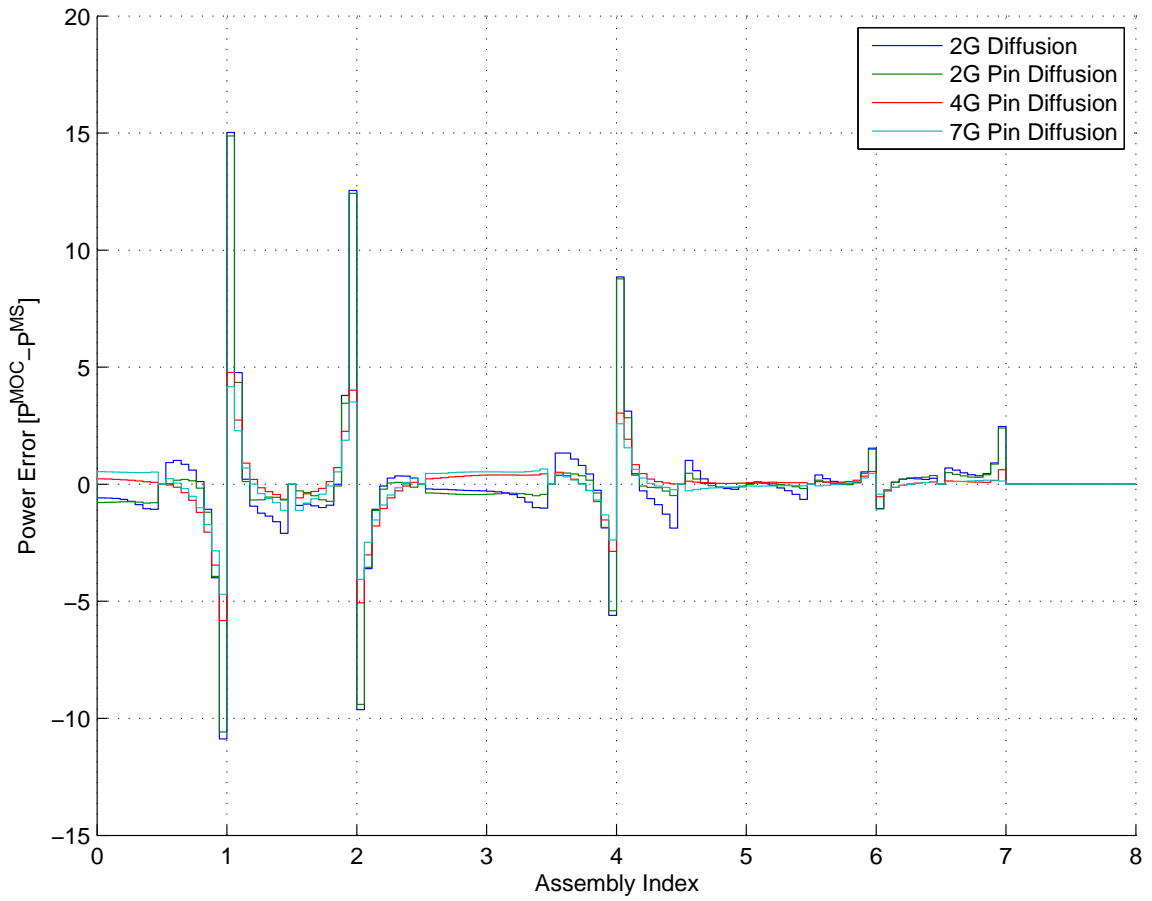


Figure 5.1: Pin Power Error Distribution for Diffusion Solvers

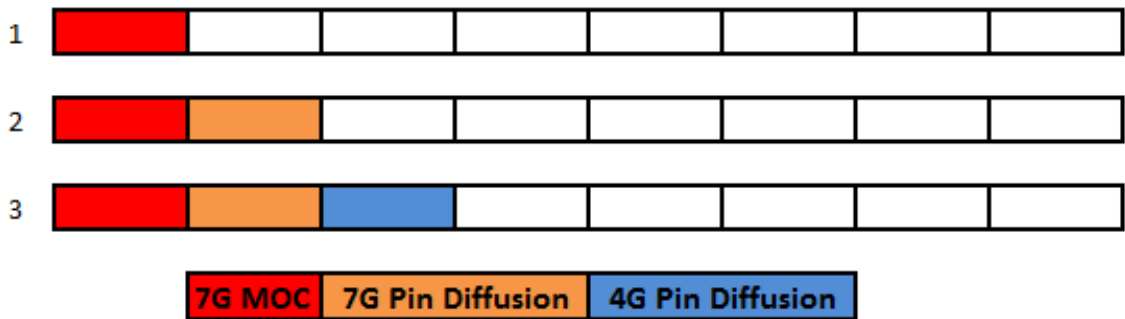


Figure 5.2: Embedded Multiscale Regions for LEU and MOX 1 Core

Table 5.1: Figures of Merit for LEU Core with Embedded Multiscale Method

	τ	Δk	E^{peak}	E^{max}	E^{RMS}	$E^{\text{RMS shape}}$
2G Diffusion	262.2	0.8	-1.00%	5.13%	0.79%	0.03%
MS - 1	5.6	1.3	-1.22%	5.13%	0.81%	0.07%
MS - 2	6.8	1.9	-1.33%	5.14%	0.85%	0.01%
MS - 3	6.4	2.4	-1.25%	5.16%	0.87%	0.01%

LEU Core

The solution of the nodal diffusion solver predicts the pin powers of the LEU core very well. The multiscale results are shown in Table 5.1. In all cases, the embedded solution is slightly less accurate than the original diffusion solution with the errors introduced by the embedded method less than half a percent in all figures of merit for the power shape.

MOX 1 Core

The PPR method have larger errors for the mox cores, and the impact of the embedded method is more apparent. Similar to the LEU core, the peak pin power is in the center assembly and embedded regions are gradually introduced to improve the solution. Figure 5.3 shows the error in the pin power distribution for the diffusion solution and the three multiscale cases. Although the peak pin power error increases slightly, the embedded method reduces the maximum pin power error and the global RMS error. The error in the pin power shape is also decreased.

As the multiscale regions are increased, the pin power errors in the center assembly become constant. This is because the transport effects at the MOX/LEU interface are not completely resolved. A fourth multiscale case is considered where the MOC solver is used in the center two assemblies. The seven group pin homogenized diffusion solver is also used in the third assembly. Figure 5.4 shows the multiscale levels used in the additional calculation.

The impact of the extension of the MOC region is significant. All of the figures of merit increase except the speedup, as shown in Table 5.2.

Figure 5.5 contrasts the original diffusion solution errors with the new multiscale solution. The interface effects are completely removed between the first two assemblies and are considerably reduced between the second and third assemblies.

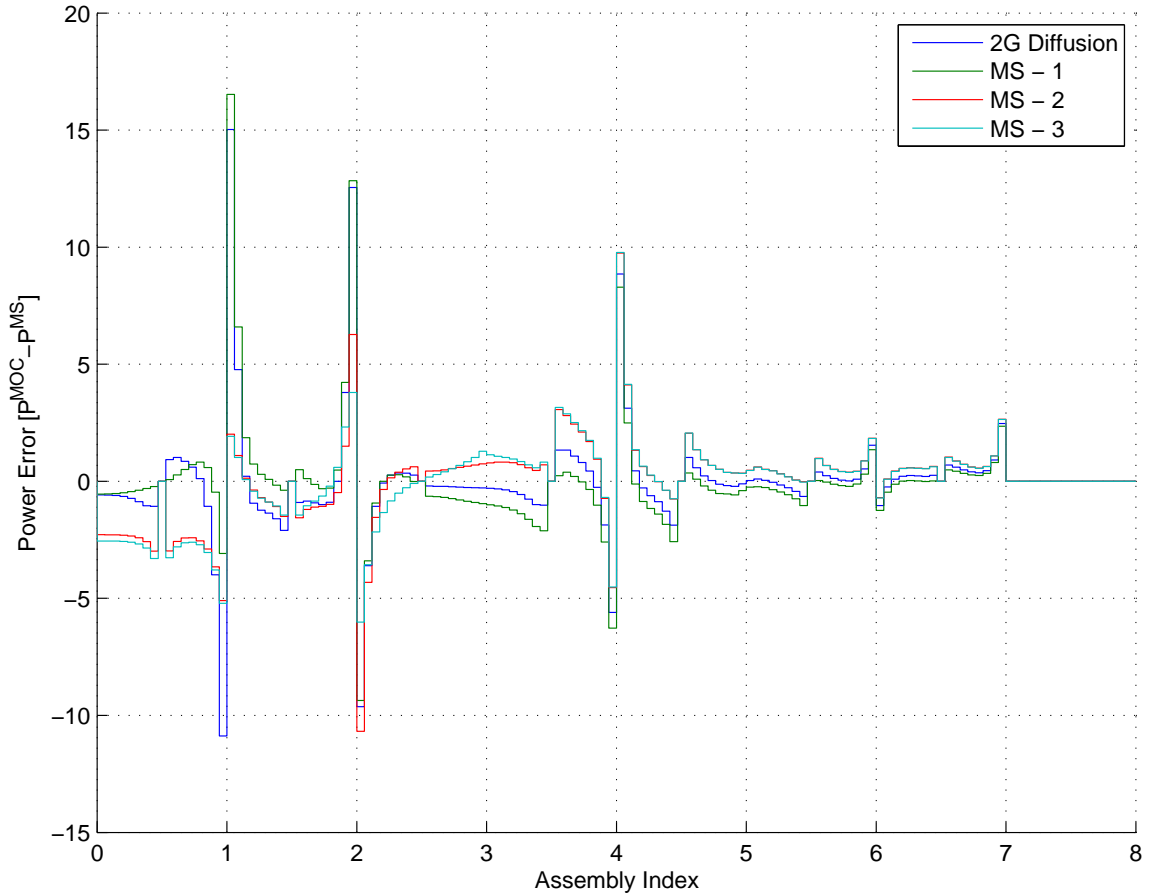


Figure 5.3: PPR in MOX1 Core for Embedded Method

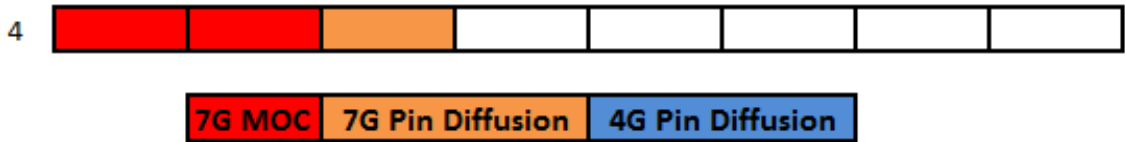


Figure 5.4: Additional Embedded Multiscale Region for MOX 1 Core

Table 5.2: Figures of Merit for MOX1 Core with Embedded Method

	τ	Δk	E^{peak}	E^{max}	E^{RMS}	$E^{\text{RMS shape}}$
2G Diffusion	256.6	-28.4	-1.07%	15.03%	2.66%	1.47%
MS - 1	5.5	-84.2	-0.23%	16.53%	2.58%	0.46%
MS - 2	5.3	64.0	-2.99%	10.68%	2.11%	0.51%
MS - 3	6.4	53.6	-3.30%	9.77%	1.94%	0.49%
MS - Extended	4.0	1.4	-0.44%	9.00%	1.22%	0.00%

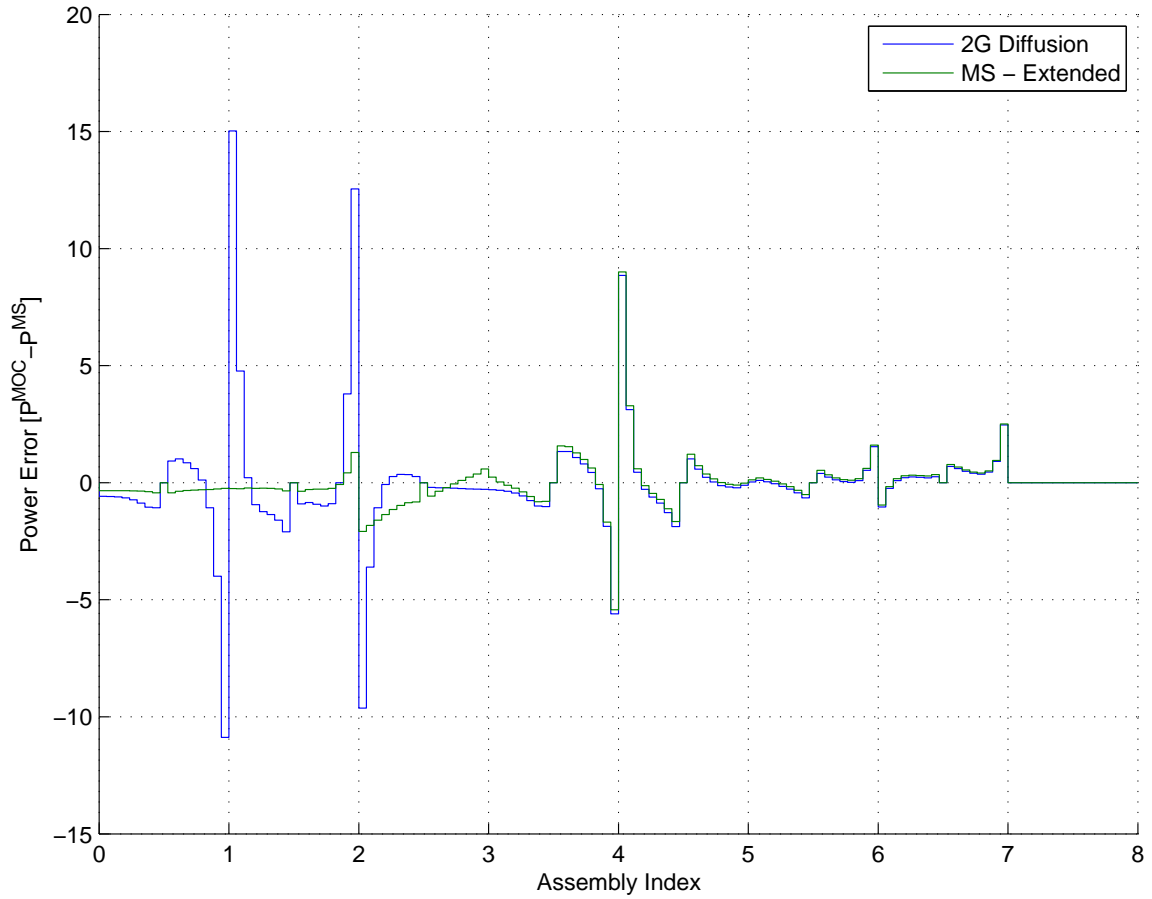


Figure 5.5: Impact of Extended MOC Region for MOX1 Core

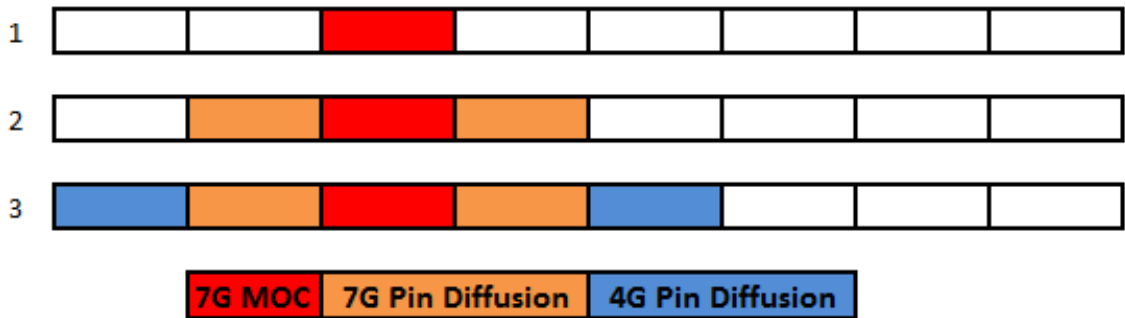


Figure 5.6: Multiscale Regions for MOX2 Core

MOX 2 Core

The MOX2 core requires the embedded region to be moved away from the center of the core, as shown in Figure 5.6.

The embedded method in this case decreases the RMS and shape errors, but

Table 5.3: Figures of Merit for MOX 2 Core

	τ	Δk	E^{peak}	E^{max}	E^{RMS}	$E^{\text{RMS shape}}$
2G Diffusion	191.6	-36.3	-1.77%	10.70%	2.60%	3.67%
MS - 1	5.2	-77.4	-1.58%	11.71%	2.66%	3.70%
MS - 2	4.6	-2.0	-1.40%	12.32%	2.23%	3.85%
MS - 3	5.0	34.5	-2.15%	8.05%	1.93%	1.37%

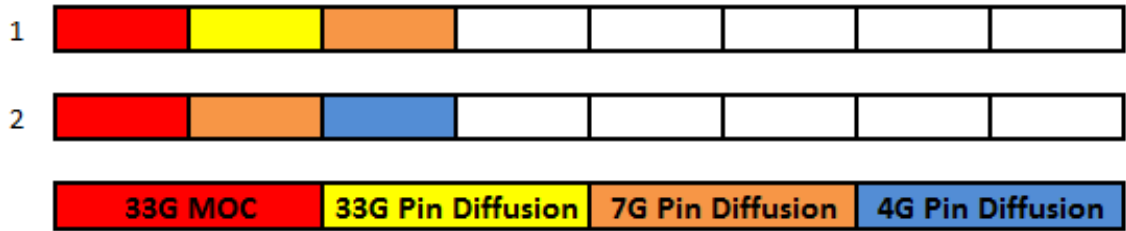


Figure 5.7: Multiscale Regions for 33 Group Embedded Calculation

as shown in Table 5.3 clear trends are not apparent in the peak pin error and the maximum overall error. The maximum error can be difficult to quantify because the location of the maximum pin error can change spatial location as the levels are expanded. It is not until the majority of the solution uses a higher level that the solution shows improvements in the maximum pin error. The principal issue with this case is that the energy structure never reaches an asymptotic spectrum. The prolongation condition relies on the energy shape to be close to symmetric at an interface.

Embedded Method with More Energy Groups

The embedded method was then extended to more energy groups, with the 33 group transport library used to assess the impact of using more energy groups. The 33 group MOC solver was embedded in the assembly with the peak power. Two different levels were examined to determine how important the energy group structure is around the MOC region. The first was a series of 33 group and 7 group pin homogenized diffusion solvers around the MOC region. The second was a series of 7 group and 4 group pin homogenized diffusion solvers around the MOC region. Figure 5.7 shows the multiscale regions for two cases using the LEU and MOX 1 cores.

All three cores were considered with these regions, and both level structures gave

Table 5.4: Comparison of Level Structure for 33 Group Embedded Calculation

	τ	Δk	E^{peak}	E^{max}	E^{RMS}	$E^{\text{RMS shape}}$
2G Diffusion	1220.6	48.4	-1.16%	18.55%	3.23%	1.70%
MS - 1	–	59.7	-3.83%	11.45%	2.14%	0.69%
MS - 2	6.8	86.8	-2.35%	11.40%	2.03%	0.68%

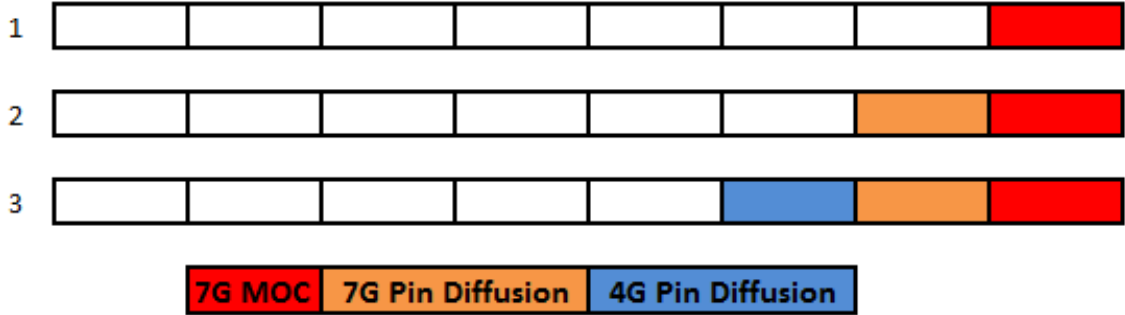


Figure 5.8: Multiscale Regions in the Reflector for the Embedded Method

very similar answers in all cases. This suggests that the impact of the reduced energy groups used in the second level structure is still sufficient to capture the spectral effects caused by adding more groups to the transport library. Table 5.4 summarizes the comparison of the two level structures for all three cores.

5.1.2 Embedded Region Around Fuel-Reflector Interface

Adding the embedded region at the fuel reflector interface is another way that the embedded method can be used to increase the local accuracy and also the global accuracy. For all three cores, the MOC region is placed in the water reflector. Additional cases are added to model the last assembly using the seven group pin homogenized diffusion solver and the next assembly using the four group pin homogenized solver. Figure 5.8 shows the three multiscale regions considered.

Although the LEU core already has a small pin power error, there is a noticeable tilt in the pin power error across the core. This is primarily because the leakage estimated at the fuel/reflector interface can have small errors that introduce a tilt in the flux and power distributions. Adding the multiscale region to the reflector will accurately model the correct effects at the boundary. Figure 5.9 shows the global shape of the pin power errors as the multiscale region is increased.

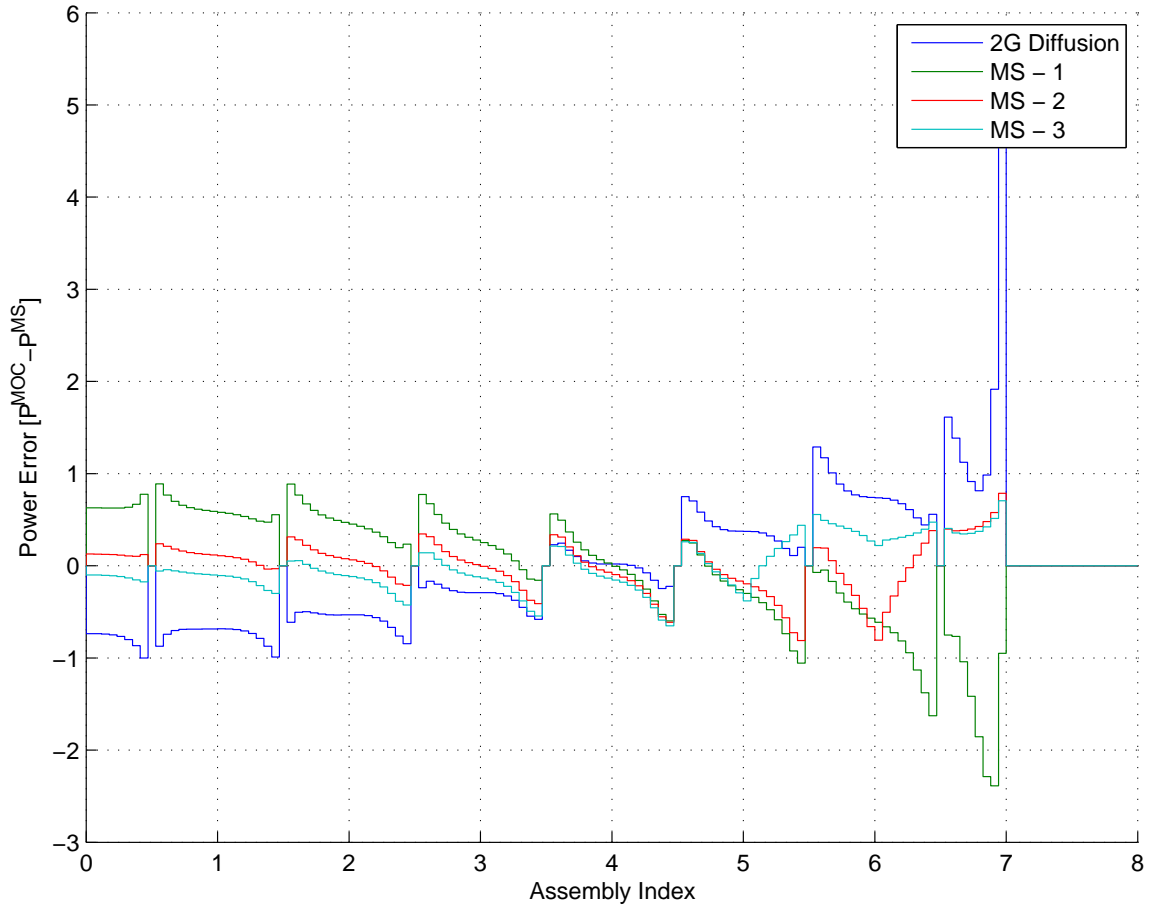


Figure 5.9: Impact of Embedded Regions in Reflector for the LEU Core

Although the pin power errors improve when the MOC region is added only in the reflector, it should be noted that the energy spectrum shape used for the prolongation operator at the core-reflector interface is approximate since the core solution is uses 2 groups and the reflector uses 7 groups. Also, since the multiscale calculation does not have a direct impact on the fission source, the solution takes a long time to converge. Adding another multiscale region at the core reflector interface increases the accuracy of the calculation and actually decreases the run time because the energy levels of the core and reflector are better coupled.

For the MOX 1 core, there is no improvement of the solution by adding multiscale regions in the reflector region. This is generally because the errors in the core leakage are overshadowed by the errors at the MOX/LEU interface.

Some improvements are observed in the MOX 2 core, as shown in Figure 5.10. Although the reductions in error are modest, because the impact is overshadowed by the MOX/LEU interface, the principal improvement is the impact of calculating the

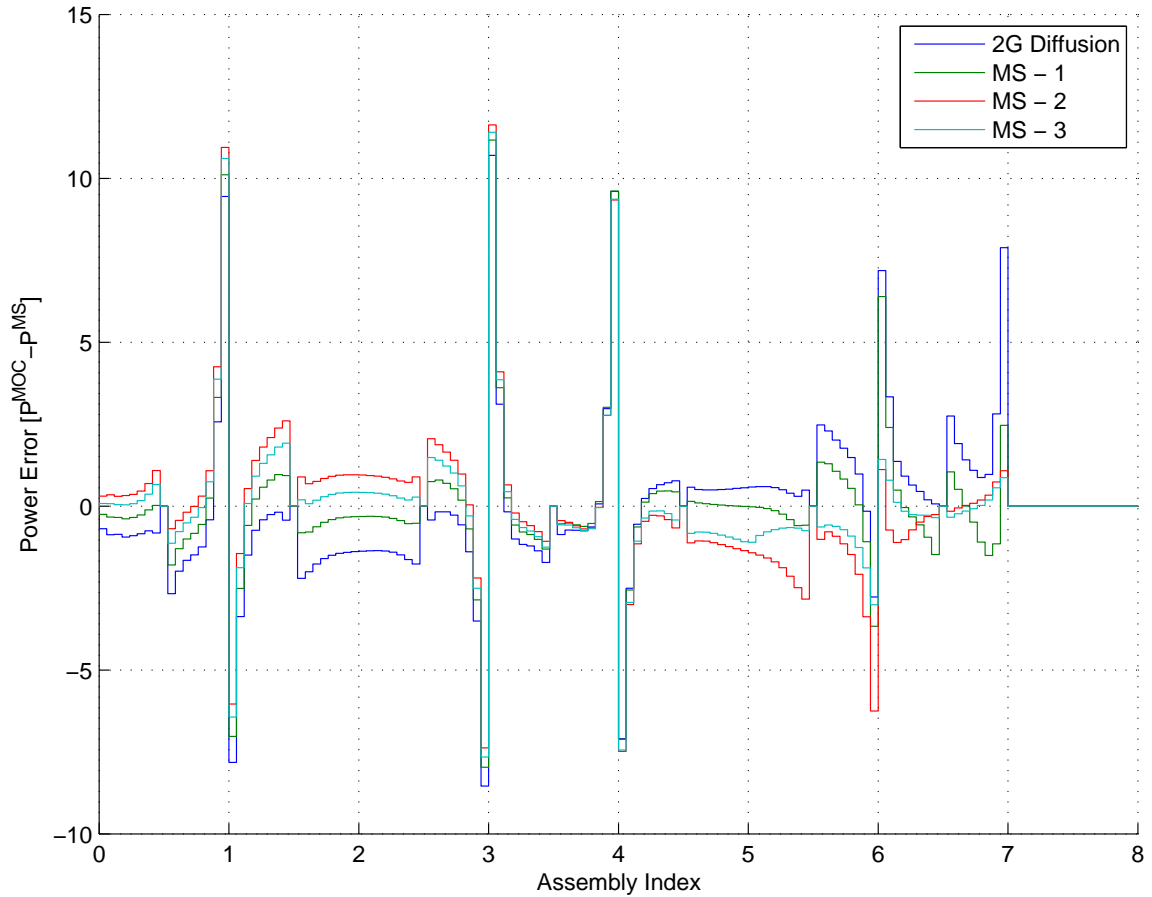


Figure 5.10: Impact of Embedded Regions in Reflector for the MOX 2 Core

correct discontinuity factor on the fuel/reflector interface. The reflector discontinuity factor was calculated using a two node problem with an LEU assembly and the reflector. Since the outgoing spectrum in LEU and MOX are different, the reflector discontinuity factor should be different for the two cases. It is not practical to generate a new discontinuity factor for every assembly facing the reflector, so the common practice is to only generate one discontinuity factor for all assemblies at the periphery.

5.1.3 Embedded Region Around Controlled Assembly

Although the change in reactivity due to a control rod (control rod worth) movement is important during transient simulations, the ability to predict the power of the fuel pins around the control rod is also important to ensure when evaluating energy deposition limits. In order to test the ability to calculate both control rod worth and the pin power error around a control rod, the LEU core was used with a control rod



Figure 5.11: Control Insertion Pattern

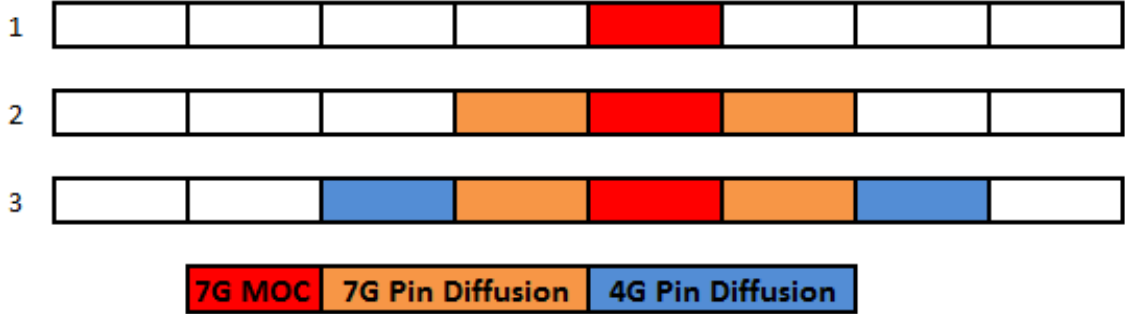


Figure 5.12: Multiscale Regions Used in Control Rod Analysis

inserted in the fourth assembly, as shown in Figure 5.11. The multiscale regions are set up in a consistent manner with the proceeding cases, and can be seen in Figure 5.12.

The control rod worth is calculated using the rodded and unrodded eigenvalues as shown in equation (5.1).

$$\rho_{CR} = \frac{k_{Unrodded} - k_{Rodded}}{k_{Unrodded}k_{Rodded}} \quad (5.1)$$

For the LEU core all methods were able to accurately predict the worth of the control rod as shown in Table 5.5.

Although the diffusion solution was able to predict the global solution accurately, the local solution has significant errors, as shown in Figure 5.13. PPR has the largest errors in pin power in the assembly with the control rod. The error in the PPR

Table 5.5: Control Rod Worth for the LEU Core

	ρ_{CR}	$\Delta\rho$
MOC	357.3	-
2G Diffusion	358.8	1.5
MS - 1	341.8	-15.5
MS - 2	345.1	-12.2
MS - 3	347.2	-10.1

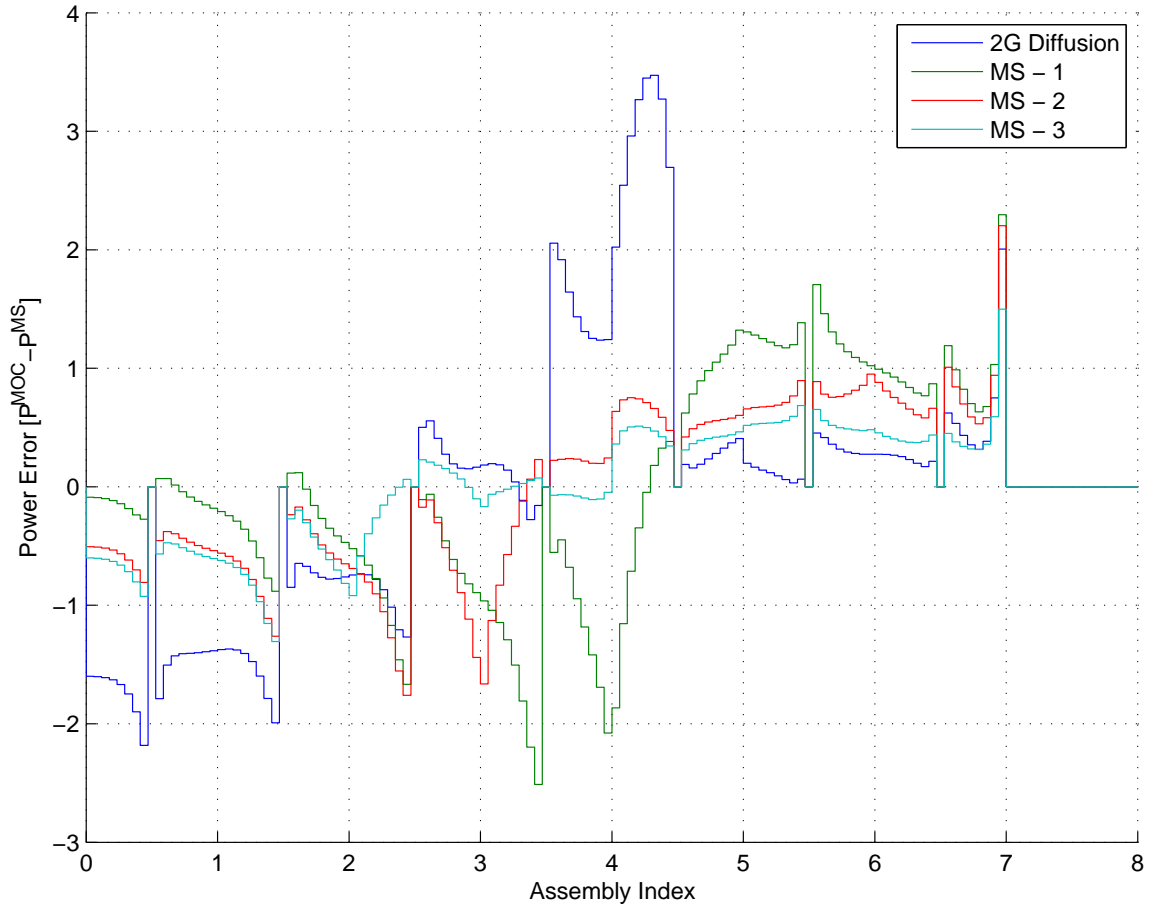


Figure 5.13: Pin Power Errors with Control Rod Inserted

solution is caused by the modulation of the pin power distribution onto an assembly where the control rod has been homogenized. The impact of the embedded region reduces the local pin power errors and improves the global solution.

Although the pin power errors occur at regions around the control rod where the power is low, the error can still be significant when considering an accident such as a control rod ejection. When the control rod is ejected from the core, a very localized power pulse occurs, and the pins closest to the control rod can experience a significant energy deposition. The design limits of the reactor are evaluated in terms of the highest energy deposition in any one fuel pin after a control rod ejection.

5.2 Discussion of Embedded Method

The embedded method evaluated in this chapter is more consistent with traditional multiscale methods used elsewhere in computational science and engineering than the post-refinement method discussed in Chapter 4. The ability to influence the global solution by locally refining the space, energy and angular mesh is a potentially powerful technique for improving the analysis of nuclear reactor performance. Several conclusions can be drawn from the results in this section to provide a set of best practice guidelines for implementing and further developing embedded methods with established computer codes such as PARCS [45] and DeCART [1].

5.2.1 Impact of Multiple Embedded Levels

As noted in the post-refinement method discussion, the energy prolongation operators are much more significant than angle or space. The ability to use multiple embedded levels provides a solution to this problem without significantly reducing runtime. The use of a fine group pin homogenized diffusion solver surrounding the MOC region decreases the impact of the prolongation operator near the MOC region and improves the solution. The introduction of an intermediate group pin homogenized solver also decreases the impact of the energy prolongation operator. By decomposing the solution into three regions with different energies, the prolongation is a much smoother transition. The impact of introducing multiple levels is very similar to the buffer region used in the post-refinement method. Both the buffer region and adding multiple levels both attempt to reduce the impact of the boundary conditions of the higher scale solutions.

The analysis using 33 energy group library also showed that a fine group diffusion solver was not necessary to capture the energy effects, and the 7 group diffusion solver was sufficient to describe the energy spectrum with a low-level transport solution such as diffusion theory. This suggests that the need for a pin homogenized diffusion solver with the same number of energy groups as the transport solution is not necessary. Reducing the size of the requirements of the homogenized diffusion solver will reduce runtime and memory requirements for the multiscale methods.

5.2.2 Prolongation Operators

The prolongation operator for energy was chosen to reflect the results of the post-refinement method. The post-refinement method assessment concluded that the albedo type boundary conditions were much more stable. For this reason, the energy shape was chosen to use the outgoing current to define the shape of the incoming current. Unfortunately, there are cases where this assumption is not valid. In these situations, higher order methods need to be implemented to make the embedded iteration method general enough to handle any arbitrary geometry. Methods such as the discrete generalized multigroup method [16] could be used to better estimate the energy spectrum at the interface but have yet to be demonstrated in multidimensional cases.

Chapter 6

Summary and Conclusion

6.1 Summary of Work

In the research here, two different multiscale methods have been investigated, which rely on a global diffusion solution to provide boundary conditions for a local region of interest. The local region is solved using a high order method which for the work here was chosen to be an integral transport MOC solver. In the post-refinement multiscale methods the boundary conditions are transferred in one direction from the low order local solution to the high order global solution, and the local solution does not attempt to correct the global solution. Two methods were investigated to implement the post-refinement method, which employ different solution procedures. The first is a fixed source problem where the flux distribution is solved for a given incoming angular flux at the boundary. The second method provides an albedo boundary condition and solves a local eigenvalue problem.

The post-refinement methods were assessed using a series of one dimensional core models with a mixture of LEU and MOX assemblies. Cases were analyzed in which the global and local solutions had the same energy group structure to analyze the effect of angular prolongation. Then, mixed energy cases were solved in which more energy groups were used in the local solution to test the energy prolongation operations. For the cases with the same energy group structure, all methods performed well and showed improvement over the standard methodology of diffusion with pin power reconstruction. The mixed energy cases exposed some problems with the energy prolongation operators. The albedo method showed improvement over the state of the art method for most cases considered, but the fixed source method showed better results only when a buffer region was included.

After analyzing the two different methods it was determined that the albedo method is more robust and consistent at improving the estimations of the peak pin

power and the shape of the pin power distribution. Therefore, the albedo method was implemented into a two dimensional multiscale code system. Both the LEU core and the MOX cores showed improved estimations of the local pin powers for the cases run.

The second multi-scale method investigated in the research here was the embedded method, which is more consistent with multiscale methods currently used in computational science and engineering in which refinements in the local solution impact the global solution. The embedded method implemented here was assessed using the same one-dimensional core models used in the post refinement method. Cases were examined where the embedded region is placed in the peak power assembly, at the fuel-reflector interface, and around a control rod. The embedded method showed the ability to reduce the global RMS pin power errors in almost every case analyzed, but the impact on the peak pin power shape was not uniform. There were several cases where the impact on the peak pin power did not change or errors even slightly increased. Embedding the local solver into the reflector region demonstrated the ability to more accurately model the leakage effects out of the reactor and significantly decreased the tilt in the error across the LEU core. The MOX cores showed little or no improvement in the global errors when the local solver was embedded into the reflector. This is primarily because the MOX/LEU interface errors overshadowed any impact of improvements in describing the core leakage. The last case considered was the impact of embedding the local solver around a control rod. No noticeable improvements were observed in the determination of the control rod worth, but improvements were observed in the accuracy of local pin power predictions which is important during core safety analysis.

Throughout the series of cases considered in this work, several observations were made. For the post-refinement methods it was observed that the pin power accuracy can only be as accurate as the global power distribution in the region of interest. If the global assembly power has large errors, the pin powers will have similar errors. The numerical stability of the fixed source and albedo methods were assessed by evaluating the impact of small errors introduced in the boundary conditions. Numerical tests of both methods showed that the albedo method is less sensitive to errors in the boundary condition. For the embedded method, it was observed that the inclusion of several solution levels increases the accuracy of the method. Specifically, the addition of multigroup pin homogenized diffusion solvers around the region of interest can decrease both local and global errors.

6.2 Future Work

Throughout this research several areas for future work have been identified, some of which are current areas of active research in the reactor physics community. A variety of minor improvements to the low order diffusion solution could be made which could improve the accuracy of the boundary conditions which have a significant impact on the local solution. The energy spectrum in which the cross-sections are homogenized can also have a significant impact and should be improved. In this work, the infinite spectrum was used to homogenize cross-sections but many standard lattice codes use the critical spectrum to estimate the impact of leakage on the homogenized cross-sections. The critical spectrum calculation is most appropriate when considering reactors where criticality is determined by changing the soluble boron concentration. Also, only two group cross-sections for the standard diffusion solution were used in this analysis, whereas in some cases a larger number of energy groups are being used in MOX core analysis.

One of the conclusions in the work here is that prolongation in energy is a large source of error in the determination of boundary conditions for the local problem. Current research [17] is investigating methods to solve for moments in energy of transport and diffusion solvers using the discrete generalized multigroup method. This involves first solving the low order equation and then solving a series of fixed source problems in energy to reconstruct the energy shape. The reconstruction of the energy shape could provide a much better estimation of the boundary conditions for the local problem.

The embedded multiscale method could also be a practical method for cases where a more sophisticated transport solver is embedded into another transport solver using the same energy grid [13]. Research is recommended into the application of this method for high fidelity embedded transport calculations (such as 3D MOC) into codes which are capable of calculating a full core transport solution with some approximations (2D-1D MOC, such as the method is implemented into DeCART [1], or 3D S_N codes, like DENOVO [2]).

Another interesting area of research would be to develop criteria to dynamically refine the multiscale region based on local error approximations. Dynamically adaptive multiscale methods have been developed and used in other research areas, but are not currently used in nuclear reactor analysis. This work provides the initial building blocks of such a scheme by allowing the user to statically specify the adaptive regions. A natural next step would be to allow the grid to refine itself dynamically.

Although the multiscale methods here were considered as improvements over the standard pin power reconstruction techniques, the true advantages of the multiscale methods will address issues in which standard pin power reconstruction methods are not effective. The prime example is the ability to couple the local problem to tools of comparable fidelity to provide density and temperature distributions in the region as well as dimensional changes. Current pin power reconstruction methods assume a predefined temperature distribution and therefore are not as accurate when the temperature distribution is different. When multiscale tools are used inside the coupled physics framework, the user will be able to take full advantage of the multiscale methods developed here.

Overall the multiscale methods considered in this work can be implemented into current software used to solve the transport equation. The extension of these codes to solve the full core with diffusion methods should be straightforward to implement. Although there are cases in which all of the methods considered here may have some advantages, the albedo method with buffer regions is suggested for implementation if only local information is desired, because of the stability it provides for a wide variety of different core configurations. If the ultimate goal of implementing a multiscale method is to improve the global solution's accuracy by modeling regions of the reactor in which the standard methods introduce errors, then the embedded method is recommended. Although there are some outstanding issues that have been identified during this work, ongoing research shows promising methods to resolve many of these issues. With the tools provided in this work and developments through ongoing research, multiscale methods can provide reactor designers and analyst with a repertoire of tools that have the ability to significantly reduce the computational burden and improve the accuracy, in order to obtain detailed local information for nuclear reactors.

Bibliography

- [1] M. Hursin, B. Kochunas, and T. J. Downar, *DeCART Theory Manual*. University of Michigan, 2008.
- [2] T. Evans, A. Stafford, R. Slaybaugh, and K. Clarno, “Denovo: A new three-dimensional parallel discrete ordinates code in scale,” *Nuclear Technology*, vol. 171, pp. 171–200, 2010.
- [3] U. Trottenberg, C. W. Oosterlee, and A. Schuller, *Multigrid*. Academic Press, 2000.
- [4] H. G. Joo and T. Downar, “An incomplete domain decomposition preconditioning method for nonlinear nodal kinetics calculation,” *Nuclear Science and Engineering*, vol. 123, pp. 403–414, 1996.
- [5] K. Koebke and M. Wagner, “The determination of the pin power distribution in a reactor core on the basis of nodal coarse mesh calculations,” *Atomkernenergie*, vol. 30, p. 136, 1977.
- [6] S. Grill, A. Jonsson, and J. Rec, “A nodal imbedded method to recover local power peaking from coarse mesh reactor calculations,” *Trans*, vol. 35, p. 580, 1980.
- [7] A. Jonsson, S. Grill, and J. R. Rec, “Nodal imbedded calculation for the retrieval of local power peaking from coarse mesh reactor analysis,” in *International Topical Meeting on Advances in Mathematical Methods for the Solution of Nuclear Engineering Problems*, 1981.
- [8] F. Nissen, *Determination of Local Pin Powers in the Framework of NODAL Coarse-Mesh Solutions*. PhD thesis, Riso National Laboratory, 1982.
- [9] K. Smith, “Assembly homogenization techniques for light water reactor analysis,” *Progress in Nuclear Energy*, vol. 17, pp. 303–335, 1986.
- [10] J. P. Jessee, W. A. Fiveland, L. H. Howell, P. Colella, and R. B. Pembe, “An adaptive mesh refinement algorithm for the radiative transport equation,” *JOURNAL OF COMPUTATIONAL PHYSICS*, vol. 139, pp. 380–398, 1998.

- [11] Y. Wang, *Adaptive Mesh Refinement Solution Techniques for the Multigroup S_n Transport Equation Using a Higher-Order Discontinuous Finite Element Method*. PhD thesis, Texas A&M University, 2009.
- [12] C. Yi and A. Haghghat, “A hybrid block-oriented discrete ordinates and characteristics method algorithm for solving linear boltzmann equation,” in *Joint International Topical Meeting on Mathematics & Computation and Supercomputing in Nuclear Applications (M&C + SNA 2007)*, (Monterey, California), 2007.
- [13] C. Yi and A. Haghghat, “A three-dimensional block-oriented hybrid discrete ordinates and characteristics method,” *Nuclear Science and Engineering*, vol. 164, pp. 221–247, 2010.
- [14] B. Forget and F. Rahnema, “A spectral unfolding method,” *Transactions of the American Nuclear Society*, vol. 1, pp. 669–671, 2007.
- [15] L. Zhu and B. Forget, “A discrete generalized multigroup energy expansion theory,” *Nuclear Science and Engineering*, vol. 166, pp. 239–253, 2010.
- [16] B. Forget and L. Zhu, “Mixed energy reactor simulations using the discrete generalized multigroup method,” in *PHYSOR 2010 Advances in Reactor Physics to Power the Nuclear Renaissance*, 2010.
- [17] B. Forget, “Mixed energy methods.” Personal Communication, 2011.
- [18] H. R. Kim and N. Z. Cho, “Global/local iterative methods for equivalent diffusion theory parameters in nodal calculation,” *Annals of Nuclear Energy*, vol. 20, pp. 767–783, 1993.
- [19] B. D. Ivanov, *Methodology for Embedded Transport Core Calculation*. PhD thesis, Pennsylvania State University, 2007.
- [20] B. D. Ivanov, M. Ouisloumen, E. Mller, and K. N. Ivanov, “Embedded lattice transport calculations based on paragon-new code system for reactor core analysis,” in *International Conference on Reactor Physics, Nuclear Power: A Sustainable Resource*, (Interlaken, Switzerland), 2008.
- [21] B. D. Ivanov, E. Mller, M. Ouisloumen, and K. N. Ivanov, “Online homogenization technique facilitating nem-driven embedded lattice physics calculations,” in *International Conference on Reactor Physics, Nuclear Power: A Sustainable Resource*, 2008.
- [22] S. Zhang, C. Tang, H. Huang, and Y. Chao, “Feasibility of embedding nodal homogenization in next generation methods for 3d pin-by-pin core simulation,” in *International Conference on Reactor Physics, Nuclear Power: A Sustainable Resource*, 2008.

- [23] K. Koebke, “A new approach to homogenization and group condensation,” in *Technical Committee Meeting on Homogenization Methods in Reactor Physics*, (Lugano, Switzerland), 1978.
- [24] K. Smith, *Spatial Homogenization Methods for Light Water Reactor Analysis*. PhD thesis, Massachusetts Institute of Technology, 1980.
- [25] Studsvik Scandpower, *HELIOS v 1.10*, 2008.
- [26] F. B. H. Finnemann and M. R. Wagner, “Interface nodal current technique for multi-dimensional reactor calculation,” *Atomkernenergie*, vol. 30, p. 123, 1977.
- [27] K. Smith, “An analytic nodal method for solving the two-group, multi-dimensional, static and transient neutron diffusion equations,” nuclear engineering, Massachusetts Institute of Technology, Cambridge, MA, 1979.
- [28] Y. Kim, S. J. K. Y. J. Kim, and T. K. Kim, “A semi-analytic multigroup nodal method,” *Annals of Nuclear Energy*, vol. 26, p. 699, 1999.
- [29] B. G. Carlson, “Transport theory: Formulations and solutions by finite difference methods,” tech. rep., Los Alamos Scientific Laboratory, 1968.
- [30] E. E. Lewis and J. W. F. Miller, *Computational Methods of Neutron Transport*. Wiley-Interscience, 1984.
- [31] J. Askew, “A characteristics formulation of the neutron transport equation in complicated geometries,” Tech. Rep. AEEW-R-1108, U.K. Atomic Energy Authority, 1972.
- [32] Z. Liu, H. Wu, L. Cao, Q. Chen, and Y. Li, “A new three-dimensional method of characteristics for the neutron transport equation,” *Annals of Nuclear Energy*, vol. 38, pp. 447–454, 2010.
- [33] J. Y. Cho, H. G. Joo, K. S. Kim, S. Q. Zee, and M. H. Chang, “Three-dimensional heterogeneous whole core transport calculation employing planar moc solution,” *Transactions of the American Nuclear Society*, vol. 87, p. 234, 2002.
- [34] N. Z. Cho, “Fundamentals and recent developments of reactor physics methods,” *Nuclear Engineering and Technology*, vol. 47, pp. 25–78, 2005.
- [35] B. Forget and F. Rahnema, “High order spatial expansion of the incident current in the heterogeneous coarse mesh transport meth,” in *Transactions of the American Nuclear Society*, 2005.
- [36] E. Lewis, M. A. Smith, N. Tsoulfanidis, G. Palmiotti, T. A. Taiwo, and R. N. Blomquist, “Benchmark specification for deterministic 2-d/3-d mox fuel assembly transport calculations without spatial homogenisation,” tech. rep., Nuclear Energy Agency, 2001.

- [37] B. Forget, “Transmittal of 33 group c5g7 library.” Personal Communication, 2011.
- [38] F. Rahnema, “Boundary condition perturbations in transport theory,” *Nuclear Science and Engineering*, vol. 124, pp. 320–326, 1996.
- [39] F. Rahnema and E. M. Nichita, “Leakage corrected spatial (assembly) homogenization technique,” *Annals of Nuclear Energy*, vol. 24, pp. 477–488, 1997.
- [40] F. Rahnema and P. Ravetto, “On the equivalence of boundary and boundary condition perturbations in transport theory and its diffusion approximation,” *Nuclear Science and Engineering*, vol. 128, pp. 209–223, 1998.
- [41] M. S. McKinley and F. Rahnema, “Higher-order boundary condition perturbation theory for the diffusion approximation,” *Nuclear Science and Engineering*, vol. 136, pp. 15–33, 2000.
- [42] M. S. McKinley and F. Rahnema, “High-order boundary condition perturbation theory for the neutron transport equation,” *Nuclear Science and Engineering*, vol. 140, pp. 285–294, 2002.
- [43] Y. Saad, *Iterative Methods for Sparse Linear Systems*. SIAM, 2003.
- [44] Y. Saad, *Numerical Methods for Large Eigenvalue Problems*. Manchester University Press, 1992.
- [45] H. G. Joo, D. Barber, G. Jiang, and T. Downar, “Parcs: Purdue advanced reactor core simulator,” tech. rep., Purdue University, 1998.